UNIVERSITÄTSKLINIKUM HAMBURG-EPPENDORF

Institut für Osteologie und Biomechanik

Heisenberg Forschungsgruppe Bioengineering/Medizintechnik
Leiter: Univ.-Prof. Dr. rer. medic. Björn Busse

Direktor: Univ.-Prof. Dr. med. Michael Amling

Collagen Fiber Organization in Human Cortical Bone and Its Functional Relationship with Matrix Composition and Biomechanical Competence

Dissertation

zur Erlangung des Doktorgrades PhD
an der Medizinischen Fakultät der Universität Hamburg.

vorgelegt von:

Kilian Elia Stockhausen
aus Köln

Hamburg 2021

(wird von der Medizinischen Fakultät ausgefüllt)

Angenommen von der
Medizinischen Fakultät der Universität Hamburg am: 24.06.2021

Veröffentlicht mit Genehmigung der
Medizinischen Fakultät der Universität Hamburg.

Prüfungsausschuss, der/die Vorsitzende: **Prof. Dr. Björn Busse**

Prüfungsausschuss, zweite/r Gutachter/in: **Prof. Dr. Thomas Oertner**

Table of Contents

1. Introduction

1.1. Scientific Context

The discovery of the osteon by Clopton Havers in the 17th century, the observation of bone-resorbing osteoclasts by Albert Kölliker in the 19th century (Kölliker, 1873), and the findings by Harold Frost regarding the coupling of bone cells as coordinated remodeling units in the 1960s (Hattner et al., 1965): these are just a few examples of pioneering discoveries that have contributed to a deeper understanding of bone as a dynamic tissue. While often intuitively viewed as a static structure, bone is in fact metabolically active and continuously renewed throughout life. In this process, the overall size and shape as well as the micro- and nanostructure of the bone matrix are extensively altered and adapted to new mechanical demands. However, while efficient mechanisms operate in healthy adult bone to provide high resistance to fracture, an increased bone fragility is recognized in certain phases of life and in disease. Specifically, an elevated fracture risk is not only documented in children and in the aging skeleton but also in various metabolic diseases including osteoporosis. It is estimated that every third child experiences at least one fracture before the age of 17, with the majority of fractures resulting from low-energy traumas (Cooper et al., 2004; Hedström et al., 2010; Landin, 1983). While the higher physical activity during childhood is often considered as a driving risk factor (Clark et al., 2008), underlying skeletal deficits have also been suggested to contribute to the high fracture incidence in children (Farr et al., 2014; Faulkner et al., 2006; Goulding, 2007). In aging and osteoporosis, an imbalance between bone formation and resorption leads to a net loss of bone mass which results in high skeletal fragility and a public health problem of epidemic proportions. In 2010, 22 million women and 5.5 million men were estimated to have osteoporosis in the European Union alone, and a total number of 3.5 million osteoporotic fragility fractures were documented (Svedbom et al., 2013). The treatment of fractures and the associated absence from work result in a large economic burden but also, and more importantly, reduce the quality of life of the affected individuals (Hernlund et al., 2013). Movement is not only an important element for an independent and active daily life but is also a prerequisite for the production of endorphins during exercise that trigger a positive body feeling. Patients suffering from a hip fracture are evidently affected in their physical and mental functioning, and do not recover to the

same level of performance they had prior to the fracture (Alexiou et al., 2018). Moreover, the life expectancy is also dramatically altered as the mortality rate following surgery is estimated to be 3% during the hospital stay (Groff et al., 2019) and 27% within one year following hospital release (Panula et al., 2011).

In view of the high fracture incidence in the developing, aging and osteoporotic skeleton, and considering the expected increase of aging- and osteoporosis-related fractures due to our aging society (Odén et al., 2015), the question arose: How does bone obtain its fracture resistance? This question has preoccupied the minds of researchers for a long time. Traditionally, high bone fragility was ascribed to a loss of bone quantity as measured by the bone mineral density (BMD). Clinically, dual-energy X-ray absorptiometry (DXA) is most often used for the diagnosis of osteoporosis in which the BMD is measured and compared to a healthy young control group to obtain a so-called T-score. While T-scores between -1.0 and -2.5 indicate low bone density, or osteopenia, T-scores of -2.5 and below lead to a diagnosis of osteoporosis (Kanis et al., 2013). However, it was shown that only 18% of osteoporotic fractures occur in patients that had T-scores in the osteoporotic range of -2.5 or less (Siris et al., 2004). *Vice versa*, 82% of the patients with fractures presented non-osteoporotic T-scores, strongly suggesting that other factors, beyond the BMD, have a substantial influence on the elevated fracture risk. Here, numerous other influencing factors that affect the mechanical competence of bone have been identified. They are collectively termed as “bone quality” and concern various aspects of the bone tissue including its micro- and nanostructure, the matrix composition and the spatiotemporally regulated cellular activity of bone cells.

While many bone quality parameters affecting the fracture risk have been elucidated in health and disease, it remains rather understudied how the organization and orientation of collagen fibers is related to compositional patterns. While it is widely accepted that both the preferential orientation of collagen fibers and the mineralization profile individually impact the mechanical competence of bone at several length scales, the coupling of distinct structural and compositional patterns is not fully characterized. Bone derives its mechanical competence from its hierarchical structure, which is established during skeletal growth and maintained throughout lifelong remodeling processes. Clarifying the relationship between the collagen fiber orientation, mineralization profile and local biomechanical properties could deepen our

understanding of how tissue properties at the nanoscale influence and guide fracture mechanisms at larger length scales. In this thesis, the organization and orientation of collagen fibers was investigated at a consistent skeletal site (mid-diaphyseal femoral bone) and related to important compositional and mechanical properties of bone quality. In the first project, bone obtained from fetal to 14-years old cases was comprehensively assessed to document bone quality changes during skeletal development that may further explain the increased fractured risk during longitudinal bone growth. Here, the collagen fiber orientation, bone composition and mechanical competence were analyzed in the period of life where the skeleton is subjected to new mechanical demands associated with the transition from crawling to walking. In the second project, the collagen fiber orientation was assessed at the nanoscale in remodeled osteons that interact differently with circularly polarized light to appear either dark or bright. Here, the changing brightness of *dark* and *bright* osteons indicates fundamentally differently aligned collagen fibers (longitudinal and transverse, respectively). In addition to the collagen fiber organization, spatially correlated compositional and mechanical properties were quantified to elucidate the structure-function relationship in cortical bone at the smallest length scales. As the adaptability of bone is reflected in its micro- and nanostructural arrangement, the formation of *dark* and *bright* osteons points at a tissue heterogeneity that is considered advantageous for its mechanical strength.

Understanding the origins of bone quality in healthy bone is essential to evaluate impaired bone quality in disease. Therefore, it is necessary to establish a benchmark whether and to what extent distinct structural arrangements in cortical bone are associated with specific compositional characteristics. By scrutinizing the structure-composition relationship in healthy cortical bone, valuable insights can be gained which could help to better understand the origins of increased fracture risk in aging and bone pathologies.

1.2. Skeletal Development and Hierarchical Structure

During skeletal development and throughout life bone undergoes extensive structural changes to adapt to its mechanical environment. In the premature skeleton, three key processes are involved in the formation, elongation, shaping and microstructural adaption of the bone matrix. At first, early stages of skeletal growth are

guided by endochondral ossification where a calcified cartilage precursor is replaced by a collagenous matrix that is able to bind bone mineral (Karaplis, 2002). Secondly, bone modeling processes continue to grow the bone in diameter and cortical thickness by a spatially uncoupled activity of osteoblasts and osteoclasts. Osteoblasts lay down new bone matrix at the periosteal surface while osteoclasts resorb tissue near the endocortical border to adapt the bone to altered mechanical loading scenarios while preserving a lightweight structure (Currey, 2002; Seeman, 2003). Lastly, on the microstructural level, the bone matrix is extensively adapted by bone remodeling processes where osteoclasts and osteoblasts operate simultaneously and spatially bound to replace less-organized primary tissue by organized secondary remodeled osteons. In this process, osteoclasts resorb bone matrix that is subsequently filled in by osteoblasts with new bone matrix rich in type I collagen that serves as a scaffold for later mineralization *via* incorporation of hydroxyapatite crystals (Lassen et al., 2017). The activity of osteoclasts and osteoblasts is guided by mechanosensitive osteocytes, the most abundant bone cells, that are distributed throughout the bone matrix.

In adults, secondary remodeled osteons are the fundamental functional unit and define its microstructural appearance. The structure of osteons spans over several hierarchical levels (**Figure 1**). At its core, the matrix is composed of type 1 collagen, hydroxyapatite and water that are spatially bound to form mineralized collagen fibrils. They contain weak but recoverable sacrificial bonds that dissipate energy through

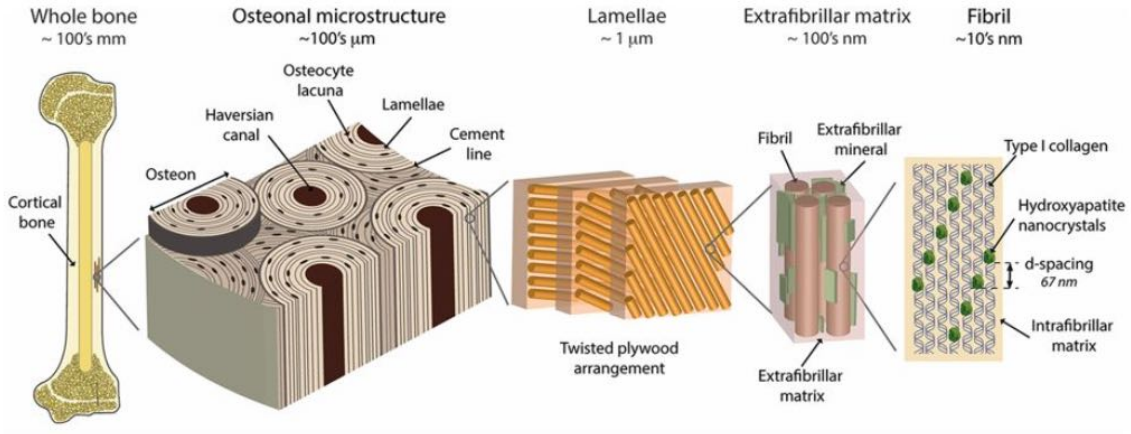

Figure 1: The hierarchical structure of bone. At the microstructural level, the cortical bone consists of cylindrically shaped osteons that are the fundamental structural units. The Haversian canal is located at the center of each osteon which contains blood and nerve vessels. Osteonal lamellae concentrically surround the Haversian canal. The lamellae consist of arrays of collagen fibers, which are assembled from arrays of collagen fibrils, composed of collagen and mineral. Adapted from Zimmermann *et al.* (2011).

rupture when mechanically loaded (Fantner et al., 2005). The mineralized collagen fibrils are assembled in fiber arrays that are aligned along their long axis and stabilized by interfibrillar crosslinks. The fiber arrays are, in turn, aggregated to form osteonal lamellae. Osteons consist of concentrically layered lamellae that surround a central vascular cavity (Haversian canal). At the periphery, osteons are bordered by the cement line that is higher mineralized in comparison to the surrounding interstitial bone matrix (Milovanovic et al., 2018). The matrix is interspersed by mechanosensitive osteocytes that reside in micrometer-scale cavities (lacunae) that are connected by nanometer-sized tunnels (canaliculi). They form a dense network and play an essential role for the skeletal metabolism and the maintenance of a healthy bone matrix. Specifically, osteocytes are able to communicate directly with each other through the canalicular network to sense mechanical and chemical stimuli in their environment. The sensory inputs are subsequently transmitted to osteoblasts and osteoclasts *via* the delivery of signaling molecules in order to initiate modeling/remodeling processes (Schaffler et al., 2014).

During skeletal growth, the bone matrix is extensively altered by modeling/remodeling processes at the tissue level. It is gradually remodeled from woven (primary) bone with irregularly assembled collagen fibers towards secondary remodeled cortical bone with highly organized collagen fibers building the osteonal lamellae. In this process, many bone quality parameters are affected: the mineral concentration increases with ongoing development while the mineral distribution becomes more homogeneous (Currey et al., 1996; Reid and Boyde, 1987). Concomitantly, the mechanical properties are altered with the bone stiffness being correlated to the children age indicating a higher resistance to fracture (Currey and Butler, 1975; Lefèvre et al., 2019; Öhman et al., 2011). On the cellular level, fetal/infantile bone is characterized by a high osteocyte density that decreases with age enabling a quick proliferation and accelerated bone remodeling rate (Ferretti et al., 1999; Hernandez et al., 2004; Remaggi et al., 1998). Moreover, osteocyte lacunae have been shown to be larger in size in infantile cases which was associated with a more heterogeneous mineral distribution (Jandl et al., 2020). Clearly, the bone matrix is subjected to extensive adaptions throughout life that affect important bone quality parameters. However, a high fracture incidence is documented not only in elderly individuals but also in children/adolescents. This points towards an impaired bone

quality that is linked to a transitory weakness of the skeleton (Bailey et al., 1989; Faulkner et al., 2006; van Staa et al., 2001).

1.3. Collagen as a Contributor to Bone Quality

Bone is a dynamic and hierarchically organized tissue with impressive mechanical properties that provide high resistance to bending, compression and torsion. It is a natural composite material built from collagen, mineral and water that jointly define its unique mechanical behavior. Mineral platelets with high elastic modulus are embedded into a collagenous framework of low elastic modulus. Hence, the mineral phase predominantly enables resistance to plastic deformation (i.e., high stiffness) whereas collagen predominantly provides ductility and the ability to absorb energy (i.e., toughness) (Currey, 1988; Wang et al., 2001; Zioupos and Currey, 1998). Despite its importance, the ability of bone to withstand repetitive loading and resist fracture is not solely dependent on the quantity of bone tissue but also on its matrix quality. The term “bone quality” is a collective term for various structural, material and cellular properties of bone that guide its mechanical competence at several length scales (**Figure 2**). Structural properties include the overall bone geometry (size and shape) as well as its microstructural (trabecular and cortical) and nanostructural arrangement (woven and osteonal bone) (Felsenberg and Boonen, 2005; McCalden et al., 1993; Vom Scheidt et al., 2019; Shapiro and Wu, 2019). Important material

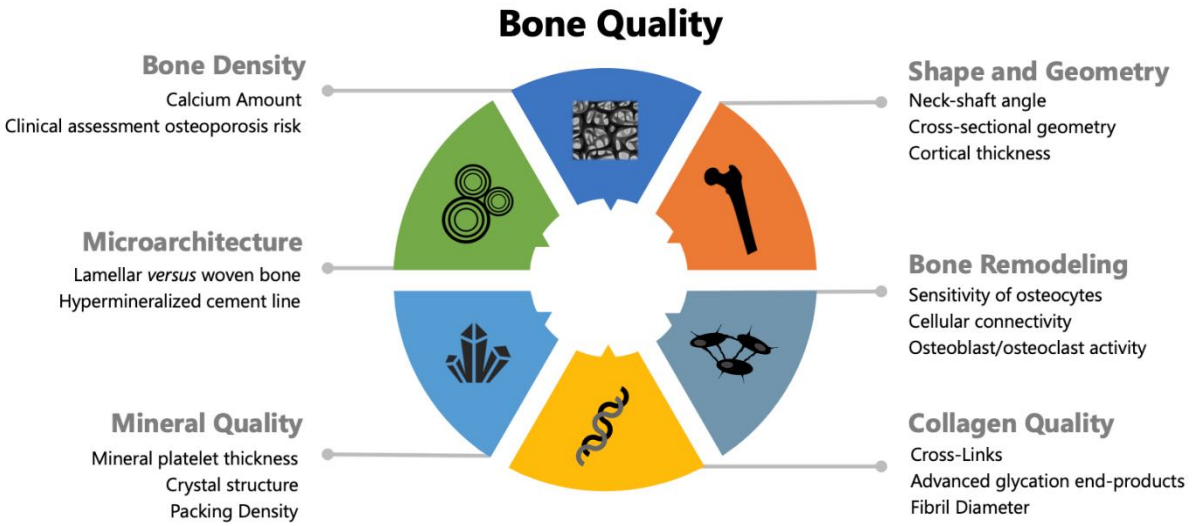

Figure 2: The term “bone quality” includes several structural, material and cellular properties at all level of hierarchy that contribute to the mechanical competence of bone.

characteristics of bone tissue comprise the quality of its organic (collagen) and inorganic (mineral) components, the bone mineral density distribution as well as water content and accumulation of microcracks (Felsenberg and Boonen, 2005; Fiedler et al., 2018; Fonseca et al., 2014; O'Brien et al., 2003; Wang et al., 2002; Willett et al., 2019). On the cellular level, the integrity of the network formed by mechanosensitive osteocytes is essential to maintain healthy bone by detecting damage and initiating repair processes (Fonseca et al., 2014; Milovanovic et al., 2015). With aging and skeletal disease several bone quality parameters can be impaired reducing the ability to withstand mechanical loading and ultimately leading to increased fragility and fracture susceptibility.

Several studies have highlighted that variations in the quality of the collagenous phase can strongly affect bone strength. The importance of collagen for fracture resistance is emphasized by clinically challenging pathologies like osteogenesis imperfecta or Paget's disease, both of which are characterized by impaired collagen formation and organization leading to increased fracture susceptibility (Carriero et al., 2014; Rauch and Glorieux, 2004; Zimmermann et al., 2015a). Collagen quality is influenced by exposing bone to ionizing radiation which has been shown to decrease bone toughness while preserving Young's modulus independent of the radiation dose (Currey et al., 1997). On a molecular level, the collagenous matrix quality is affected by the formation and extent of inter- and intramolecular crosslinks (Saito and Marumo, 2010) as well as the accumulation of advanced glycation end-products (Gautieri et al., 2017; Schmidt et al., 2017). In addition, the structure and arrangement of collagen fibrils also affect the mineral quality as possible nucleation sites for bone mineral crystals are determined by the collagen framework which also limits the size of the crystals (Wang et al., 2012). Moreover, the collagen fiber orientation (CFO) is considered as an contributor to bone's ability to resist fracture and an impact of preferentially aligned collagen fibers on the mechanical properties is postulated (Ritchie, 2011; Viguet-Carrin et al., 2006). The distribution pattern of secondary remodeled osteons with differently aligned collagen fibers is reported to be non-randomly distributed and corresponds to the distribution pattern of loading forces acting on the bone, with longitudinal collagen fibers being found in regions supporting tensile loads while transverse fibers are located in regions under compression (Ascenzi, 1988; Martin and Boardman, 1993; Martin and Ishida, 1989). The

dependency of population densities of distinct osteon types with specific loading modes suggests that collagen fibers align according to specific strain modes and serve different mechanical functions (Riggs et al., 1993a; Skedros et al., 2009, 2011).

1.4. Bone Toughness and Strength

In healthy adults, remodeled osteonal bone can tolerate significant loading by capable fracture resistance mechanisms operating at different hierarchical levels of the matrix. While the most dominant toughening mechanisms have been classified in mature bone (Fantner et al., 2005; Gupta et al., 2005; Koester et al., 2008; Nalla et al., 2003; Poundarik et al., 2012; Zimmermann et al., 2011), the mechanisms and underlying bone quality still remain understudied during longitudinal skeletal growth (<20 years of age).

Cortical bone obtains its fracture toughness by intrinsic and extrinsic mechanisms operating at different length scales (**Figure 3**) (Launey et al., 2010). While intrinsic resistance is generated at micro- to nanometer length scales to hamper the initiation of cracks, extrinsic mechanisms act at the micro- to macroscale to limit the propagation of already initiated cracks. The most influential intrinsic mechanisms include the molecular uncoiling of tropocollagen, the breaking of sacrificial bonds between fibril arrays, as well as fibrillar sliding between mineralized collagen fibrils. At larger length scales, the extrinsic mechanisms operate by collagen fiber bridging, crack bridging by uncracked ligaments and crack deflection at hypermineralized cement

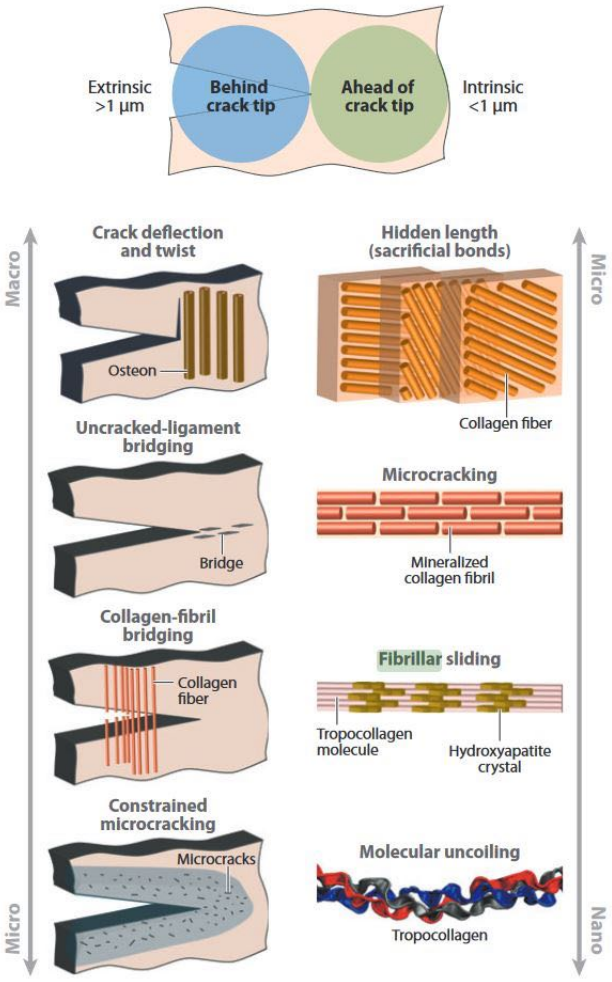

Figure 3: Extrinsic and intrinsic toughening mechanisms of bone. Extrinsic mechanisms act behind the crack tip at the micro- and macroscale whereas intrinsic mechanisms act ahead of the crack tip at the nano- and microscale. Figure from Launey *et al.* (2010).

lines. Here, the stiffness mismatch at interfaces of different mineralization content plays a crucial role as the crack follows the paths of lowest resistance. Hence, when a crack propagates in a relatively low mineralized volume and reaches an interface to a volume with higher mineral content, the crack is deflected and continues to travel in the less stiff volume. By elongating the total microcrack path, more energy is dissipated in the process and large-scale fractures are prevented. In view of their underlying operating principles, intrinsic mechanisms act ahead of the crack tip while extrinsic mechanisms act behind it (Ritchie, 2011; Zimmermann et al., 2015b). In addition to the mineralization heterogeneity that induces a stiffness mismatch in the matrix, the overall mineral content also plays a major role in bone strength and strongly affects the mechanical properties (Boivin et al., 2008; Follet et al., 2004). The stiffness and resistance to fracture increases with higher densities of mineral due to the higher stiffness of the inorganic mineral phase of bone compared to the organic collagenous phase (Berteau et al., 2015; Landis et al., 1995; Öhman et al., 2011). However, excessive mineralization is detrimental as it makes the bone tissue brittle and increases the fracture risk (Bala et al., 2010). Therefore, the degree and quality of mineralization in bone is used as an indicator of the mechanical competence of bone.

Previous studies have identified a lower modulus and hardness in pathologic or callus tissue consisting of woven bone compared to healthy lamellar tissue (Manjubala et al., 2009; Zimmermann et al., 2015a), implying that primary tissue types are inherently weaker than healthy, secondary remodeled bone tissue types. Considering that further important structural features for toughness (i.e., lamellar interfaces or cement lines) have not yet developed in primary non-osteonal tissue suggests that bone quality deviates or is, at least, explained differently for primary and secondary bone tissue. In fully remodeled osteonal bone of healthy adults, the adaptive capabilities to mechanical demands are reflected in the microstructural arrangement and composition. Here, the existence of *dark* and *bright* osteons with contrasting CFO patterns points at a required heterogeneity of the tissue matrix that is considered advantageous for the mechanical properties of bone. Most studies seized on the idea that *dark* osteons are more capable to resist tensile forces and bending while *bright* osteons, assembled of oblique-angled collagen fibrils, can better withstand compressive forces and torsion (McMahon et al., 1995; Riggs et al., 1993b). Consequently, it was postulated that *bright* osteons are found in regions supporting

tensile loads, while *dark* osteons dominate in regions under compressive loading. This was confirmed in quadrupedal mammalians, where significant bending stresses created by angulation of the joints lead to distinct volumes being loaded in tension or compression (Bergmann et al., 1984; Boyde and Riggs, 1990; Shahar et al., 2003; Skedros et al., 1996). However, the diaphysis of human femoral bone is primarily loaded in compression with little impact of bending and tensile forces (Duda et al., 1997; Taylor et al., 1996; Zheng et al., 1998). Yet, both *dark* and *bright* osteons are present in femoral cross-sections. This clearly suggests that, in view of this rather uniform loading scenario, spatial changes in the preferential CFO of osteons might serve further mechanical functions beyond the resistance to tensile and compressive stresses indicating a more profound mechanical function of *dark* and *bright* osteons. This is further supported by the fact that, even though the overall CFO pattern appeared non-randomly distributed, no single pattern of CFO was found to exist in the human diaphyseal femur suggesting that the microstructure is sensitive to individual and localized adaptation (Bromage et al., 2003).

1.5. Collagen Fiber Organization in Osteonal Bone

The question of how collagen is organized in osteonal lamellar bone has sparked interest for a long time and has led to a number of proposed models over the years. In 1906, Gebhard *et al.* proposed a model in which osteonal lamellae are consistently fibrous layers with the fibril orientation being unidirectional in individual lamellae but undergoing a change in orientation of 90° between neighboring lamellae (Gebhardt, 1905). In the 1960s, Ascenzi and Bonucci reconceived this view and postulated that three representative patterns of lamellar organization exist in osteons: longitudinal, transverse and alternating (**Figure 4**) (Ascenzi and Bonucci, 1967, 1968). These observations were based on polarized light micrographs that allow for the visualization of the preferential collagen fiber. Here, lamellae containing transverse and oblique-angled collagen fibers with respect to the osteon axis appear bright. In contrast, lamellae appear dark when the collagen fibers run in parallel with the osteon axis. Lastly, alternating osteons are built from lamellae that alternate between a transverse and longitudinal orientation. Structurally, *bright* osteons are characterized by predominant fiber orientations of ±45° with respect to the osteon axis. Contrarily, *dark* osteons are rather homogeneous and distinguished by longitudinal collagen fibers

(Ascenzi et al., 2003). In 1988, Giraud-Guille proposed a more complex model of collagen fiber organization using polarized light and transmission electron microscopy (Giraud-Guille, 1988). Two different types of plywood-like architecture were reported to exist in osteonal bone, namely “orthogonal plywood” and “twisted plywood”. While the “orthogonal plywood” conforms with the classical concept of alternating and orthogonal orientations of collagen fibrils between neighboring lamellae, the “twisted plywood” model suggested a novel perspective. In this arrangement, no clear structural boundary between individual lamellae exists as collagen fibers are continuously shifted in their direction. The oriented collagen fibers rotate through 180° cycles, so that superimposed series of nested arcs become visible in oblique sections. Later studies supported the idea of plywood-like structures in osteonal bone even though the models were further refined. Weiner *et al.* demonstrated four to five parallel fibril arrays that are followed by an abrupt change in fibril orientation. The authors termed this characteristic structural feature as “back-flip” fibril arrays (Weiner et al., 1997). Both Varga *et al.* in 2013 and Schrof *et al.* in 2014 found oscillating plywood patterns in lamellae, in addition to twisted plywood arrangements, where the fibrils undergo continuous sinusoidal oscillation rather than rotating from 0 to 180° (Schrof et al., 2014; Varga et al., 2013). However, no consensus on the spatial distribution of each structure type was reported: either the outermost lamella was stated as twisted followed by oscillatory ones (Varga et al., 2013), or most lamellae displayed a twisted plywood pattern with only a few lamellae near the Haversian canal having a oscillating structure (Schrof et al., 2014). Despite the different proposed models, it is generally agreed on that the collagen-mineral assembly is spatially correlated. The collagen fibers are reinforced by bone mineral particles to form a spatially related composite material where the mineral long axis is co-aligned with the collagen fibers that provide bone with its unique mechanical properties

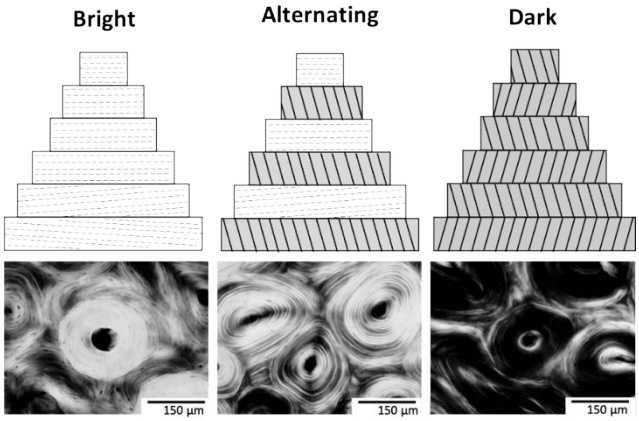

Figure 4: Three types of lamellar organization of secondary remodeled osteons according to Ascenzi et al. Osteons containing transversely oriented collagen appear bright under polarized light (type 1, left). The collagen orientation is shifted by 90° between neighboring lamellae (type 2, middle). Osteons built for longitudinally oriented collagen appear dark (type 3, right). Figure adapted from Ascenzi *et al.* (1968).

(Fratzl et al., 2004; McNally et al., 2013). More recently, further insights into the collagen-mineral assembly have been gained showing that bone mineral is fractal-like and hierarchically assembled at the nanoscale (Reznikov et al., 2018) and that localized differences between the orientation of mineral nanocrystals and collagen fibrils exist within single lamellae that might add an additional layer of mechanical adaptation towards compressive loading (Grünewald et al., 2020).

1.6. Objectives

The origins of bone quality are many-faceted and often closely interrelated (Stock, 2015). In this context, it is essential to include comprehensive bone quality parameters on all relevant length scales to elucidate the underlying mechanisms of bone fragility. The aim of this thesis is to investigate the organization and orientation of collagen fibers in human femoral bone taken from the mid-diaphysis and to comprehensively evaluate important structural, compositional and mechanical properties to deepen our understanding of how nanoscale tissue properties influence and guide fracture mechanisms at larger length scales. As bone is a dynamic tissue that adapts its matrix organization in response to mechanical stimuli during skeletal growth and throughout life, two key questions were addressed:

i.) It was investigated how bone quality and mechanical competence develop during skeletal growth. As a high fracture incidence is not only documented in the elderly but also in children and adolescents, this indicates that bone quality might also be inferior in the latter groups compared to healthy adult bone. To better understand the transitory weakness and increased fracture risk in children, the microstructure including the CFO was analyzed in the femoral mid-diaphysis of fetal to 14-years old cases and linked to its composition and mechanical performance. Here, the cases were split into two groups: fetal/infantile bone consisting of primary bone with no osteons and 2- to 14-years old cases composed of remodeled tissue (i.e., secondary osteons).

ii.) Secondly, adult femoral bone was studied to assess the structural heterogeneity of osteons that appear dark or bright in circularly polarized light microscopy. As the microstructural appearance of bone reflects its adaptability to mechanical strains, *dark* and *bright* osteons with diverging collagen fiber arrangements could provide valuable

insights into the collagen-mineral relationship in cortical bone and elucidate the need for localized matrix modifications.

In the present thesis, important bone quality parameters on the nano- and microscale are comprehensively assessed to elucidate the relationship between the CFO and nano-compositional patterns in human femoral bone. By concurrent evaluation of mechanical characteristics, this thesis aims to elucidate the origins of cortical bone fragility in the developing skeleton and to quantify cortical bone quality adaptions in adult bone beneficial for its mechanical competence.

2. Materials and Methods

2.1. Sample Cohort

Several high-resolution techniques were included in the comprehensive evaluation of bone quality parameters. The sample preparation and methodology are described in more detail in the original manuscripts (Stockhausen et al., 2021; Zimmermann et al., 2019). In short, femoral bone from the mid-diaphysis was obtained from healthy human cases during autopsy at the Department of Forensic Medicine at the University Medical Center Hamburg-Eppendorf (Hamburg, Germany) in accordance with the local ethics regulations and following ethical approval as stated in the manuscripts. To evaluate bone quality parameters during skeletal development, a cross-sectional study was adopted, and bone was acquired from a Caucasian female cohort (22 weeks of gestation, n = 1; age of 2 months, n = 2; 1 year, n = 1; 2 years, n = 1; 5 years, n = 1; 14 years, n = 2). To assess intra-individual structural heterogeneity

Table 1: Overview of methods used in the respective study. The sample preparation method is denoted in superscript (1 = ground section, 2 = block sample, 3 = microtome section, 4 = hydrated sample)

Fetal – 14-years Old Cases	***Dark* and *Bright* Osteons**
Circularly Polarized Light Microscopy [1]	Circularly Polarized Light Microscopy [1]
Quantitative Backscattered Electron Imaging [2]	Quantitative Backscattered Electron Imaging [1]
Fourier Transform Infrared Spectroscopy [3]	Fourier Transform Infrared Spectroscopy [1]
Tensile Testing [4]	Nanoindentation Testing [1]
SAXS/WAXD [4]	Synchrotron Nano-Computed Tomography [1]
Histomorphometry [3]	FIB-SEM Imaging [1]
	Finite Element Modeling

in terms of *dark* and *bright* osteons, bone was obtained from a 44-year-old organ donor. Cross sections from the femoral mid-diaphysis were prepared using a diamond saw (EXAKT Advanced Technologies GmbH, Norderstedt, Germany). The specimens were fixed in 3.7% formaldehyde for 3 days followed by dehydration in an increasing alcohol series and undecalcified embedding in methylmethacrylate. Samples were prepared from the embedded block as ground sections with a thickness of 100µm using an automatic grinding machine and as microtome sections with a thickness of 5µm. Additionally, the embedded blocks were ground to a coplanar finish, carbon-coated and used for compositional analysis. Lastly, hydrated cortical bone samples (15 mm × 1 mm × 250 µm) from fresh-frozen fetal to 14-years old cases were prepared using a low-speed saw for synchrotron-based mechanical testing. The methods used in the respective study and their corresponding sample preparation method are summarized in table 1.

2.2. Structural Evaluation

Histomorphometric evaluation in the fetal to 14-years old cases was performed on microtome-cut sections stained with von Kossa/van Gieson stain. The stain allows for the differentiation between mineralized bone (von Kossa precipitation in black) and unmineralized osteoid (van Gieson stain in pink). Here, the osteoid volume per bone volume (OV/BV), osteoid surface per bone surface (OS/BS) and osteoid thickness (O.Th) were quantified using the software “OsteoMeasure” (OsteoMetrics, Decatur, GA, USA) (Dempster et al., 2013).

Circularly polarized light microscopy (CPL) was used to assess the preferential CFO (**Figure 5**). Here, bone areas containing obliquely orientated collagen fibers appear bright while dark areas are composed of collagen fibers parallel with the long axis of the bone. While

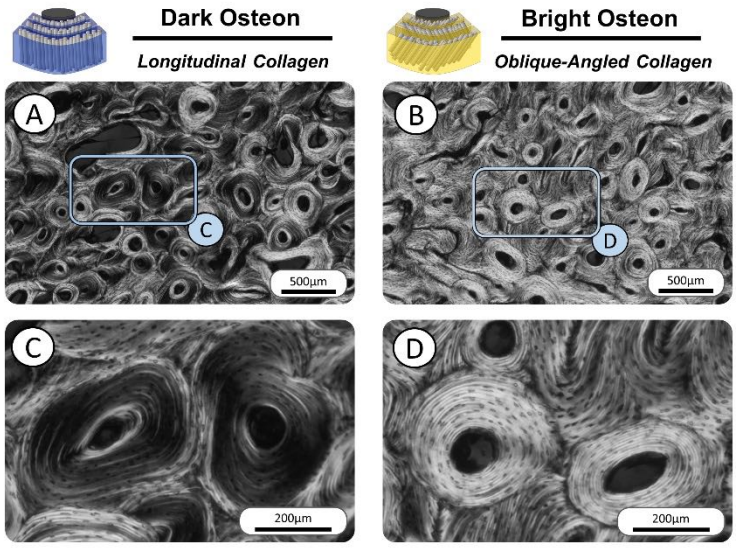

Figure 5: Circularly polarized light microscopy was used to identify 20 osteons of contrasting brightness. The brightness reflects changes in collagen fiber orientation originating at the nanoscale.

the dark appearance of longitudinally oriented collagen arises from its optically anisotropic properties, porous spaces, vascular canals or osteocyte lacunae also appear dark but due to the absence of birefringent tissue. To exclude these areas from the evaluation, a masking procedure was applied. In the fetal to 14-years old cases, the structural appearance and the CPL brightness were evaluated in the medial cortex of the cross-section. In the 44-years old case, CPL was utilized to detect *dark* and *bright* osteons for subsequent structural, compositional and mechanical analysis. Twenty (ten *dark* and ten *bright*) osteons were selected from the anterolateral quadrant of the femoral cross-section. Osteons were only included if (i.) they were surrounded by at least two partially resorbed osteons, i.e. to exclude primary osteons and (ii.) they displayed a continuous outer border, i.e. to exclude osteons that have been resorbed. In addition, micro-computed tomography was performed and co-registered to the CPL image to validate that the Haversian canals of the investigated *dark* and *bright* osteons are oriented perpendicular to the analyzed plane (**Figure 6**). Lastly, a control experiment was conducted to deconvolute the influence of the mineral phase on the CPL brightness. Here, a test sample was decalcified in 20% EDTA and prepared as a ground section of identical thickness (100µm). Successful decalcification was confirmed radiographically using a cabinet X-ray system (Faxitron, Inc., USA). Then, the decalcified sample was imaged by CPL and compared to undecalcified samples in terms of CPL brightness.

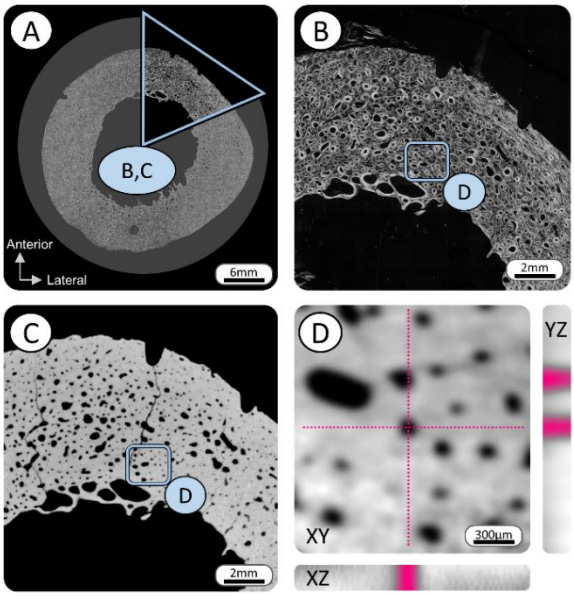

Figure 6: (A) Osteons were selected unbiasedly from the anterolateral quadrant. (B, C) CPL images and micro-computed tomography scans were co-registered to confirm the perpendicular orientation of the osteons with respect to the cutting plane. (D) The orientation of the Haversian canal (highlighted in pink) was verified in the orthogonal projections.

The three-dimensional spatial organization of collagen fibers in *dark* and *bright* osteons was visualized by synchrotron nano-computed tomography with Zernike phase contrast. By utilizing Zernike phase contrast, the contrast can be enhanced in weakly absorbing specimen that appear transparent to conventional absorption

tomography (Langer et al., 2012; Varga et al., 2013). The experiments were carried out at the P05 beamline operated by the Helmholtz Zentrum Geesthacht (HZG) at the PETRA III storage ring of the German Electron Synchrotron (DESY) (Flenner et al., 2020; Ogurreck et al., 2013). The nanoindentations (chapter 2.4) were localized and cylindrical volumes with a diameter of 25 µm were extracted using a focused ion beam (FIB). The nano-tomograms were acquired with a Fresnel zone plate of 130 µm diameter, a beam shaping optics and Zernike phase rings at an energy of 11 keV with a three-dimensional spatial resolution of 77.7nm (determined by Fourier shell correlations).

The internal matrix structure within *dark* and *bright* osteons was further verified by focused ion beam - scanning electron microscopy (FIB-SEM) imaging. The FIB was used to mill trenches into the osteons exposing imaging planes with radial-longitudinal orientation with respect to the Haversian canal. Firstly, a coarse trench was milled at 30 kV and 30 nA, followed by polishing of the exposed image plane at 30 kV and 2 nA. Then, images were acquired at 2 kV (InlensDuo Detector, Zeiss) and post-processed using a band-pass filter to remove curtaining artefacts (Schindelin et al., 2012).

2.3. Compositional Assessment

The bone mineral density distribution (BMDD) and osteocyte lacunar morphology was determined by quantitative backscattered electron imaging (qBEI). Calibration of the brightness and contrast was achieved with carbon and aluminum standards, so that the intensity of the backscattered electrons linearly correlated with the mean atomic number and, hence, the calcium content (Roschger et al., 1998). Accordingly, lower and higher brightness values translate to a low and high calcium content of the tissue, respectively. Similar to the masking procedure applied to CPL micrographs, osteonal areas were isolated to exclude surrounding tissue from evaluation in qBEI. A custom-made MATLAB routine was used to calculate the following parameters from the backscattered electron images: mean calcium content of the BMDD (Ca_{mean}), most frequent calcium content (Ca_{peak}), the heterogeneity of the calcium distribution (Ca_{width}), percentage of bone area which is mineralized below the 5^{th} percentile or above the 95^{th} percentile (Ca_{low} and Ca_{high}, respectively). Moreover, the backscattered electron images were used to quantify the bone volume per tissue volume (BV/TV) as well as osteocyte lacunae characteristics. Specifically, the number

of osteocyte lacunae per bone area (N.Ot.Lc./B.Ar., #/mm²), the mean osteocyte lacunar area (Ot.Lc.Ar, µm²), and the circularity index of osteocyte lacunae were assessed.

The composition was further assessed using Fourier transform infrared spectroscopy (FTIR) operated in transmission mode (for the fetal to 14-years old cases) or attenuated total reflection-mode (*dark* and *bright* osteons). Spectra were acquired over a spectral range of 570 to 4000 cm^{-1} at a 4 cm^{-1} spectral resolution. After correction for the spectral presence of atmospheric gases, and subtraction of background and PMMA signals, the areas under the curve of the amide I peak (1700-1600 cm^{-1}), the phosphate peak (1154 - 900 cm^{-1}) and the carbohydrate peak (890 - 850 cm^{-1}) were integrated to measure the mineral-to-matrix ratio (MMR) and carbonate-to-phosphate ratio (CPR) (Boskey and Pleshko Camacho, 2007; Schmidt et al., 2017). Additionally, the ratio of the 1030 cm^{-1} and 1110 cm^{-1} subbands was used to assess the mineral maturity in the fetal to 14-years old cases (Farlay et al., 2010).

2.4. Mechanical Properties

In the fetal to 14-years old cases, mechanical competence and deformation at the tissue, fibril, and mineral length scales were assessed by tensile testing with simultaneous small-angle x-ray scattering (SAXS) and wide-angle X-ray diffraction (WAXD). Experiments were performed at beamline 7.3.3 at the Advanced Light Source synchrotron (Lawrence Berkeley National Laboratory, Berkeley, CA, USA) (Hexemer et al., 2010). Here, the hydrated cortical bone samples were loaded in tension and SAXS/WAXD data were collected at an energy of 10 keV at ~4000 mm and 150 mm sample-to-detector distance, respectively. By combining tensile testing with SAXS/WAXD measurements, the overall tissue strength can be assessed while evaluating deformations occurring at the nanoscale at the same time (Zimmermann et al., 2011). Changes in the average collagen d-spacing and mineral lattice were deduced from the 1D SAXS and WAXD data, respectively (Ilavsky, 2012). Tissue stress was calculated during tensile testing by normalizing the acting load to the cross-sectional area. Tissue strain was measured by monitoring the spacing between horizontal marks that were placed on the sample.

The local biomechanical properties of *dark* and *bright* osteons were assessed by nanoindentation testing where four indents were placed in each osteon using the

depth-sensing continuous stiffness mode: one per osteonal quadrant at half the distance between the osteon center and the outer border. Indentations with 2 µm depth were performed with a Berkovich tip preceded and followed by calibration on fused silica. The hardness and the elastic modulus were calculated according to Oliver and Pharr with the NanoSuite software provided by the manufacturer (Oliver and Pharr, 1992).

To predict how overlying levels of hierarchy are affected by shifts in preferential CFO, multi-scale modeling using the Finite Element Method (FEM) was applied (Qwamizadeh et al., 2016, 2017a, 2017b). Here, the orthotropic mechanical properties of three distinct hierarchical levels were calculated by modeling finite representative volume elements (RVEs) (Omairey et al., 2019). The three hierarchical levels included were (i.) mineral-coated collagen fibers, (ii.) osteonal lamellae, and (iii.) fully remodeled secondary osteons. Each hierarchical level was modeled for different scenarios of CFO to represent *dark*, *bright* and alternating osteons. The respective RVE was used as input for the overlying hierarchical level. Specific input parameters and assumptions are noted in (Stockhausen et al., 2021) and were taken from (Buenzli and Sims, 2015; Dong et al., 2014; Hamed et al., 2010, 2012; Hellmich and Ulm, 2002; Rho et al., 1997).

2.5. Statistical Analysis

Shapiro-Wilk tests were used to evaluate normality of the data. Homogeneity of variances was tested using Levene's test. In the fetal to 14-years old cases, data was averaged on the individual level and separated into two groups based on microstructural observations: the 2- to 14-year-old samples contained secondary remodeled osteons while the fetal to 1-year-old samples did not. Because of the small sample size, a nonparametric statistical analysis was used (Mann-Whitney U). To determine statistical differences between *dark* and *bright* osteons independent t-tests were performed. Pearson product-moment correlations were used to check for correlations between structural, compositional, and mechanical properties. Statistical tests were performed using SPSS with a level of significance of $\alpha=0.05$. All data are represented as the mean ± standard deviation.

3. Results

3.1. Matrix Characteristics in Cortical Bone Development

3.1.1. Cortex Densification and Collagen Fiber Reorganization

Substantial structural variations were observed in the femoral mid-diaphysis of the developing skeleton (**Figure 7**). Microstructurally, the fetal/infantile cases presented a scaffold-like structure characterized by a high porosity and a disorganized collagen fiber organization resembling woven bone. No remodeling events or lamellar structures in form of secondary osteons are visible. Contrarily, the 2- to 14-years old cases displayed a denser matrix with significantly less porosity and a lamellar structure with secondary remodeled osteons. Histomorphometric evaluation revealed a significantly lower bone volume fraction (BV/TV) in the infantile cases ($p = 0.03$), accompanied by a significantly higher osteoid surface per bone surface (OS/BS) ($p = 0.03$). Despite the significant difference in OS/BS, the osteoid thicknesses (O.Th) were similar in both groups. Moreover, a significantly higher density of osteocyte lacunae

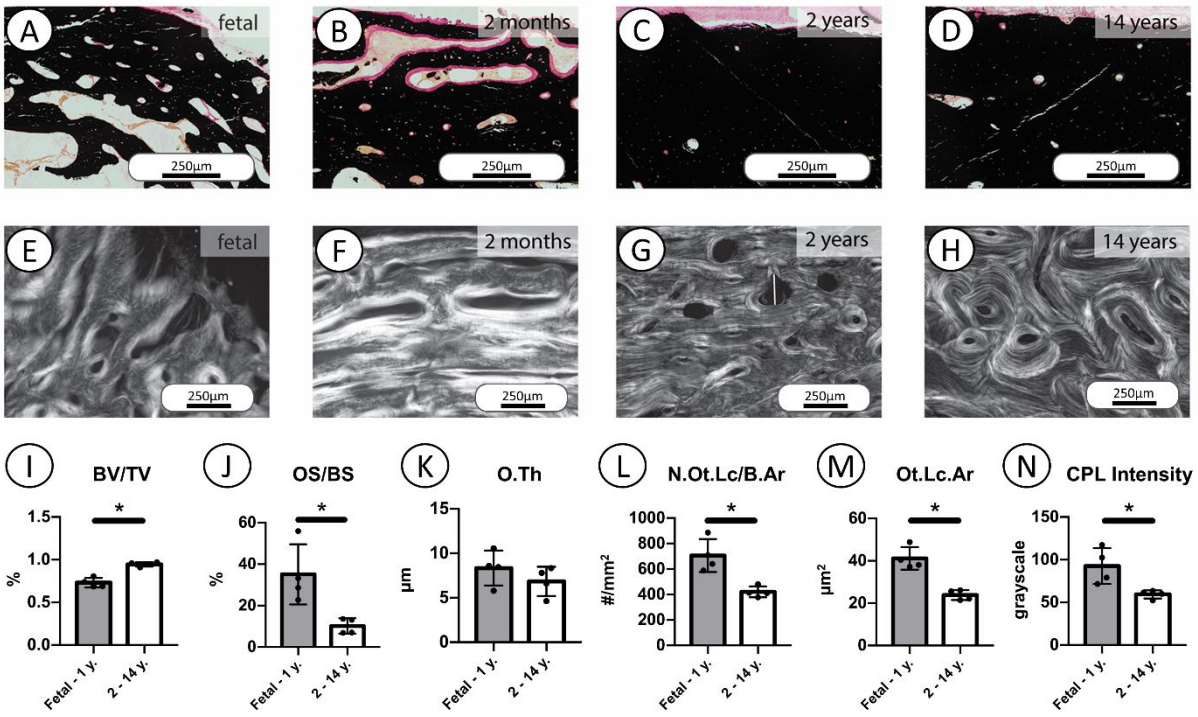

Figure 7: (A-D) Histomorphometry on von Kossa/van Gieson-stained sections was used to differentiate mineralized bone (black) from unmineralized osteoid (pink). (E-F) The microstructural arrangement and collagen fiber orientation was assessed by circularly polarized light microscopy. The fetal/infantile cases have a more porous cortex (I) and a more rapid bone formation rate (J). However, the osteoid thickness is similar for both groups. Osteocyte lacunae are larger in size and more frequent in fetal/infantile bone (L, M). Higher CPL intensities reflect a higher fraction of transversely oriented collagen fibers.

(N.Ot.Lc/B.Ar) was quantified that were also 73% larger in size. Lastly, quantitative evaluation of CPL micrographs showed significantly higher brightness values in woven bone in fetal/infantile cases signifying a higher fraction of transversely oriented collagen fibers. The preferential collagen fiber orientation becomes more longitudinally oriented in the 2- to 14-years old cases as indicated by lower CPL intensities.

3.1.2. Changing Mineralization Patterns During Skeletal Growth

Compositionally, the qBEI data demonstrated a significantly lower mean calcium content in fetal/infantile cases that increases with age (10% higher in the 2- to 14-years old cases) (**Figure 8**). Despite the elevated mean mineral content, the most frequent calcium concentration (Ca_{peak}) is similar in both age groups. In addition, a decrease in mineralization heterogeneity was measured with advancing age as reflected by a 34% lower Ca_{Width} in the 2- to 14-years old cases. In support of the lower mean calcium content, the area fraction of bone regarded as lowly mineralized (Ca_{low}) is significantly higher in fetal/infantile cases, even though both groups present similar area fractions

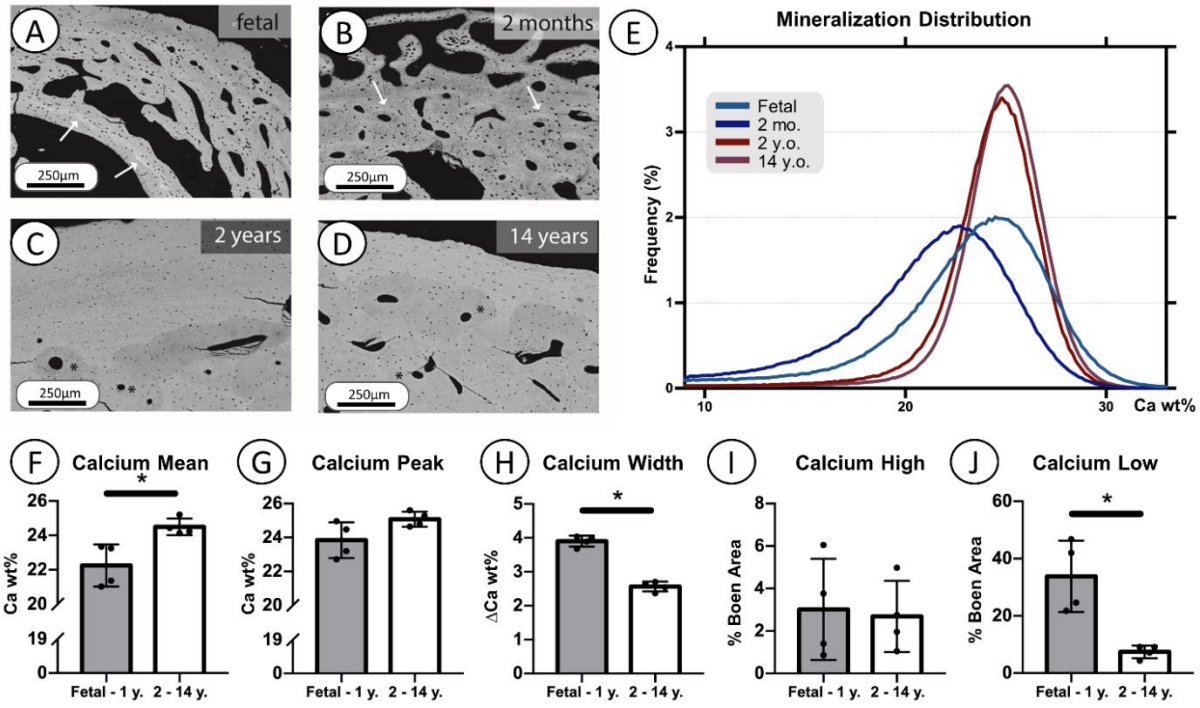

Figure 8: Bone mineralization was quantified using quantitative backscattered electron imaging. (A. B) Remnants of calcified cartilage are present in fetal/infantile bone (white arrows). (C, D) Remodeling events are visible in the 2- to 14-years old cases as reflected by areas with low mineralization (black asterisks). (E) Histogram analysis shows a higher mineralization in the older cases. (F, G) Despite a higher mean calcium content, the peak calcium shows no significant difference. (H) The mineral is more heterogeneously distributed in fetal/infantile cases. In line with the mean and peak calcium content, no significant differences were measured for calcium high whereas calcium low was significantly lower for the 2- to 14-years old cases.

of highly mineralized tissue (Ca_{high}). Secondary osteons, that are generally lower mineralized than the interstitial bone, are evident in the femoral mid-diaphysis of the 2- to 14-years old cases reflecting an advanced bone remodeling history. The observed trends in the mineralization profile are supported by FTIR data. In accordance with the higher mineral content, a 12% higher mineral-to-matrix ratio is quantified in the 2- to 14-years old cases that is also more homogeneously distributed. The FTIR spectra were also used to evaluate the carbonate-to-phosphate ratio (CPR) and the mineral maturity, but no significant differences could be demonstrated.

3.1.3. Development of Mechanical Resistance

Structural and compositional differences were linked to the mechanical resistance at multiple length scales *via* tensile testing (macroscale deformation) and simultaneous SAXS/WAXD experiments (deformation at the fibril and mineral levels, respectively). By gradually applying loads and measuring the concomitant deformation of the samples, stress-strain curves are obtained from which the mechanical behavior at the macroscale can be deduced. At low strains, the samples showed linear elastic behavior that derives from stretching of molecular bonds. Here, a 160% higher elastic modulus was quantified in the 2- to 14-years old cases. With increasing strain, plastic deformation commences, and the tissue starts to deform nonlinearly. At this strain rate, the ultimate bone strength was measured to be 83% greater in the older age group. However, no significant differences were observed for the failure strain.

The simultaneously obtained SAXS/WAXD data was used to measure the deformation at the fibril and mineral level. Here, the fibril deformation showed a linear increase in fibril strain during tensile tests for all cases. However, differences in the mechanical response at the nano-level were revealed in the mineral phase by WAXS where a higher mineral strain to tissue strain suggests that the more organized microstructure in the older cases allows the mineral to deform more easily. At higher tissue strains, the linear stress-strain relationship becomes nonlinear and remains constant indicating sliding within/between fibrils or nonlinear deformation in the collagen matrix.

3.2. Regional Bone Matrix Modifications: *Dark* and *Bright* Osteons

3.2.1. Lamellar Interfaces and Changing Collagen Fiber Orientation

In the mature skeleton, the bone matrix has been extensively remodeled, and its microstructural appearance is characterized by secondary remodeled osteons of changing brightness under polarized light. Here, increasing brightness corresponds to a shift in predominant CFO towards more oblique-angled collagen fibers. After deconvoluting the impact of the mineral phase on the CPL brightness and confirming that osteons were sectioned transversely, osteons with significantly different brightness values (67.22 ± 9.31 *versus* 162.00 ± 10.17, $p<0.001$) were used for

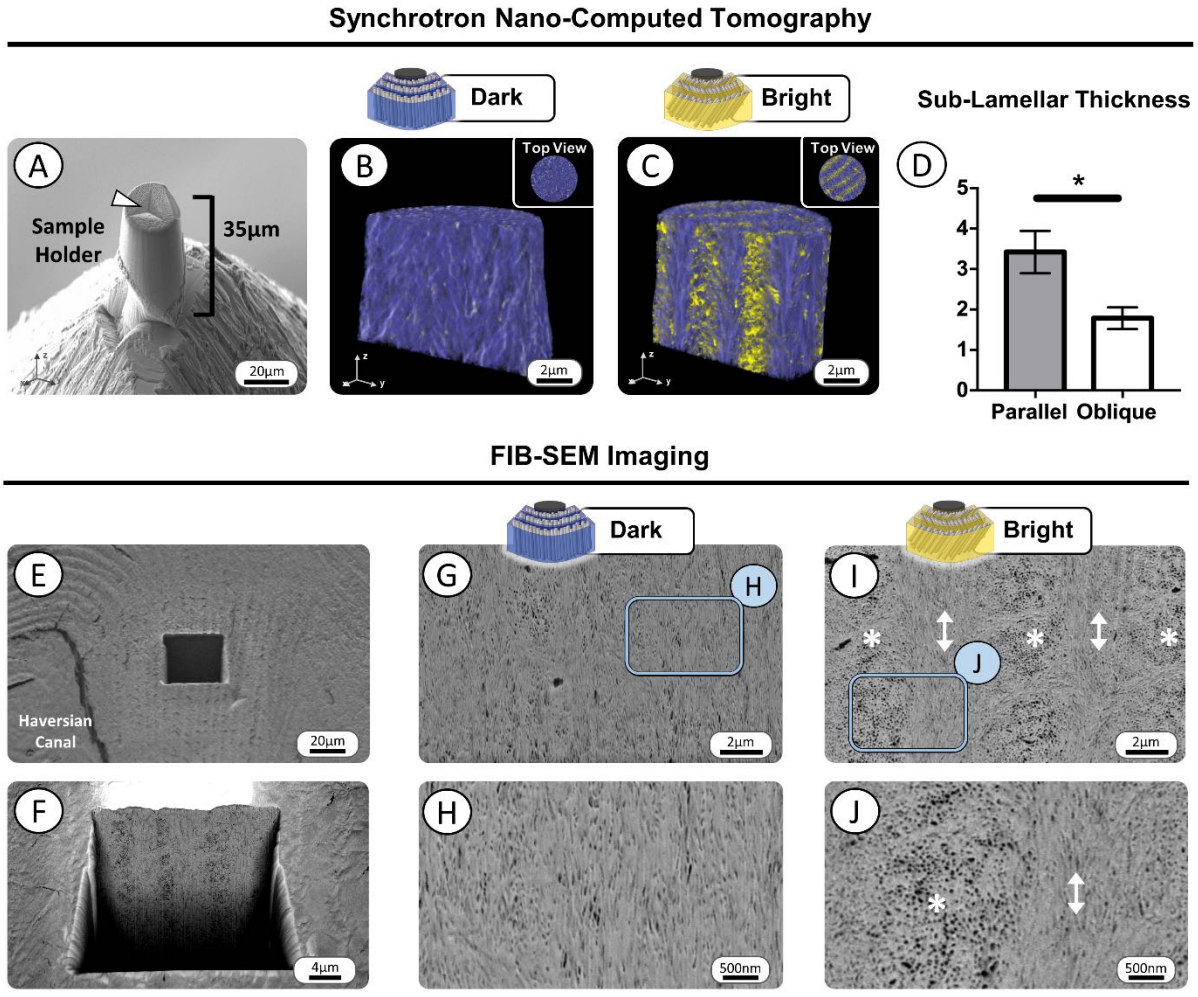

Figure 9: (A -D) Synchrotron nano-computed tomography in bone volumes beneath the nanoindents shows that *dark* osteons are structurally rather homogenous with collagen fibers running longitudinally. *Bright* osteons present a lamellar with changing collagen fiber orientation between neighboring lamellae. Parallel-fibered lamellae were found to be significantly thicker compared to lamellae composed of oblique-angled fibers. (E-J) These results were further confirmed by FIB-SEM imaging: *bright* osteons display a lamellar pattern with fibrils being oriented parallel (double-headed arrows) and oblique-angled to the analyzed plane (asterisk).

subsequent evaluation. Specifically, both decalcified and undecalcified samples showed similar overall CPL brightness and a lamellar pattern with varying brightness independent of the mineralization state. Therefore, differences in CPL intensity can be ascribed to orientation shifts of optically anisotropic type 1 collagen which are not affected by the mineralization profile of individual osteons. To confirm the orthogonality of the selected osteons, micro-computed tomography was used. Here, the three-dimensional orientation of the Haversian canal was assessed in the orthogonal projections for the selected osteons and co-registered to the CPL micrograph (**Figure 6**).

Using synchrotron nano-computed tomography with Zernike phase contrast the structural heterogeneity of both types was verified in three dimensions and with high resolution **(Figure 9A-D)**. It was shown that *dark* osteons are structurally rather homogeneous with collagen fibers running predominantly parallel to the long axis of the bone. Moreover, they show no lamellar pattern. *Bright* osteons display a higher degree of orientational heterogeneity and a distinct lamellar pattern with changing CFO between neighboring lamellae is visible. Here, the longitudinally oriented fraction of collagen fibers (blue lamellae) corresponds to the slightly darkened lamellae of the otherwise *bright* osteon under CPL. Quantification of the sub-lamellar thicknesses showed that lamellae composed of longitudinally oriented collagen fibers were significantly thicker compared to lamellae built from oblique-angled fibers (3.42 ± 0.55 µm *versus* 1.79 ± 0.27 µm, $p<0.001$). Additional validation of the structural disparities between *dark* and *bright* osteons was obtained by FIB-SEM imaging. Here, trenches with radial-longitudinal orientation with respect to the Haversian canal were milled to expose the internal matrix organization of the osteons **(Figure 9E-J)**. In support of the nano-computed tomography findings, a higher structural homogeneity was observed in parallel-fibered *dark* osteons compared to *bright* osteons that are composed of individual lamellae with oblique-angled collagen fibers that are bordered by lamellae built from parallel-oriented fibers. The lamellar layout of *bright* osteons is further signified in two dimensions in backscattered electron images where lamellae with a thickness of ~6 µm are clearly visible whereas no lamellar pattern is present in *dark* osteons. Here, it is important to mention that the lamellar thickness as assessed in backscattered electron images denotes the total thickness of a repeating unit of lamellae (Pazzaglia et al., 2012). However, as visualized by nano-computed

tomography and FIB-SEM imaging, a lamellar unit contains two sub-lamellae of contrasting CFO. Backscattered electron images were further used to quantify characteristics of osteocyte lacunae. Here, it was found that osteocyte lacunar areas are smaller in size in *dark* osteons compared to *bright* osteons (41.17 ± 5.92 *versus* 49.21 ± 4.83 μm^2, $p<0.001$) and are characterized by a higher circularity index (0.631 ± 0.059 *versus* 0.536 ± 0.056, $p<0.001$) representing a rounder shape. No significant difference in osteocyte lacunar density was verified between both osteon types (0.00083 ± 0.00024 *versus* 0.00091 ± 0.00033 #/μm^2, $p = 0.588$).

3.2.2. Discrete Mineralization Profiles

Significant differences in the mineral distribution were quantified by analysis of the qBEI histograms (**Figure 10**). A higher mean calcium content (Ca_{mean}) was quantified in *dark* osteons. The Ca_{mean} is 5.68% higher in *dark* osteons compared to the *bright* ones (26.25 ± 0.32 *versus* 24.84 ± 0.34 Ca wt%, $p<0.001$). The peak calcium content (Ca_{peak}) displays the same trend with a 5.42% higher peak mineralization (26.67 ± 0.36 *versus* 25.30 ± 0.32 Ca wt%, $p<0.001$). In line with the higher mean and peak calcium content, a higher percentage of bone area exhibiting a high mineral

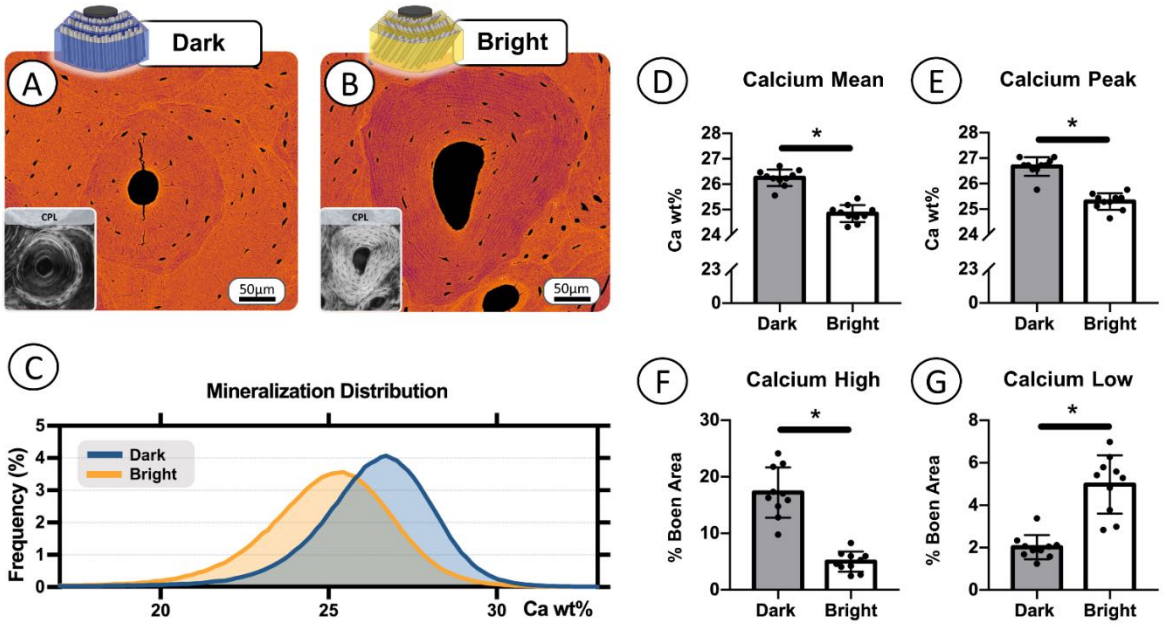

Figure 10: (A-C) Using qBEI, a higher mineralization was quantified in *dark* osteons. (D, E) Both mean and peak calcium contents are significantly higher compared to *bright* osteons. (F, G) Accordingly, a smaller percentage of bone area displays a low mineralization and a higher percentage a high mineralization.

content (Ca_{high}, $p<0.001$) and a lower percentage of bone area with a low mineral content (Ca_{low}, $p<0.001$) was quantified in *dark* osteons compared to *bright* osteons.

The differences measured by qBEI are further validated by the FTIR results: *dark* osteons show a 14.77% higher MMR compared to *bright* osteons (3.21 ± 0.17 *versus* 2.80 ± 0.18, $p<0.001$). Moreover, the MMR positively correlates with the mean calcium content underlining that *dark* osteons in fact contain more mineral ($r = 0.7292$, $p<0.001$). The higher MMR was accompanied by a higher carbonate-to-phosphate ratio (CPR) in *dark* osteons (0.01463 ± 0.00044 *versus* 0.01370 ± 0.00028, 6.79% higher, $p<0.001$) which also correlated positively with the mean calcium content ($r = 0.4914$, $p<0.001$). Spatial assessment of the MMR revealed a ring of elevated MMR towards the Haversian canal that was observed in both in *dark* and *bright* osteons. Here, it was observed that the thickness of the high-MMR ring positively correlates with the osteon wall thickness ($r = 0.681$, $p<0.001$). To eliminate the CFO as a potential interference factor on the MMR, a second integration of the peak areas of amide I plus amide II with respect to the mineral peak area was performed. However, the results showed similar differences as the usual MMR confirming that the CFO has no relevant influence.

3.2.3. Deviations in Biomechanical Competence

Nanoindentation testing was used to link the detected structural and compositional differences of *dark* and *bright* osteons to the local mechanical matrix characteristics (**Figure 11**). In line with the differing mineralization patterns as evaluated by qBEI and FTIR, both the hardness and stiffness measured *via* nanoindentation are significantly higher in *dark* osteons. The elastic modulus and hardness are 31.05% and 33.33% higher in *dark* osteons, respectively. The mean calcium content also correlated positively with both the elastic modulus and hardness,

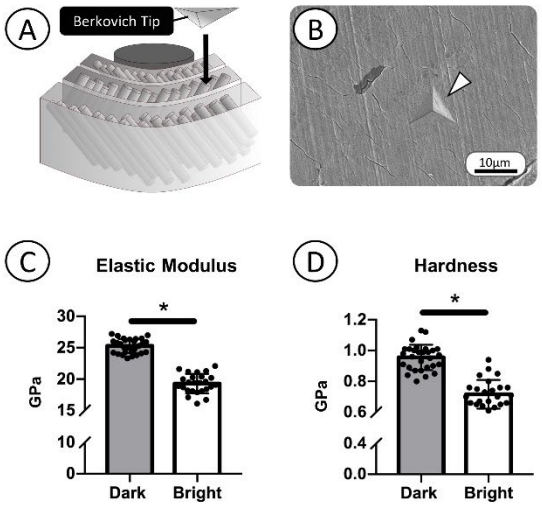

Figure 11: (A, B) Nanoindentation testing was performed with Berkovich tips and successful indents were verified using electron microscopy. (C, D) *Dark* osteons have a significantly higher elastic modulus and hardness.

whereas the preferential CFO correlated negatively with the material mechanical properties.

By modeling RVEs for different CFOs using the finite element methods, a substantially higher effective modulus was calculated for longitudinally oriented mineral-coated fibers. The differences at the fiber level are carried over to the osteonal lamellar level where a shift in CFO from 45° to 0° led to an 26.70% increase in the effective modulus in the direction of indentation. Comparing the predicted values to the experimentally obtained values by nanoindentation reveals similar results. While the FEM model predicted an elastic modulus of 26.15 GPa for *dark* and 20.64 GPa for *bright* osteons, 25.28 ± 1.12 GPa and 19.29 ± 1.54 GPa were measured experimentally. The elastic constants calculated for the lamellar level were used to predict the effective elastic modulus of fully remodeled osteons. Here, the influence of changing CFO in individual lamellae was emphasized as the osteonal effective modulus was found to be 14.38% higher in *dark* osteons compared to *bright* osteons.

4. Discussion

4.1. Bone Quality Develops During Skeletal Growth

Long bones in the human skeleton undergo large structural adaptations during skeletal growth that affect the overall size and shape as well as the microstructural appearance of the bone tissue. In endochondral ossification, bone is initially formed by replacing a calcified cartilage precursor and the bone develops in length, while periosteal appositional growth and endocortical resorption increase the diameter and cortical thickness at later stages of development. In this process, the cortical microstructure in the mid-diaphyseal femur is also adapted in response to the mechanical environment, and less-organized bone is replaced by highly organized lamellar bone. However, an elevated fracture risk is not only recognized in aging bone, where an unbalanced remodeling activity results in a net loss of bone mass along with impaired bone quality of the remaining matrix, but also in children and adolescents below 20 years of age. This suggests that bone quality in the developing skeleton has not fully developed and is inherently lower compared to mature bone or reflects different mechanical demands experienced in this period of life (Bailey et al., 1989; Boyce and Gafni, 2011; Faulkner et al., 2006; van Staa et al., 2001; Verbruggen et al.,

2018). Within the context of this thesis, fetal to 14-years old cases were comprehensively assessed to better understand the structural and compositional framework that may help to elucidate the underlying mechanisms of increased fracture risk during longitudinal bone growth.

4.1.1. Structural Adaption to Changing Mechanical Demands

Often, woven bone is regarded as only a transitional phase in bone development or as tissue with inferior properties formed following fracture or in pathological cases (Buckwalter et al., 1995; Hoerth et al., 2014; Holguin et al., 2014; Manjubala et al., 2009; Zimmermann et al., 2015a). Hence, the focus of most studies is placed on remodeled lamellar bone and there are relatively few studies centered on compositional and mechanical characteristics of woven bone. Histological studies have established the presence of woven bone in early phases of bone formation that is also characterized by a lower density, higher porosity and higher vascularity compared to adult bone (Humphries, 2011). With ongoing age, the cortical porosity and vascularity decreases with the formation of primary osteons and their subsequent remodeling into secondary osteons (Feik et al., 1997). Previous studies investigated the development of long bones in mice and found that the growing femur undergoes large transformations likely induced by changing mechanical demands that temporally coincide with the beginning of walking (Bortel et al., 2015; Sharir et al., 2011). These findings are in accordance with our results where the femur showed a porous scaffold-like structure in fetal/infantile bone that densifies near the time of walking. Here, a densification of the cortex was observed in the older age group as highlighted by a significantly higher BV/TV. As the cortex becomes denser with age, the available surface area for osteoblast to secrete new bone decreases. Accordingly, the higher OS/BS in the fetal/infantile cases emphasizes a higher bone formation rate that decreases with age. Even though the OS/BS is significantly lower in the 2- to 14-year-old cases, the osteoid thickness is comparable with the fetal/infantile group which suggests that the acting mineralization processes are alike in both age groups. Microstructurally, the fetal/infantile cases showed a non-osteonal, woven bone structure emphasized by disorganized collagen fibers consisting of randomly distributed but spatially separated packets of matrix in which the collagen fibers are similarly oriented (either longitudinally or more transversely). With advancing age, the

microstructure is remodeled, and highly organized lamellar bone progressively replaces the less organized woven bone. This structural arrangement is characterized by a higher fraction of longitudinally oriented collagen fibers, possibly in response to changing mechanical demands (Boyde and Riggs, 1990; Bromage et al., 2003; Portigliatti Barbos et al., 1984). The appearance of osteocyte lacunae and their distribution density are also reported to differ between woven and lamellar bone. While osteocyte lacunae in adult lamellar bone are generally elongated and elliptical, they appear larger in size and more round and oval in woven bone with no preferential three-dimensional spatial orientation (Jandl et al., 2020; Remaggi et al., 1998). Moreover, they appear more frequently in woven compared to lamellar bone suggesting that the remodeling rate in woven bone is accelerated. Previous studies have shown that a higher osteocyte lacunar density is associated with a higher bone remodeling/formation (Hernandez et al., 2004), and an increased ability to detect and remove microcracks (Vashishth et al., 2000). This is in line with our results of increased osteocyte lacunar density and osteocyte lacunar area in the fetal/infantile age group, raising the question whether the matrix organization guides the lacunar size or whether enlarged osteocyte lacunae serve a more profound mechanical function by altered mechanosensory potential as suggested by previous studies (Bacabac et al., 2008; van Hove et al., 2009; van Oers et al., 2015). Enlarged osteocyte lacunae have also been verified in woven bone that is rapidly formed in Paget's disease (Zimmermann et al., 2015a) and in cranial suture synostosis (Regelsberger et al., 2012). However, even though differences in osteocyte lacunar morphology may be the result of different mechanical loading and could indicate altered mechanosensitivity, further studies are needed to verify this relationship in health and disease.

4.1.2. Increased Homogeneity and Degree of Mineralization

Accompanying the structural adaption with age, the mineralization pattern also undergoes extensive changes in this process. In general, a lower mineral content is measured in fetal and immature bone at the tissue level that increases with ongoing age (Currey and Butler, 1975; Currey et al., 1996). Moreover, is has been reported that the mineral content reaches a plateau and remains rather constant between 1.5 to 23 years of age (Fratzl-Zelman et al., 2009). At the microstructural level, an increase in mineralization is associated with an increase in tissue age, such that newly formed

bone is lower mineralized than older bone (Bala et al., 2010). In our cross-sectional study, a coupling between the mineralization profile and the structural appearance/tissue age was observed. Here, the woven bone showed a divergent mineralization pattern compared to the osteonal bone with an overall lower and more heterogeneously distributed mineralization profile. In the older age group, the mineralization profile was higher and more homogeneously distributed. This conforms with other findings where a lower mineral content was verified in woven bone found in Paget's disease of bone and also in fracture calli (Hoerth et al., 2014; Manjubala et al., 2009; Zimmermann et al., 2015a). These trends towards a lower mineral content with a more homogeneous distribution are also reflected in the MMR obtained by FTIR. Here, a 12% higher MMR was measured in the older cases that was also more homogeneously distributed. This indicates that the mineralization profile may be related to the different structural framework the mineral is located in. The rapidly deposited and disorganized woven bone matrix in the fetal/infantile cases could affect the mineralization period and limit the size of hydroxyapatite crystals. This is in accordance with published data that reported similarly shaped but smaller hydroxyapatite crystals in woven compared to lamellar bone which was linked to the high bone remodeling rate (Su et al., 2003). Generally, the degree of mineralization heterogeneity is considered as a contributor to the mechanical competence of bone as the energy needed for microcrack propagation is lower in homogeneously mineralized tissue (Bala et al., 2012). However, the mineralization heterogeneity is usually assessed in structurally comparable tissues (i.e., secondary remodeled bone). Here, an increasing homogenization is believed detrimental as energy dissipation proceeds less effectively due to fewer interfaces between lowly and highly mineralized bone areas. In this context, the age-dependent relatively more homogenous mineralization pattern in the 2- to 14-year-old cases may be considered advantageous as the origin of the mineral heterogeneity in the fetal/infantile cases is inherently different compared to the aging skeleton. Due to the absence of remodeled osteons in the fetal/infantile cases, the higher heterogeneity can be attributed to the remnants of calcified cartilage that are still incorporated in an otherwise lower mineralized matrix. The calcified cartilage also explains the statistically indifferent peak calcium content (Ca_{peak}) despite the discrepancy in Ca_{mean}.

4.1.3. Development of Mechanical Resistance

The observed changes in bone structure and composition coincide with a distinct change in mechanical demands that occurs between one and two years of age suggesting that both the micro- and nanostructure are modified and adapted in the process. At this time of life children begin to walk, which establishes a new scenario of directional mechanical loading on the femoral diaphysis. The weight bearing increases greatly with the onset of independent walking making efficient adaptation processes of the bone especially important (Boskey and Coleman, 2010; Lynch et al., 2011; Martin and Ishida, 1989; Portigliatti Barbos et al., 1984). This was reflected in the obtained mechanical results. Here, the structural and compositional disparities translate directly into the biomechanical competence where an advancing age was associated with significantly higher strength and stiffness. Conversely, this suggests that the fetal/infantile femur is mechanically weaker than the 2- to 14-yead old cases when using the same basis of assessment for bone quality as in mature bone. This conforms with previous studies that have shown that woven bone is structurally and mechanistically more isotropic but weaker in any loading direction possibly due to the lower degree of mechanical stimuli experienced at this age (García-Rodríguez and Martínez-Reina, 2017; Ip et al., 2016; Shapiro and Wu, 2019; Verbruggen et al., 2018).

Mechanistically, the mechanical behavior by mineral-collagen interaction was evaluated by SAXS/WAXD experiments under simultaneous tensile testing. Here, it was shown that the contribution of the mineral to deformation increases with age while the collagen fibril deformation was similar both study groups. This behavior is possibly influenced by the local mineral content and mineral particle thickness that is reported to be significantly lower in younger children and increasing with age (Fratzl-Zelman et al., 2014). Although differences in the collagen deformation were not detected by SAXS, the preferential CFO is considered to contribute to the mechanical behavior of bone as longitudinally oriented collagen are reported to be better adapted to resist axial tensile loads (Ascenzi and Bonucci, 1967; Ascenzi et al., 2003). However, with the second publication included in this thesis, it has been shown that the collagen fiber organization is linked to specific nano-compositional patterns where longitudinally oriented collagen fibers incorporate more mineral and, hence, facilitate more stiffness (as discussed in chapter 4.2) (Stockhausen et al., 2021). As stiffer materials are better able to resist plastic deformation in uniaxial loading this would suggest that the 2- to

14-year-old cases are better adapted to directional loading in both compression and tension. On the other hand, the fetal/infantile cases with oblique-angled collagen and a lower mineral content would have superior ductility and energy dissipation capabilities. Therefore, it can also be argued that the limited and non-directional mechanical stimulation during fetal development and the first two years of life requires a more isotropic matrix organization that can withstand more random loading scenarios and dissipate more energy.

It is well established that impairment of bone quality proceeds in aging and disease and affects the mechanical resistance and fracture risk (Busse et al., 2013; Carriero et al., 2014; Zimmermann et al., 2011, 2015a). However, high bone fragility is also documented in children indicating that the fracture susceptibility in children might have a different origin. With the present study, it has been shown how bone quality, and, by association, mechanical competence differs in the first two years of life and develops with ongoing skeletal growth (**Figure 12**). This concerns both the bone

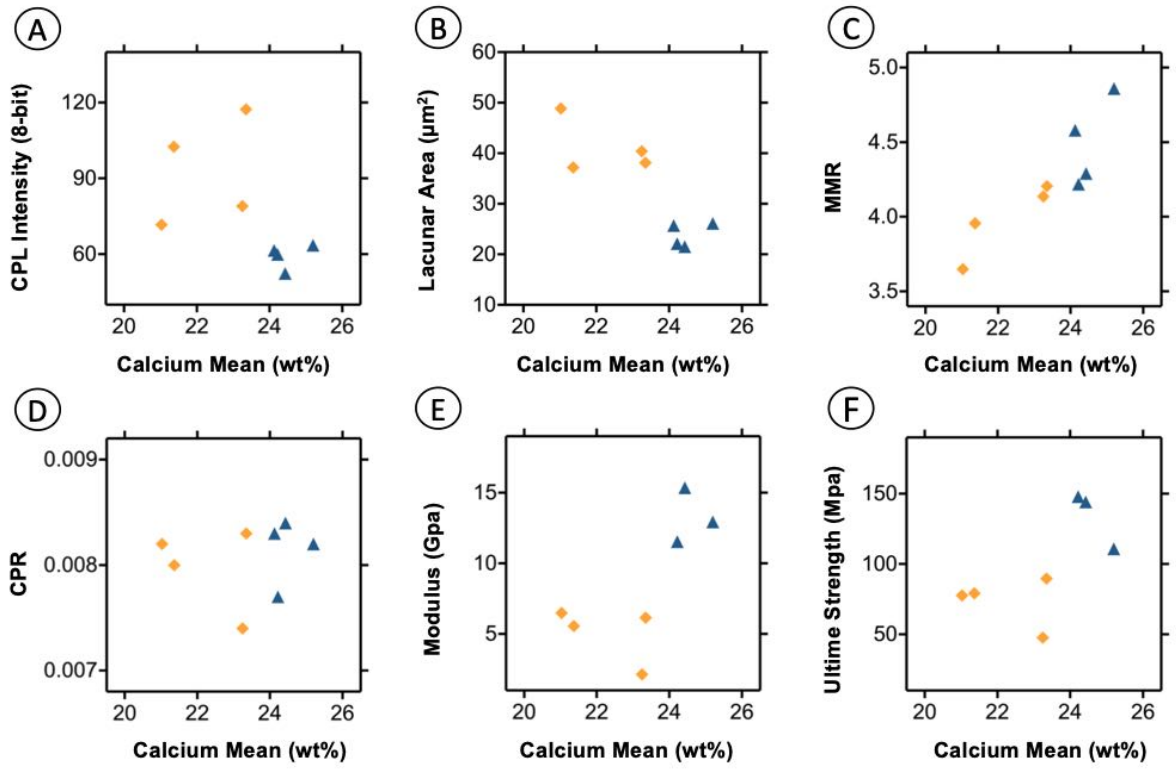

Figure 12: Structural, compositional and mechanical bone quality parameters during skeletal growth as a function of mineral content. A higher mineral content in the 2- to 14-years old cases is associated with (A) more longitudinally oriented collagen and (B) smaller osteocyte lacunae. (C, D) The mineral-to-matrix ratio showed a positive correlation with the calcium content whereas the carbonate-to-phosphate ratio was similar in both groups. (E, F) The changes in collagen fiber orientation and calcium content translate to a higher elastic modulus and ultimate strength with ongoing age.

volume fraction and the absence of microstructural features in woven bone (i.e., lamellar interfaces and cement lines) that diminish the ability to deflect or bridge cracks (Fantner et al., 2005; Koester et al., 2008; Nalla et al., 2003; Zimmermann and Ritchie, 2015; Zimmermann et al., 2015a) but also the collagen orientation and mineralization profile. The obtained results suggest that the less organized woven bone formed by endochondral ossification is mechanically weaker than secondary remodeled osteonal bone. Specifically, the changes in mechanical behavior on small length scales during skeletal growth is largely guided by changes in the preferential CFO that are coupled to specific mineralization patterns.

4.2. Localized Matrix Adaptations: The Presence of *Dark* and *Bright* Osteons

With the previous study, it has been established that femoral bone undergoes extensive structural and compositional changes during skeletal development in which the mechanical competence is adapted. The fetal/infantile femoral mid-diaphysis presents a woven bone structure that is characterized by a lower mineral content and a higher fraction of transversely oriented collagen fibers. With ongoing skeletal development, the structural adaption continues, and the entire femoral cross-section becomes dominated by secondary remodeled osteons with a higher mineral content and more longitudinally oriented collagen fibers. This structural arrangement is maintained from adolescence into old age. While the osteon long axis is generally aligned with the long axis of the femur, the orientation of collagen fibers within individual lamellae can differ substantially. Here, *dark* and *bright* osteons present the two extreme cases that differ fundamentally in their nanostructural arrangement. The tissue heterogeneity in terms of *dark* and *bright* osteons indicates the ability of the cortical bone matrix to locally adapt its structure in functional interaction with its composition.

4.2.1. Structural Heterogeneity of Secondary Osteons

The presence of *dark* and *bright* osteons is well recognized and has drawn interest in the past (Ascenzi and Bonucci, 1967, 1968; Boyde et al., 1984; Martin and Ishida, 1989; Mason et al., 1995). Due to the birefringent properties of optically anisotropic collagen type I, CPL has been used for decades to visualize changes in CFO and postulate models of lamellar organization in cortical bone (chapter 1.5).

However, most studies concerned with the structure of lamellar cortical bone either selected osteons without pre-characterization under CPL or assessed CPL brightness without characterization of compositional and mechanical properties (Ascenzi et al., 2003; Giraud-Guille, 1988; Grandfield et al., 2018; Reznikov et al., 2014). In a similarly focused study, *dark* and *bright* osteons were isolated and structurally analyzed using synchrotron x-ray diffraction and confocal microscopy (Ascenzi et al., 2003). Here, it was found that *dark* osteons are structurally homogeneous with collagen fibers being preferentially aligned with the long axis of the osteon whereas *bright* osteons contain collagen fibers oriented bidirectionally at ±45° with respect to the osteon axis. In our study, a combination of CPL, synchrotron nano-computed tomography and FIB-SEM imaging was used to discern the nanostructural arrangement of *dark* and *bright* osteons in 2D, 3D and at high resolution. Using synchrotron nano-computed tomography, *dark* osteons were characterized as structurally homogeneous with preferentially longitudinally oriented collagen fibers and no evident boundary between neighboring lamellae. This was confirmed in different imaging planes: transversely viewed from the top using qBEI imaging and in radial-longitudinal orientation by FIB-SEM imaging. As the lamellar interface in osteonal bone is thought to inhibit crack growth by crack deflection/bridging increasing the toughness (Yeni and Norman, 2000), the absence of lamellar boundaries in *dark* osteons could impair their toughening mechanism at this level of hierarchy. The structural arrangement is inherently different in *bright* osteons where a distinct lamellar pattern with changing CFO between neighboring lamellae is present. In 2D qBEI images, lamellae appear approximately 6µm thick, but nano-computed tomography and FIB-SEM imaging reveal sub-lamellae with varying thickness of 3.42 ± 0.55 µm and 1.79 ± 0.27 µm that compose a repeating lamellar unit. Organizational motifs in secondary osteons have been reported before (Gebhardt, 1905; Giraud-Guille, 1988; Marotti, 1993; Reid, 1986; Reznikov et al., 2014). Here, sub-lamellar structures with changing CFO have also been documented. Notably, Reid *et al.* used scanning electron microscopy on human femoral bone samples that were etched by chick osteoclasts to expose the underlying collagen organization (Reid, 1986). Here, they found that the thickness of sub-lamellar units is not uniform but is associated with the orientation of collagen fibers. Specifically, they found lamellae composed of transversely oriented collagen to be thinner compared to lamellae with longitudinal CFO. This conforms with our findings as we

also found transversely fibered lamellae to be significantly thinner compared to longitudinally fibered lamellae. However, they also noted the wide range of appearances of osteonal bone, including the absence of lamellae in areas composed of longitudinal fibers. More recently, Reznikov *et al.* used a dual beam microscope to visualize the hierarchical organization of lamellar bone and reported different structural motifs (Reznikov et al., 2014). Firstly, an ordered motif where the collagen fibrils are aligned with respect to each other, which can occur in two preferred orientations, either within 10-20° of the femur long axis (“high angle”) or orthogonal to the femur long axis (“low angle”). Secondly, a disordered motif where collagen fibrils show little preferred orientation and poor alignment within the lamella. In our study, we also found “high angle” and “low angle” motifs but could not confirm the existence of the disordered motif. Following the definition of Reznikov *et al.* and applying it to our findings suggests that *dark* osteons are built in its entirety from “high angle” lamellar motifs with the collagen fiber orientation being preferentially aligned with the long axis. In comparison, *bright osteons* alternatingly contain “high angle” and “low angle” sub-lamellae that also differ in their lamellar thickness. Images obtained by high-angle annular darkfield scanning transmission electron microscopy of osteonal FIB sections have also revealed lamellae with fibrils in parallel with the osteon axis which are bordered by lamellae with perpendicular collagen fiber orientation (Grandfield et al., 2018). Consistent with our findings, the change in collagen fiber orientation between neighboring lamellae is not continuous but rather abrupt. In addition, they have also reported a disordered zone with randomly oriented collagen fibers. The absence of the disordered motif in our studied cohort of *dark* and *bright* osteons might be explained by the selection of the osteons themselves. The osteons in the above-mentioned studies were selected randomly with no pre-characterization under polarized light. Therefore, it remains unknown which group of osteons (e.g., *dark* or *bright*) the analyzed specimens belong to. While disordered motifs were ascertained in osteons selected with no prior characterization of their collagen fiber orientation by CPL microscopy, we have focused on *dark* and *bright* osteons that lie on opposite sides of the collagen orientation spectrum.

The change in collagen orientation is also implied by the detected differences in osteocyte characteristics. As it is commonly accepted that osteoblasts are aligned with the collagen fibers they synthesize during the formation phase (Jones et al., 1975), the

long axis of the osteocyte lacunae is aligned with the CFO (Kerschnitzki et al., 2011; Marotti, 1979). In our study, smaller and rounder cross-sectioned osteocyte lacunae were verified in *dark* osteons indicating that the long axis of the lacunae is oriented in parallel with the long axis of the osteon (considering the section plane to be perpendicular to the osteon long axis, but not to the CFO). Contrarily, the elongated shape with larger lacunar area in *bright* osteons suggests that osteocyte lacunae are more transversely oriented. In sum, it has been shown that the observed differences in CPL intensity reflect fundamental structural discrepancies at the nanometer scale in terms of the predominant CFO between different osteons within the same individual.

4.2.2. Coupling of Structural Variations and Nano-Compositional Patterns

In general, heterogeneity in the mineralization profile of secondary remodeled bone is considered advantageous for crack deflection due to an elastic mismatch between higher- and lower-mineralized bone volumes (Zimmermann et al., 2015b). Usually, a heterogeneous mineralization is maintained through remodeling process where newly formed osteons are relatively lower mineralized. During the formation phase of bone, the matrix is mineralized by successive steps that define the compositional properties of individual osteons (Meunier and Boivin, 1997). Following the synthesis of the organic, collagenous framework of the matrix, osteons undergo two distinct mineralization steps. During primary mineralization the bone matrix is rapidly mineralized to reach 50-70% of its maximum mineral content, followed by a secondary mineralization that progresses over an extended period of time (Bala et al., 2012; Ruffoni et al., 2007). As bone remodeling events occur asynchronous and spatially separated, cortical bone has a heterogeneous mineralization profile, and the most advanced secondary osteons are characterized by the highest mineral content (Bala et al., 2010; Currey, 2002). Therefore, a higher mean calcium content as assessed by qBEI is usually considered to indicate a higher tissue age and maturation (Busse et al., 2013; Grynpas, 1993; Schmidt et al., 2019). In our study, a higher mineral content was validated in *dark* osteons with longitudinal collagen fibers demonstrating a connection between the CFO and degree of mineralization. Following the line of argumentation laid out above, the higher mineral content would imply that *dark* osteons are on average older and more mature compared to *bright* osteons. However, this seems improbable as this would require a structural reorganization of the collagenous

scaffold from lamellar and oblique-angled to homogeneous and longitudinal over time. As of now, no evidence exists that bone is able to undergo such extensive structural adaptions that are not part of the remodeling cycle and, hence, involve prior resorption. Therefore, the presented qBEI data for *dark* and *bright* osteons indicates that additional matrix heterogeneity exists also between fully remodeled osteons that goes beyond the heterogeneity generated during bone remodeling processes. In line with the greater mean and peak calcium content as quantified by qBEI, a higher MMR was measured by FTIR. Here, a positive correlation between the MMR and both the mean and peak mineral content underlines that *dark* osteons indeed contain more mineral. The CPR was also found to be significantly higher in *dark* osteons compared to *bright* osteons, presenting a positive correlation with the mean and peak mineral content as well. Previous studies have established that the MMR and CPR increase with ongoing age (Boskey and Imbert, 2017; McCreadie et al., 2015) and that the highest CPRs are measured in the oldest tissue volumes regardless of the developmental age (Boskey et al., 2016; Gourion-Arsiquaud et al., 2009; Paschalis et al., 1997). Accordingly, higher ratios of MMR and CPR would suggest again that *dark* osteons are older than *bright* osteons which is improbable due to the required structural reorganization over time, as discussed above. However, it is also possible for bone to adapt for a very specific mechanical function as, for example, observed in auditory ossicles of sperm whales (Schmidt et al., 2018). In their study, it has been shown that the extent of carbonate substitution for phosphorus may reflect differences in the mineralization speed and/or secondary hypermineralization for mechanical purposes. Following this interpretation, a higher CPR in *dark* osteons would suggest an accelerated mineralization as a functional adaption to serve a specific biomechanical purpose. As the biomechanical competence of cortical bone is closely linked to the density and quality of the mineral phase (Donnelly et al., 2010; Landis et al., 1995; Rho et al., 2002), it can be surmised that the revealed mineralization disparities between *dark* and *bright* osteons are related to the structural collagenous framework the mineral is located in (**Figure 13**). Therefore, it can be reasoned that *dark* and *bright* osteons play a practical role in providing biomechanical competence and that the higher mineralization of *dark* osteons is not a consequence of tissue aging.

4.2.3. The Mechanical Relevance of *Dark* and *Bright* Osteons

The biomechanical significance of both osteon types was verified by nanoindentation testing where the variational mineral content was reflected in the measured elastic moduli and hardness. Both parameters were significantly higher in *dark* osteons underlining their functional adaption to mechanical loads. Specifically, the higher elastic modulus translates into a high stiffness and an improved ability to withstand high loads before elastic deformation takes place, whereas the higher hardness reveals an improved resistance to plastic deformation. This clearly shows that *dark* osteons are more rigid structures compared to *bright* osteons. *Vice versa*, *bright* osteons are able to undergo more elastic deformation and return to their initial state when the load is removed. Moreover, the lower hardness is reflective of a more ductile structure that can sustain more plastic deformation. In the literature, the material properties of cortical bone have been studied in the past using different analytical techniques. In studies that utilized indentation testing, a high variability and heterogeneity in both hardness and elastic moduli were reported at different anatomical sites, but also within individual femoral cross-sections (Hoc et al., 2006; Hoffler et al., 2000; Rho et al., 1997; Turner et al., 1999; Zysset et al., 1999). In this context, our results of osteonal heterogeneity offer a new perspective on the reported values. When indentation testing on cortical bone is performed, the material properties are usually obtained in the longitudinal or transverse plane of the specimen, and the preferential CFP is either assumed to run parallel to the long axis of the bone or is entirely neglected. Therefore, localized structural heterogeneities are generally not accounted for and the obtained results can fluctuate considerably. These variations have been ascribed to underlying changes in the cortical microstructure, collagen fibril orientation and differences in the local mineral content generated by bone remodeling processes (Franzoso and Zysset, 2009). Extending these findings, we have shown that further variations also exist between fully remodeled and matured osteons providing an additional level of compositional and mechanical heterogeneity. This agrees with a previous study that has applied nanoindentation testing to investigate variations in elastic moduli within individual osteons and reported the presence of a structural anisotropy supporting the view that changes in CFO occur between neighboring lamellae (Faingold et al., 2012). Despite all lamellae having similar elastic moduli on average, they highlighted the relatively large standard deviations for the elastic moduli

measured within single lamellae that reflect local fluctuations in mechanical properties. Moreover, they measured a 30% higher elastic modulus in the lamellae closest to the Haversian canal. As a ring of elevated MMR towards the center of the Haversian canal was confirmed both in *dark* and *bright* osteons in the context of this thesis, the origin of these variations can be traced back to fundamental structural disparities that are linked to specific nano-compositional patterns. In view of these considerable differences in mechanical properties, it is suggested that future studies should ideally thoroughly pre-characterize the local collagen fiber orientation and mineral profile before commencing with indentation testing.

By generating finite element models of mineral-coated collagen fibers, osteonal lamellae and entire osteons starting from the basic building block of the bone matrix (mineralized collagen fibrils), the mechanical behavior was predicated at different length scales dependent on structural variations arising from the nanoscale. Here, two key conclusions could be derived. Firstly, on the lamellar level, the results of the FEM

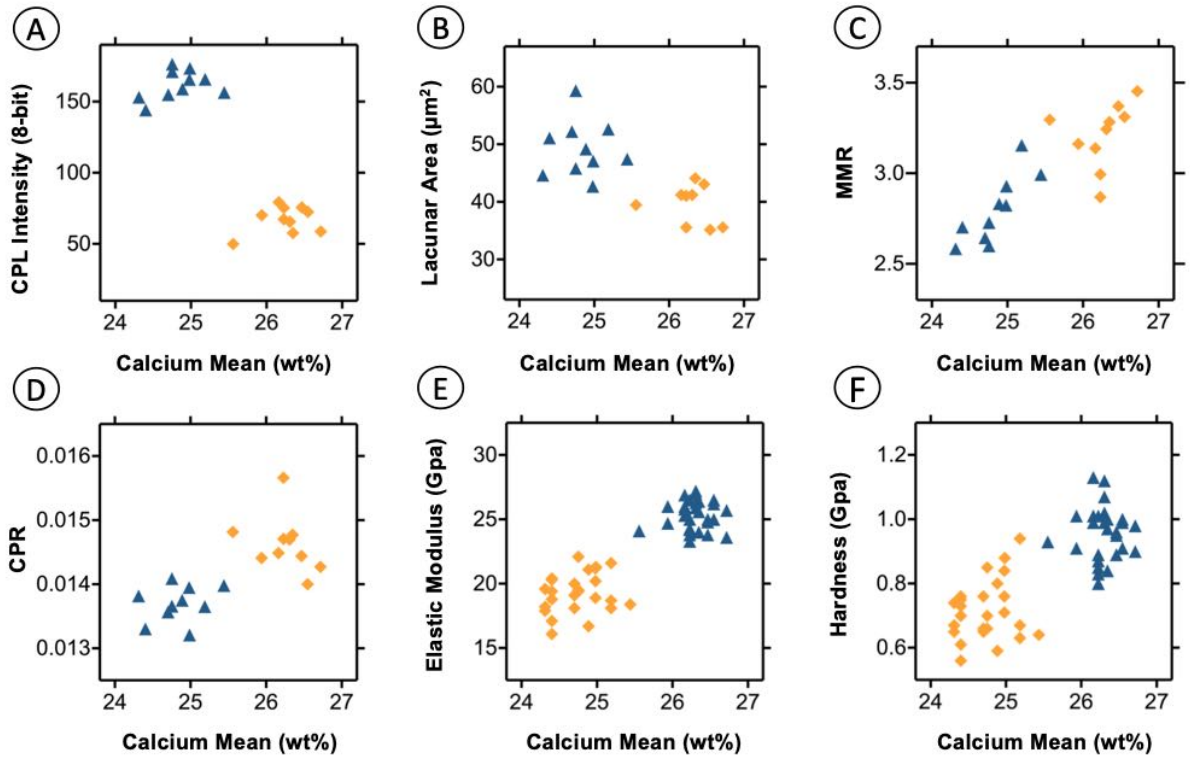

Figure 13: Structural, compositional and mechanical bone quality parameters in *dark* and *bright* osteons as a function of mineral content. (A, B) Longitudinally fibered *dark* osteons are higher mineralized and contain smaller osteocyte lacunae. (C, D) The mineral-to-matrix ratio and carbonate-to-phosphate are positively correlated with the mean calcium content. (E, F) The mechanical properties are guided by the contrasting nanostructural arrangements and mineralization profiles, and both the elastic modulus hardness proportionally increase with increasing mineral content.

models are in accordance with the elastic moduli experimentally measured by nanoindentation for *dark* and *bright* osteons, respectively. This shows that the bottom-up and multi-scale modeling approach from bone's basic matrix constituents is a capable tool to predict the mechanical properties when accounting for shifts in collagen fiber orientation. Due to the hierarchical assembly of bone, the results from the lamellar level translate to the overlying hierarchical levels, where the lamellar CFO plays a key role for the osteonal mechanical properties providing *dark* osteons with a 14.38% higher effective modulus compared to *bright* osteons. In view of these results, it can be recognized that the nanoscale CFO indeed has biomechanical consequences at larger length scales, where more rigid *dark* osteons act as a stiff matrix constituent while more ductile *bright* osteons serve as an energy dissipation and damping matrix element.

4.2.4. New Perspectives on Strain-Mode Specific Matrix Adaptations

It is widely accepted that *dark* osteons occupy volumes that are subjected to tensile loads whereas *bright* osteons are located in volumes that are under compression. This interpretation was initially put forward by Gebhardt *et al.* based on observations from a macroscopic mechanical model built from elastic brass or steel wires representing oriented collagen patterns (Gebhardt, 1905), and tested in later studies where *dark* osteons were reported to have higher tensile strength and a higher modulus of elasticity and *bright* osteons to have higher ultimate compressive strength (Ascenzi and Bonucci, 1967, 1968). The coincident distribution density of *dark* and *bright* osteons in regions under tension and compression, respectively, was also observed in other studies (Bromage et al., 2003; Mason et al., 1995; Portigliatti Barbos et al., 1984; Skedros et al., 1996). However, our results indicate a different structural response to the mechanical stimuli the femur experiences that stands in contrast to the established view. In view of the revealed coupling of structural and compositional properties (**Figure 13**), an alternative view on the formation of *dark* and *bright* osteons in the diaphyseal femur is proposed: We believe that longitudinally fibered *dark* osteons, that contain more mineral and have a higher rigidity, are built in volumes that required more stiffness for biomechanical reasons. As stiffer materials are better able to resist deformation when exposed to uniaxial loads, *dark* osteons might be favored in volumes that are loaded in either compression or tension, rather than just tension.

Conversely, *bright* osteons with more oblique-angled collagen fibers and a lower mineral content might be advantageous in regions that experience some bending stresses (while still being mainly loaded in compression) as they provide more flexibility and a superior capability to absorb and dissipate energy. Interestingly, this in line with observations of collagen fiber orientation in the ovine calcaneal shaft where, contrary to previous findings, areas of bone experiencing significant compression had longitudinally oriented collagen fibers (McMahon et al., 1995). This is in agreement with our interpretation as well as previous findings that noted that bone with longitudinal collagen fiber orientation was stiffer both in tension and compression (Riggs et al., 1993b).

Matrix heterogeneity at the nano- and micrometer length scale of bone are, to a certain extent, deemed beneficial for the mechanical competence of bone at higher level of hierarchy (Boivin et al., 2000; Donnelly et al., 2012; Milovanovic et al., 2018; Seref-Ferlengez et al., 2015). Several studies have reported that the heterogeneity in material properties is lowered when comparing fracture and non-fracture cohorts, including the carbonate-to-phosphate ratio (Wang et al., 2016), collagen maturity (Donnelly et al., 2012) and the mineral distribution (Roschger et al., 2008). Further contributors to tissue heterogeneity, also acting as toughening mechanisms, include the mineralization profile of individual osteons (Wittig et al., 2019), the higher mineralization and accumulation of cross-links in interstitial bone (Schmidt et al., 2017) and the stiffness mismatch occurring at hypermineralized cement lines (Milovanovic et al., 2018). In health, mechanosensitive osteocytes act in response to mechanical stimuli and initiate continuous bone remodeling cycles in which damaged bone is replaced by new bone, that becomes mineralized over time. In this process, microcracks are timely and efficiently removed, bone is adapted to new mechanical demands and a constant tissue heterogeneity is preserved for increased fracture toughness (Phelps et al., 2000; Seref-Ferlengez et al., 2015). While matrix heterogeneity is usually related to structural features that all osteons, including *dark* and *bright* osteons, have in common (i.e., cement lines) or to mineralization heterogeneity as a result of bone remodeling, our results suggest that it also applies to the organic structural framework. We demonstrated that bone is able to modulate its nanostructural arrangement together with its compositional properties, potentially

adding another layer of matrix heterogeneity that limits the growth and propagation of microcracks.

The process of bone remodeling is highly complex and requires a delicate equilibrium between bone-resorbing osteoclasts and bone-forming osteoblasts (Eriksen, 2010). It depends on the viability of osteocytes and their interconnectedness through canaliculi (Milovanovic et al., 2013). However, osteoclasts have been reported to resorb cortical bone non-randomly and to preferentially target osteons with specific compositional and mechanical characteristics (Pernelle et al., 2017). Specifically, it has been shown that osteons with a lower degree of mineralization, a higher CPR and both lower elastic modulus and hardness are preferentially resorbed by osteoclasts. The nanostructural heterogeneity between *dark* and *bright* osteons could therefore serve a further purpose, in addition to locally providing stiffness and ductility. Linking these results to our findings implicates that *dark* osteons with longitudinally CFO and a greater mineral content are deemed more beneficial in specific loading modes and less likely to be resorbed by osteoclasts. Interestingly, the effect of dissimilar cortical microstructure on the remodeling activity has been noted in the equine radius, where the caudal cortex, dominated by *bright* osteons, showed significantly more remodeling events than the cranial cortex, characterized by more *dark* osteons (Riggs et al., 1993b). At this point, it should be noted that the mechanisms discussed above apply to non-targeted, stochastic remodeling activity. However, a second mode of remodeling exists that operates target oriented (Eriksen, 2010; Parfitt, 2002). While the stochastic remodeling acts to prevent bone quality impairment as result of aging, targeted remodeling operates to remove micro-damaged bone. Here, the structural and compositional heterogeneity between *dark* and *bright* osteons could also enhance the ability to detect microdamage. The path and length of initiated cracks is in particular guided by the extrinsic toughening mechanisms of cortical bone (chapter 1.4) and takes the direction of lowest resistance (Zimmermann et al., 2015b). In a compositionally heterogeneous matrix with more interfaces of elastic mismatches (i.e., *dark* and *bright* osteons), the crack is deflected more often, effectively elongating the total crack path. Hence, as deformation can spread out over greater distances due to the heterogeneity of the bone matrix, osteocytes might be able to detect damage more quickly and initiate repair processes more promptly (Klein-Nulend et al., 2012, 2013; Milovanovic et al., 2013; Tai et al., 2007).

5. Summary and Conclusion

With the work presented in this dissertation, it was shown that the functional adaption of the bone matrix begins with fetal development and proceeds throughout life to advance bone strength and ensure high fracture resistance to mechanical activity. At early stages of skeletal development, new bone is rapidly formed as reflected by the high amounts of osteoid present. With ongoing aging, a densification of the cortex is observed that is accompanied by reorganization of the microstructural appearance where less organized woven bone is continuously replaced by highly organized secondary remodeled osteonal bone. The distinct changes in composition and mechanical competence that go along with the structural reorganization during ossification, modeling, and remodeling processes reflect the adaptive capabilities of bone and deepen our understanding of how bone quality develops during skeletal growth. It was shown that bone quality in children less than 2-years old is inherently lower compared to healthy adolescents and adults when using the same criteria of bone quality assessment. Specifically, the matrix is more porous, scaffold-like and structurally less organized. Moreover, a higher fraction of transversely oriented collagen fibers is present in the fetal to 1-year old cases, accompanied by a lower mineral content and more heterogeneous mineral distribution. The micro- and nanostructural adaption also shows in the mechanical properties. A significantly lower modulus and ultimate strength reflect an inferior ability to resist mechanical loading before fracturing. In the age span from one to two years, the matrix is extensively remodeled providing a stiffer matrix and greater resistance to plastic deformation. In this remodeling process, the collagen fibrils are re-organized and shifted towards a more longitudinal orientation. Traditionally, this would be explained by a better resistance to tensile forces. However, in view of the results obtained from *dark* and *bright* osteons in the adult skeleton, it can also be argued that the changes in CFO and mineral distribution constitute to more stiffness, and better resistance to both tension and compression. This temporally coincides with the transition from crawling to walking where the biomechanical stimulation becomes more unidirectional, creating new mechanical demands for the mid-diaphyseal femur.

In healthy adult human bone, effective fracture resistance mechanisms have developed at all levels of hierarchy that enable bone to withstand complex loading

pattern that go along with an active lifestyle. The new findings presented in this thesis suggest that *dark* and *bright* osteons might serve as an additional fracture resistance mechanism that locally provide the matrix with more stiffness or ductility where needed. Here, the role of *dark* and *bright* osteons was re-interpreted by revealing a functional relationship between the collagen fiber arrangement and specific nano-compositional patterns that guide the biomechanical competence. It was commonly accepted that a higher distribution density of *dark* osteons is found in regions of tensile stress while more *bright* osteons are located in regions under compression. However, the presented results point at a more profound mechanical function of both osteon types and suggest that the microstructure is sensitive to localized and individual adaptation. Whereas structurally homogeneous *dark* osteons with longitudinal CFO and a higher degree of mineralization provide better resistance to elastic and plastic deformation in both tension and compression, *bright* osteons with more oblique-angled fibers and a lamellar pattern provide more ductility where needed.

In summary, this thesis aimed to elucidate the relationship between CFO and the matrix composition in human bone (**Figure 14**). Here, a distinct coupling of nanostructural arrangements and compositional patterns was revealed. During skeletal growth and in mature bone, bone matrix arrangements with more transversely oriented collagen fibers are associated with a lower degree of mineralization that translates to lower tissue moduli and could provide better energy dissipation capabilities. In contrast, longitudinally oriented collagen fibers are linked to a relatively higher mineral content and higher stiffness underlining that the bone matrix is sensitive

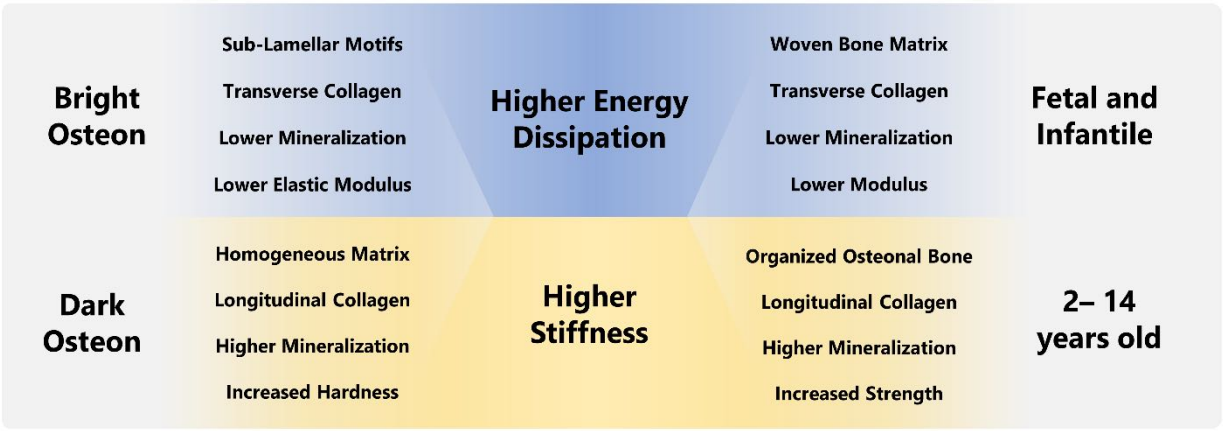

Figure 14: Distinct matrix characteristics were revealed in the developing and mature skeleton that underline the adaptive capabilities of bone. The preferential collagen fiber orientation is coupled with specific compositional patterns that guide the mechanical properties.

and capable to adapt its structure and composition at the smallest length scale. Both studies contribute to a deeper understanding of how nanostructural variations of the collagen phase guide the mechanical behavior of bone.

6. Outlook

In the two publications included in this thesis, important bone matrix characteristics at different length scales were evaluated to provide a new view on the structure-composition relationship in both the developing skeleton and mature bone. This research was carried out on healthy bone and cases with known bone pathologies were excluded. Hence, the results represent the state the human skeleton evolved into and that was regarded as beneficial. Consequently, the influences of aging and diseases on bone quality are not elucidated. As a higher risk of fractures is associated with the aging skeleton as well as numerous genetic disorders and metabolic diseases, the potential for future studies is given. Even though most conditions, both in children and adults, can be reliably diagnosed and treated better with progressing advancements of the health care system, the underlying mechanisms leading to increased fragility are often not fully understood. Of special interest would be pathologies characterized by a high fracture incidence with no apparent differences in BMD (e.g., type 2 diabetes mellitus) to assess if potential compositional deviations are also reflected in the nano- and micro-structural arrangement.

To better understand bone quality impairment in aging and disease, *dark* and *bright* osteons are excellent test objects due to their distinct nanostructure and composition that make inter-individual comparison promising. By focusing on *dark* and *bright* osteons, the underlying structural framework is established, and the emphasis can be placed on other important bone quality parameters. Specifically, the age- and disease-dependent mineralization profile (including MMR and CPR) and non-enzymatic cross-linking profile of the collagenous matrix could provide valuable insight into the mechanisms underlying the increased fragility in age and disease.

As regions dominated by *bright* osteons showed significantly more remodeling events compared to regions characterized by *dark* osteons (Riggs et al., 1993b), this could be indicative for the fact that the spatial interconnectedness and organization of the lacuna-canalicular network could differ between *dark* and *bright* osteons. Here, nano-tomographic scans of larger volumes of interest could be used to provide three-

dimensional data with nanometer-resolution to assess the integrity of the cellular network. Previous studies have established that the spatial organization of the collagen matrix is linked to the organization of the lacuno-canalicular network (Repp et al., 2017). However, this was only investigated for alternating osteons with an apparent lamellar structure. To this end, future studies could extend these findings and deepen the understanding of the cellular network that is essential for bone health. In this context, the ability to initiate bone remodeling processes in response to mechanical stimuli is also impaired with age and in disease which further underlines the importance of the lacuno-canalicular network (Wu et al., 2011). The reasons for this are diverse and are also linked to reduced cellular communication following osteocyte apoptosis (Busse et al., 2010; Milovanovic et al., 2013). As significantly more mineralized osteocyte lacunae, as a sign of osteocyte apoptosis, are reported with aging and osteoporosis (Milovanovic et al., 2015) raises the question whether certain volumes with distinct compositional patterns are more susceptible to cell death. In this regard, an evaluation of the mechanosensation and transduction potential of osteocytes located in structurally and compositionally different matrices could provide valuable information on the ability of bone tissue to adapt to mechanical loading. Osteocytes play a vital role for the maintenance of bone strength by detecting matrix strains, initiating modeling and remodeling processes and regulating mineral homeostasis and mineralization. As both osteoblasts and osteoclasts are orchestrated by osteocytes, an impairment of the osteocyte network would be expected to affect the overall cellular activity (Hemmatian et al., 2017). Therefore, the activity of osteoblast and osteoclast activity could also be addressed in future studies to scrutinize the underlying mechanisms leading to healthy and mechanically strong bone.

Bone obtains its toughness by various mechanisms that operate at different length scales. These include sliding mechanisms between mineralized collagen fibrils as well as crack deflection at hypermineralized cement lines and energy dissipation at lamellar interfaces in osteons. In health, microcracks are also initiated in response to loading activity but their propagation is guided by the toughening mechanisms to prevent crack growth that could potentially result in clinically relevant fractures. However, so far, it remains unknown how specific nanostructural arrangements with different compositional and mechanical properties affect the crack growth behavior. In future studies, a combination of synchrotron nano-computed tomography and *in situ*

nanoindentation could be used to initiate cracks at the nanoscale and visualize their propagation depending on the underlying nanostructural arrangement.

7. Abbreviations and Terminology

BMDD	Bone Mineral Density Distribution
BV/TV	Bone Volume to Tissue Volume Ratio
Ca_{Mean}	Mean Calcium Content
Ca_{Peak}	Peak Calcium Content
CFO	Collagen Fiber Orientation
CPL	Circularly Polarized Light Microscopy
CPR	Carbonate to Phosphate Ratio
DXA	Dual-Energy X-ray Absorptiometry
FTIR	Fourier Transform Infrared Spectroscopy
FIB-SEM	Focused Ion Beam - Scanning Electron Microscopy
MMR	Mineral to Matrix Ratio
N.Ot.Lc/B.Ar	Number of Osteocyte Lacunae per Bone Area
OS/BS	Osteoid Surface per Bone Surface
Ot.Lc.Ar	Osteocyte Lacunar Area
O.Th	Osteoid Thickness
qBEI	Quantitative Backscattered Electron Imaging
RVE	Representative Volume Elements
SAXS	Small Angle X-Ray Scattering
WAXD	Wide Angle X-Ray Diffraction
Wt%	Weight percent

8. References

Alexiou, K.I., Roushias, A., Varitimidis, S.E., and Malizos, K.N. (2018). Quality of life and psychological consequences in elderly patients after a hip fracture: a review. Clin. Interv. Aging *13*, 143–150.

Ascenzi, A. (1988). The micromechanics versus the macromechanics of cortical bone - A comprehensive presentation. J. Biomech. Eng. *110*, 357–363.

Ascenzi, A., and Bonucci, E. (1967). The tensile properties of single osteons. Anat. Rec. *158*, 375–386.

Ascenzi, A., and Bonucci, E. (1968). The compressive properties of single osteons. Anat. Rec. *161*, 377–391.

Ascenzi, M.G., Ascenzi, A., Benvenuti, A., Burghammer, M., Panzavolta, S., and Bigi, A. (2003). Structural differences between “dark” and “bright” isolated human osteonic lamellae. J. Struct. Biol. *141*, 22–33.

Bacabac, R.G., Mizuno, D., Schmidt, C.F., MacKintosh, F.C., Van Loon, J.J.W.A., Klein-Nulend, J., and Smit, T.H. (2008). Round versus flat: Bone cell morphology, elasticity, and mechanosensing. J. Biomech. *41*, 1590–1598.

Bailey, D.A., Wedge, J.H., McCulloch, R.G., Martin, A.D., and Bernhardson, S.C. (1989). Epidemiology of fractures of the distal end of the radius in children as associated with growth. J. Bone Joint Surg. Am. *71*, 1225–1231.

Bala, Y., Farlay, D., Delmas, P.D., Meunier, P.J., and Boivin, G. (2010). Time sequence of secondary mineralization and microhardness in cortical and cancellous bone from ewes. Bone *46*, 1204–1212.

Bala, Y., Farlay, D., and Boivin, G. (2012). Bone mineralization: from tissue to crystal in normal and pathological contexts. Osteoporos. Int. *24*, 2154–2166.

Bergmann, G., Siraky, J., Rohlmann, A., and Koelbel, R. (1984). A comparison of hip joint forces in sheep, dog and man. J. Biomech. *17*, 907—921.

Berteau, J.-P., Gineyts, E., Pithioux, M., Baron, C., Boivin, G., Lasaygues, P., Chabrand, P., and Follet, H. (2015). Ratio between mature and immature enzymatic cross-links correlates with post-yield cortical bone behavior: An insight into greenstick fractures of the child fibula. Bone *79*, 190–195.

Boivin, G., Bala, Y., Doublier, A., Farlay, D., Ste-Marie, L.G., Meunier, P.J., and Delmas, P.D. (2008). The role of mineralization and organic matrix in the microhardness of bone tissue from controls and osteoporotic patients. Bone *43*, 532–538.

Boivin, G.Y., Chavassieux, P.M., Santora, A.C., Yates, J., and Meunier, P.J. (2000). Alendronate increases bone strength by increasing the mean degree of mineralization of bone tissue in osteoporotic women. Bone *27*, 687–694.

Bortel, E.L., Duda, G.N., Mundlos, S., Willie, B.M., Fratzl, P., and Zaslansky, P. (2015). Long bone maturation is driven by pore closing: A quantitative tomography investigation of structural formation in young C57BL/6 mice. Acta Biomater. *22*, 92–102.

Boskey, A., and Coleman, R. (2010). Aging and Bone. J. Dent. Res. *89*, 1333–1348.

Boskey, A., and Pleshko Camacho, N. (2007). FT-IR imaging of native and tissue-engineered bone and cartilage. Biomaterials *28*, 2465–2478.

Boskey, A.L., and Imbert, L. (2017). Bone quality changes associated with aging and disease: a review. Ann. N. Y. Acad. Sci. *1410*, 93–106.

Boskey, A.L., Donnelly, E., Boskey, E., Spevak, L., Ma, Y., Zhang, W., Lappe, J., and Recker, R.R. (2016). Examining the Relationships between Bone Tissue Composition, Compositional Heterogeneity, and Fragility Fracture: A Matched Case-Controlled FTIRI Study. J. Bone Miner. Res. *31*, 1070–1081.

Boyce, A.M., and Gafni, R.I. (2011). Approach to the child with fractures. J. Clin. Endocrinol. Metab. *96*, 1943–1952.

Boyde, A., and Riggs, C.M. (1990). The quantitative study of the orientation of collagen in compact bone slices. Bone *11*, 35–39.

Boyde, A., Bianco, P., Portigliatti Barbos, M., and Ascenzi, A. (1984). Collagen orientation in compact bone: I. A new method for the determination of the proportion of collagen parallel to the plane of compact bone sections. Metab. Bone Dis. Relat. Res. *5*, 299–307.

Bromage, T.G., Goldman, H.M., McFarlin, S.C., Warshaw, J., Boyde, A., and Riggs, C.M. (2003). Circularly polarized light standards for investigations of collagen fiber orientation in bone. Anat. Rec. B. New Anat. *274*, 157–168.

Buckwalter, J.A., Glimcher, M.J., Cooper, R.R., and Recker, R. (1995). Bone Biology. J. Bone Jt. Surg. *77*, 1276–1289.

Buenzli, P.R., and Sims, N.A. (2015). Quantifying the osteocyte network in the human skeleton. Bone *75*, 144–150.

Busse, B., Djonic, D., Milovanovic, P., Hahn, M., Püschel, K., Ritchie, R.O., Djuric, M., and Amling, M. (2010). Decrease in the osteocyte lacunar density accompanied by hypermineralized lacunar occlusion reveals failure and delay of remodeling in aged human bone. Aging Cell *9*, 1065–1075.

Busse, B., Bale, H.A., Zimmermann, E.A., Panganiban, B., Barth, H.D., Carriero, A., Vettorazzi, E., Zustin, J., Hahn, M., Ager, J.W., et al. (2013). Vitamin D deficiency induces early signs of aging in human bone, increasing the risk of fracture. Sci. Transl. Med. *5*, 188–193.

Carriero, A., Zimmermann, E.A., Paluszny, A., Tang, S.Y., Bale, H., Busse, B., Alliston, T., Kazakia, G., Ritchie, R.O., and Shefelbine, S.J. (2014). How Tough Is Brittle Bone? Investigating Osteogenesis Imperfecta in Mouse Bone. J. Bone Miner. Res. *29*, 1392–1401.

Clark, E.M., Ness, A.R., and Tobias, J.H. (2008). Vigorous physical activity increases fracture risk in children irrespective of bone mass: A prospective study of the independent risk factors for fractures in healthy children. J. Bone Miner. Res. *23*, 1012–1022.

Cooper, C., Dennison, E.M., Leufkens, H.G., Bishop, N., and van Staa, T.P. (2004). Epidemiology of childhood fractures in Britain: A study using the general practice research database. J. Bone Miner. Res. *19*, 1976–1981.

Currey, J.D. (1988). The effect of porosity and mineral content on the Young's modulus of elasticity of compact bone. J. Biomech. *21*, 131–139.

Currey, J.D. (2002). Bones: Structure and Mechanics (Princeton University Press).

Currey, J.D., and Butler, G. (1975). The Mechanical Properties in Children. J. Bone Jt. Surg. *57-A*, 810–814.

Currey, J.D., Brear, K., and Zioupos, P. (1996). The effects of ageing and changes in mineral content in degrading the toughness of human femora. J. Biomech. *29*, 257–260.

Currey, J.D., Foreman, J., Laketi, I., Mitchell, J., Pegg, D.E., and Reilly, G.C. (1997). Effects of ionizing radiation on the mechanical properties of human bone. J. Orthop. Res. *15*, 111–117.

Dempster, D.W., Compston, J.E., Drezner, M.K., Glorieux, F.H., Kanis, J.A., Malluche, H., Meunier, P.J., Ott, S.M., Recker, R.R., and Parfitt, A.M. (2013). Standardized nomenclature, symbols, and units for bone histomorphometry: A 2012 update of the report of the ASBMR Histomorphometry Nomenclature Committee. J. Bone Miner. Res. *28*, 2–17.

Dong, P., Haupert, S., Hesse, B., Langer, M., Gouttenoire, P.-J.J., Bousson, V.V., and Peyrin, F.F. (2014). 3D osteocyte lacunar morphometric properties and distributions in human femoral cortical bone using synchrotron radiation micro-CT images. Bone *60*, 172–185.

Donnelly, E., Boskey, A.L., Baker, S.P., and van der Meulen, M.C.H. (2010). Effects of tissue age on bone tissue material composition and nanomechanical properties in the rat cortex. J. Biomed. Mater. Res. A *92*, 1048–1056.

Donnelly, E., Meredith, D.S., Nguyen, J.T., Gladnick, B.P., Rebolledo, B.J., Shaffer, A.D., Lorich, D.G., Lane, J.M., and Boskey, A.L. (2012). Reduced cortical bone compositional heterogeneity with bisphosphonate treatment in postmenopausal women with intertrochanteric and subtrochanteric fractures. J. Bone Miner. Res. *27*, 672–678.

Duda, G.N., Schneider, E., and Chao, E.Y.S. (1997). Internal forces and moments in the femur during walking. J. Biomech. *30*, 933–941.

Eriksen, E.F. (2010). Cellular mechanisms of bone remodeling. Rev. Endocr. Metab. Disord. *11*, 219–227.

Faingold, A., Cohen, S.R., and Wagner, H.D. (2012). Nanoindentation of osteonal bone lamellae. J. Mech. Behav. Biomed. Mater. *9*, 198–206.

Fantner, G.E., Hassenkam, T., Kindt, J.H., Weaver, J.C., Birkedal, H., Pechenik, L., Cutroni, J.A., Cidade, G.A.G., Stucky, G.D., Morse, D.E., et al. (2005). Sacrificial bonds and hidden length dissipate energy as mineralized fibrils separate during bone fracture. Nat. Mater. *4*, 612–616.

Farlay, D., Panczer, G., Rey, C., Delmas, P.D., and Boivin, G. (2010). Mineral maturity and crystallinity index are distinct characteristics of bone mineral. J. Bone Miner. Metab. *28*, 433–445.

Farr, J.N., Amin, S., Melton III, L.J., Kirmani, S., McCready, L.K., Atkinson, E.J., Müller, R., and Khosla, S. (2014). Bone Strength and Structural Deficits in Children and Adolescents With a Distal Forearm Fracture Resulting From Mild Trauma. J. Bone Miner. Res. *29*, 590–599.

Faulkner, R.A., Davison, K.S., Bailey, D.A., Mirwald, R.L., and Baxter-Jones, A.D. (2006). Size-corrected BMD decreases during peak linear growth: Implications for fracture incidence during adolescence. J. Bone Miner. Res. *21*, 1864–1870.

Feik, S.A., Thomas, C.D., and Clement, J.G. (1997). Age-related changes in cortical porosity of the midshaft of the human femur. J. Anat. *191*, 407–416.

Felsenberg, D., and Boonen, S. (2005). The bone quality framework: Determinants of bone strength and their interrelationships, and implications for osteoporosis management. Clin. Ther. *27*, 1–11.

Ferretti, M., Muglia, M.A., Remaggi, F., Canè, V., and Palumbo, C. (1999). Histomorphometric study on the osteocyte lacuno-canalicular network in animals of different species. II. Parallel-fibered and lamellar bones. Ital. J. Anat. Embryol. *104*, 121–131.

Fiedler, I.A.K., Schmidt, F.N., Wölfel, E.M., Plumeyer, C., Milovanovic, P., Gioia, R., Tonelli, F., Bale, H.A., Jähn, K., Besio, R., et al. (2018). Severely Impaired Bone Material Quality in Chihuahua Zebrafish Resembles Classical Dominant Human Osteogenesis Imperfecta. J. Bone Miner. Res. *33*, 1489–1499.

Flenner, S., Storm, M., Kubec, A., Longo, E., Döring, F., Pelt, D.M., David, C., Müller, M., and Greving, I. (2020). Pushing the temporal resolution in absorption and Zernike phase contrast nanotomography: enabling fast in situ experiments. J. Synchrotron Radiat. *27*, 1339–1346.

Follet, H., Boivin, G., Rumelhart, C., and Meunier, P.J. (2004). The degree of mineralization is a determinant of bone strength: A study on human calcanei. Bone *34*, 783–789.

Fonseca, H., Moreira-Gonçalves, D., Coriolano, H.J.A., and Duarte, J.A. (2014). Bone quality: The determinants of bone strength and fragility. Sport. Med. *44*, 37–53.

Franzoso, G., and Zysset, P.K. (2009). Elastic anisotropy of human cortical bone secondary osteons measured by nanoindentation. J. Biomech. Eng. *131*, 1–11.

Fratzl-Zelman, N., Roschger, P., Misof, B.M., Pfeffer, S., Glorieux, F.H., Klaushofer, K., and Rauch, F. (2009). Normative data on mineralization density distribution in iliac bone biopsies of children, adolescents and young adults. Bone *44*, 1043–1048.

Fratzl-Zelman, N., Schmidt, I., Roschger, P., Glorieux, F.H., Klaushofer, K., Fratzl, P., Rauch, F., and Wagermaier, W. (2014). Mineral particle size in children with osteogenesis imperfecta type I is not increased independently of specific collagen mutations. Bone *60*, 122–128.

Fratzl, P., Gupta, H.S., Paschalis, E.P., and Roschger, P. (2004). Structure and mechanical quality of the collagen-mineral nano-composite in bone. J. Mater. Chem. *14*, 2115–2123.

García-Rodríguez, J., and Martínez-Reina, J. (2017). Elastic properties of woven bone: effect of mineral content and collagen fibrils orientation. Biomech. Model. Mechanobiol. *16*, 159–172.

Gautieri, A., Passini, F.S., Silván, U., Guizar-Sicairos, M., Carimati, G., Volpi, P., Moretti, M., Schoenhuber, H., Redaelli, A., Berli, M., et al. (2017). Advanced glycation end-products: Mechanics of aged collagen from molecule to tissue. Matrix Biol. *59*, 95–108.

Gebhardt, W. (1905). Über funktionell wichtige Anordnungsweisen der feineren und gröberen Bauelemente des Wirbeltierknochens. Arch. Für Entwicklungsmechanik Der Org. *20*, 187–322.

Giraud-Guille, M.M. (1988). Twisted plywood architecture of collagen fibrils in human compact bone osteons. Calcif. Tissue Int. *42*, 167–180.

Goulding, A. (2007). Risk Factors for Fractures in Normally Active Children and Adolescents. Med. Sport Sci. *51*, 102–120.

Gourion-Arsiquaud, S., Burket, J.C., Havill, L.M., DiCarlo, E., Doty, S.B., Mendelsohn, R., Van Der Meulen, M.C.H., and Boskey, A.L. (2009). Spatial variation in osteonal bone properties relative to tissue and animal age. J. Bone Miner. Res. *24*, 1271–1281.

Grandfield, K., Vuong, V., and Schwarcz, H.P. (2018). Ultrastructure of Bone: Hierarchical Features from Nanometer to Micrometer Scale Revealed in Focused Ion Beam Sections in the TEM. Calcif. Tissue Int. *103*, 606–616.

Groff, H., Kheir, M.M., George, J., Azboy, I., Higuera, C.A., and Parvizi, J. (2019). Causes of in-hospital mortality after hip fractures in the elderly. HIP Int. *30*, 204–209.

Grünewald, T.A., Liebi, M., Wittig, N.K., Johannes, A., Sikjaer, T., Rejnmark, L., Gao, Z., Rosenthal, M., Guizar-Sicairos, M., Birkedal, H., et al. (2020). Mapping the 3D orientation of nanocrystals and nanostructures in human bone: Indications of novel structural features. Sci. Adv. *6*.

Grynpas, M. (1993). Age and disease-related changes in the mineral of bone. Calcif. Tissue Int. *53*, 57–64.

Gupta, H.S., Wagermaier, W., Zickler, G.A., Raz-Ben Aroush, D., Funari, S.S., Roschger, P., Wagner, H.D., and Fratzl, P. (2005). Nanoscale deformation mechanisms in bone. Nano Lett. *5*, 2108–2111.

Hamed, E., Lee, Y., and Jasiuk, I. (2010). Multiscale modeling of elastic properties of cortical bone. Acta Mech. *213*, 131–154.

Hamed, E., Jasiuk, I., Yoo, A., Lee, Y.H., and Liszka, T. (2012). Multi-scale modelling of elastic moduli of trabecular bone. J. R. Soc. Interface *9*, 1654–1673.

Hattner, R., Epker, B.N., and Frost, H.M. (1965). Suggested Sequential Mode of Control of Changes in Cell Behaviour in Adult Bone Remodelling. Nature *206*, 489–490.

Hedström, E.M., Svensson, O., Bergström, U., and Michno, P. (2010). Epidemiology of fractures in children and adolescents: Increased incidence over the past decade: A population-based study from northern Sweden. Acta Orthop. *81*, 148–153.

Hellmich, C., and Ulm, F.-J. (2002). Micromechanical Model for Ultrastructural Stiffness of Mineralized Tissues. J. Eng. Mech. *128*, 898–908.

Hemmatian, H., Bakker, A.D., Klein-Nulend, J., and van Lenthe, G.H. (2017). Aging, Osteocytes, and Mechanotransduction. Curr. Osteoporos. Rep. *15*, 401–411.

Hernandez, C.J., Majeska, R.J., and Schaffler, M.B. (2004). Osteocyte density in woven bone. Bone *35*, 1095–1099.

Hernlund, E., Svedbom, A., Ivergård, M., Compston, J., Cooper, C., Stenmark, J., McCloskey, E. V, Jönsson, B., and Kanis, J.A. (2013). Osteoporosis in the European Union: medical management, epidemiology and economic burden. A report prepared in collaboration with the International Osteoporosis Foundation (IOF) and the European Federation of Pharmaceutical Industry Associations (EFPIA). Arch. Osteoporos. *8*, 136.

Hexemer, A., Bras, W., Glossinger, J., Schaible, E., Gann, E., Kirian, R., MacDowell, A., Church, M., Rude, B., and Padmore, H. (2010). A SAXS/WAXS/GISAXS beamline with multilayer monochromator. J. Phys. Conf. Ser. *247*, 012007.

Hoc, T., Henry, L., Verdier, M., Aubry, D., Sedel, L., and Meunier, A. (2006). Effect of microstructure on the mechanical properties of Haversian cortical bone. Bone *38*, 466–474.

Hoerth, R.M., Seidt, B.M., Shah, M., Schwarz, C., Willie, B.M., Duda, G.N., Fratzl, P., and Wagermaier, W. (2014). Mechanical and structural properties of bone in non-critical and critical healing in rat. Acta Biomater. *10*, 4009–4019.

Hoffler, C.E., Moore, K.E., Kozloff, K., Zysset, P.K., and Goldstein, S.A. (2000). Age, gender, and bone lamellae elastic moduli. J. Orthop. Res. *18*, 432–437.

Holguin, N., Brodt, M.D., Sanchez, M.E., and Silva, M.J. (2014). Aging diminishes lamellar and woven bone formation induced by tibial compression in adult C57Bl/6. Bone *65*, 83–91.

van Hove, R.P., Nolte, P.A., Vatsa, A., Semeins, C.M., Salmon, P.L., Smit, T.H., and Klein-Nulend, J. (2009). Osteocyte morphology in human tibiae of different bone pathologies with different bone mineral density — Is there a role for mechanosensing? Bone *45*, 321–329.

Humphries, A.L. (2011). Basic Juvenile Skeletal Anatomy and Growth and Development. In The Juvenile Skeleton in Forensic Abuse Investigations, A.H. Ross, and S.M. Abel, eds. (Totowa, NJ: Humana Press), pp. 19–31.

Ilavsky, J. (2012). Nika: software for two-dimensional data reduction. J. Appl. Crystallogr. *45*, 324–328.

Ip, V., Toth, Z., Chibnall, J., and McBride-Gagyi, S. (2016). Remnant Woven Bone and Calcified Cartilage in Mouse Bone: Differences between Ages/Sex and Effects on Bone Strength. PLoS One *11*, 1–15.

Jandl, N.M., von Kroge, S., Stürznickel, J., Baranowsky, A., Stockhausen, K.E., Mushumba, H., Beil, F.T., Püschel, K., Amling, M., and Rolvien, T. (2020). Large osteocyte lacunae in iliac crest infantile bone are not associated with impaired mineral distribution or signs of osteocytic osteolysis. Bone *135*, 115324.

Jones, S.J., Boyde, A., and Pawley, J.B. (1975). Osteoblasts and collagen orientation. Cell Tissue Res. *159*, 73–80.

Kanis, J.A., McCloskey, E. V, Johansson, H., Cooper, C., Rizzoli, R., and Reginster, J.Y. (2013). European guidance for the diagnosis and management of osteoporosis in postmenopausal women. Osteoporos. Int. *24*, 23–57.

Karaplis, A.C. (2002). Embryonic Development of Bone and the Molecular Regulation of Intramembranous and Endochondral Bone Formation. In Principles of Bone Biology, J.P. Bilezikian, L.G. Raisz, and G.A. Rodan, eds. (San Diego: Academic Press), pp. 33–58.

Kerschnitzki, M., Wagermaier, W., Roschger, P., Seto, J., Shahar, R., Duda, G.N., Mundlos, S., and Fratzl, P. (2011). The organization of the osteocyte network mirrors the extracellular matrix orientation in bone. J. Struct. Biol. *173*, 303–311.

Klein-Nulend, J., Bacabac, R.G., and Bakker, A.D. (2012). Mechanical loading and how it affects bone cells: the role of the osteocyte cytoskeleton in maintaining our skeleton. Eur. Cell. Mater. *24*, 278–291.

Klein-Nulend, J., Bakker, A.D., Bacabac, R.G., Vatsa, A., and Weinbaum, S. (2013). Mechanosensation and transduction in osteocytes. Bone *54*, 182–190.

Koester, K.J., Ager, J.W., and Ritchie, R.O. (2008). The true toughness of human cortical bone measured with realistically short cracks. Nat. Mater. *7*, 672–677.

Kölliker, A. (1873). Die normale Resorption des Knochengewebes und ihre Bedeuting für die Entstehung der typischen Knochenformen (F.C.W. Vogel).

Landin, L.A. (1983). Fracture patterns in children. Analysis of 8,682 fractures with special reference to incidence, etiology and secular changes in a Swedish urban population 1950-1979. Acta Orthop. Scand. Suppl. *202*, 1–109.

Landis, W.J., Librizzi, J.J., Dunn, M.G., and Silver, F.H. (1995). A study of the relationship between mineral content and mechanical properties of turkey gastrocnemius tendon. J. Bone Miner. Res. *10*, 859–867.

Langer, M., Pacureanu, A., Suhonen, H., Grimal, Q., Cloetens, P., and Peyrin, F. (2012). X-Ray Phase Nanotomography Resolves the 3D Human Bone Ultrastructure. PLoS One *7*, 1–7.

Lassen, N.E., Andersen, T.L., Pløen, G.G., Søe, K., Hauge, E.M., Harving, S., Eschen, G.E.T., and Delaisse, J.-M. (2017). Coupling of Bone Resorption and Formation in Real Time: New Knowledge Gained From Human Haversian BMUs. J. Bone Miner. Res. *32*, 1395–1405.

Launey, M.E., Buehler, M.J., and Ritchie, R.O. (2010). On the Mechanistic Origins of Toughness in Bone. Annu. Rev. Mater. Res. *40*, 25–53.

Lefèvre, E., Farlay, D., Bala, Y., Subtil, F., Wolfram, U., Rizzo, S., Baron, C., Zysset, P., Pithioux, M., and Follet, H. (2019). Compositional and mechanical properties of growing cortical bone tissue : a study of the human fibula. Sci. Rep. *9*, 17639.

Lynch, M.E., Main, R.P., Xu, Q., Schmicker, T.L., Schaffler, M.B., Wright, T.M., and van der Meulen, M.C.H. (2011). Tibial compression is anabolic in the adult mouse skeleton despite reduced responsiveness with aging. Bone *49*, 439–446.

Manjubala, I., Liu, Y., Epari, D.R., Roschger, P., Schell, H., Fratzl, P., and Duda, G.N. (2009). Spatial and temporal variations of mechanical properties and mineral content of the external callus during bone healing. Bone *45*, 185–192.

Marotti, G. (1979). Osteocyte orientation in human lamellar bone and its relevance to the morphometry of periosteocytic lacunae. Metab. Bone Dis. Relat. Res. *1*, 325–333.

Marotti, G. (1993). A new theory of bone lamellation. Calcif. Tissue Int. *53*, 47–55.

Martin, R.B., and Boardman, D.L. (1993). The effects of collagen fiber orientation, porosity, density, and mineralization on bovine cortical bone bending properties. J. Biomech. *26*, 1047–1054.

Martin, R.B., and Ishida, J. (1989). The relative effects of collagen fiber orientation, porosity, density, and mineralization on bone strength. J. Biomech. *22*, 419–426.

Mason, M.W., Skedros, J.G., and Bloebaum, R.D. (1995). Evidence of strain-mode-related cortical adaptation in the diaphysis of the horse radius. Bone *17*, 229–237.

McCalden, R.W., McGeough, J.A., Barker, M.B., and Court-Brown, C.M. (1993). Age-related changes in the tensile properties of cortical bone. The relative importance of changes in porosity, mineralization, and microstructure. J. Bone Joint Surg. Am. *75*, 1193—1205.

McCreadie, B.R., Morris, M.D., Chen, T., Rao, D.S., Finney, W.F., Widjaja, E., and Goldstein, S.A. (2015). Bone tissue compositional differences in women with and without osteoporotic fracture. Bone *39*, 1190–1195.

McMahon, J.M., Boyde, A., and Bromage, T.G. (1995). Pattern of collagen fiber orientation in the ovine calcaneal shaft and its relation to locomotor-induced strain. Anat. Rec. *242*, 147–158.

McNally, E., Nan, F., Botton, G.A., and Schwarcz, H.P. (2013). Scanning transmission electron microscopic tomography of cortical bone using Z-contrast imaging. Micron *49*, 46–53.

Meunier, P.J., and Boivin, G. (1997). Bone mineral density reflects bone mass but also the degree of mineralization of bone: Therapeutic implications. Bone *21*, 373–377.

Milovanovic, P., Zimmermann, E.A., Hahn, M., Djonic, D., Püschel, K., Djuric, M., Amling, M., and Busse, B. (2013). Osteocytic canalicular networks: morphological implications for altered mechanosensitivity. ACS Nano *7*, 7542–7551.

Milovanovic, P., Zimmermann, E.A., Riedel, C., vom Scheidt, A., Herzog, L., Krause, M., Djonic, D., Djuric, M., Puschel, K., Amling, M., et al. (2015). Multi-level characterization of human femoral cortices and their underlying osteocyte network reveal trends in quality of young, aged, osteoporotic and antiresorptive-treated bone. Biomaterials *45*, 46–55.

Milovanovic, P., vom Scheidt, A., Mletzko, K., Sarau, G., Püschel, K., Djuric, M., Amling, M., Christiansen, S., and Busse, B. (2018). Bone tissue aging affects mineralization of cement lines. Bone *110*, 187–193.

Nalla, R.K., Kinney, J.H., and Ritchie, R.O. (2003). Mechanistic fracture criteria for the failure of human cortical bone. Nat. Mater. *2*, 164–168.

O'Brien, F.J., Taylor, D., and Lee, T.C. (2003). Microcrack accumulation at different intervals during fatigue testing of compact bone. J. Biomech. *36*, 973–980.

Odén, A., McCloskey, E. V, Kanis, J.A., Harvey, N.C., and Johansson, H. (2015). Burden of high fracture probability worldwide: secular increases 2010-2040. Osteoporos. Int. *26*, 2243–2248.

van Oers, R.F.M., Wang, H., and Bacabac, R.G. (2015). Osteocyte Shape and Mechanical Loading. Curr. Osteoporos. Rep. *13*, 61–66.

Ogurreck, M., Wilde, F., Herzen, J., Beckmann, F., Nazmov, V., Mohr, J., Haibel, A., Müller, M., and Schreyer, A. (2013). The nanotomography endstation at the PETRA III imaging beamline. J. Phys. Conf. Ser. *425*, 182002.

Öhman, C., Baleani, M., Pani, C., Taddei, F., Alberghini, M., Viceconti, M., and Manfrini, M. (2011). Compressive behaviour of child and adult cortical bone. Bone *49*, 769–776.

Oliver, W.C., and Pharr, G.M. (1992). An improved technique for determining hardness and elastic modulus using load and displacement sensing indentation experiments. J. Mater. Res. *7*, 1564–1583.

Omairey, S.L., Dunning, P.D., and Sriramula, S. (2019). Development of an ABAQUS plugin tool for periodic RVE homogenisation. Eng. Comput. *35*, 567–577.

Panula, J., Pihlajamäki, H., Mattila, V.M., Jaatinen, P., Vahlberg, T., Aarnio, P., and Kivelä, S.-L. (2011). Mortality and cause of death in hip fracture patients aged 65 or older: a population-based study. BMC Musculoskelet. Disord. *12*, 105.

Parfitt, A.M. (2002). Targeted and nontargeted bone remodeling: Relationship to basic multicellular unit origination and progression. Bone *30*, 5–7.

Paschalis, E.P., Betts, F., DiCarlo, E., Mendelsohn, R., and Boskey, A.L. (1997). FTIR microspectroscopic analysis of normal human cortical and trabecular bone. Calcif. Tissue Int. *61*, 480–486.

Pazzaglia, U.E., Congiu, T., Marchese, M., Spagnuolo, F., and Quacci, D. (2012). Morphometry and Patterns of Lamellar Bone in Human Haversian Systems. Anat. Rec. *295*, 1421–1429.

Pernelle, K., Imbert, L., Bosser, C., Auregan, J.C., Cruel, M., Ogier, A., Jurdic, P., and Hoc, T. (2017). Microscale mechanical and mineral heterogeneity of human cortical bone governs osteoclast activity. Bone *94*, 42–49.

Phelps, J.B., Hubbard, G.B., Wang, X., and Agrawal, C.M. (2000). Microstructural heterogeneity and the fracture toughness of bone. J. Biomed. Mater. Res. *51*, 735–741.

Portigliatti Barbos, M., Bianco, P., Ascenzi, A., and Boyde, A. (1984). Collagen orientation in compact bone: II. Distribution of lamellae in the whole of the human femoral shaft with reference to its mechanical properties. Metab. Bone Dis. Relat. Res. *5*, 309–315.

Poundarik, A.A., Diab, T., Sroga, G.E., Ural, A., Boskey, A.L., Gundberg, C.M., and Vashishth, D. (2012). Dilatational band formation in bone. Proc. Natl. Acad. Sci. U. S. A. *109*, 19178–19183.

Qwamizadeh, M., Liu, P., Zhang, Z., Zhou, K., and Wei Zhang, Y. (2016). Hierarchical Structure Enhances and Tunes the Damping Behavior of Load-Bearing Biological Materials. J. Appl. Mech. *83*, 51009.

Qwamizadeh, M., Lin, M., Zhang, Z., Zhou, K., and Zhang, Y.W. (2017a). Bounds for the dynamic modulus of unidirectional composites with bioinspired staggered distributions of platelets. Compos. Struct. *167*, 152–165.

Qwamizadeh, M., Zhou, K., and Zhang, Y.W. (2017b). Damping behavior investigation and optimization of the structural layout of load-bearing biological materials. Int. J. Mech. Sci. *120*, 263–275.

Rauch, F., and Glorieux, F.H. (2004). Osteogenesis imperfecta. Lancet (London, England) *363*, 1377–1385.

Regelsberger, J., Milovanovic, P., Schmidt, T., Hahn, M., Zimmermann, E.A., Tsokos, M., Zustin, J., Ritchie, R.O., Amling, M., and Busse, B. (2012). Changes to the cell, tissue and architecture levels in cranial suture synostosis reveal a problem of timing in bone development. Eur. Cells Mater. *24*, 441–458.

Reid, S.A. (1986). A study of lamellar organisation in juvenile and adult human bone. Anat. Embryol. (Berl). *174*, 329–338.

Reid, S.A., and Boyde, A. (1987). Changes in the mineral density distribution in human bone with age: Image analysis using backscattered electrons in the SEM. J. Bone Miner. Res. *2*, 13–22.

Remaggi, F., Canè, V., Palumbo, C., and Ferretti, M. (1998). Histomorphometric study on the osteocyte lacuno-canalicular network in animals of different species. I. Woven-fibered and parallel-fibered bones. Ital. J. Anat. Embryol. *103*, 145–155.

Repp, F., Kollmannsberger, P., Roschger, A., Berzlanovich, A., Gruber, G.M., Roschger, P., Wagermaier, W., and Weinkamer, R. (2017). Coalignment of osteocyte canaliculi and collagen fibers in human osteonal bone. J. Struct. Biol. *199*, 177–186.

Reznikov, N., Shahar, R., and Weiner, S. (2014). Three-dimensional structure of human lamellar bone: The presence of two different materials and new insights into the hierarchical organization. Bone *59*, 93–104.

Reznikov, N., Bilton, M., Lari, L., Stevens, M.M., and Kröger, R. (2018). Fractal-like hierarchical organization of bone begins at the nanoscale. Science *360*, 6388.

Rho, J.Y., Tsui, T.Y., and Pharr, G.M. (1997). Elastic properties of human cortical and trabecular lamellar bone measured by nanoindentation. Biomaterials *18*, 1325–1330.

Rho, J.Y., Zioupos, P., Currey, J.D., and Pharr, G.M. (2002). Microstructural elasticity and regional heterogeneity in human femoral bone of various ages examined by nano-indentation. J. Biomech. *35*, 189–198.

Riggs, C.M., Lanyon, L.E., and Boyde, A. (1993a). Functional associations between collagen fibre orientation and locomotor strain direction in cortical bone of the equine radius. Anat. Embryol. (Berl). *187*, 231–238.

Riggs, C.M., Vaughan, L., Evans, G.P., Lanyon, L.E., and Boyde, A. (1993b). Mechanical implications of collagen fibre orientation in cortical bone of the equine radius. Anat. Embryol. (Berl). *187*, 239–248.

Ritchie, R.O. (2011). The conflicts between strength and toughness. Nat. Mater. *10*, 817–822.

Roschger, P., Fratzl, P., Eschberger, J., and Klaushofer, K. (1998). Validation of quantitative backscattered electron imaging for the measurement of mineral density distribution in human bone biopsies. Bone *23*, 319–326.

Roschger, P., Paschalis, E.P., Fratzl, P., and Klaushofer, K. (2008). Bone mineralization density distribution in health and disease. Bone *42*, 456–466.

Ruffoni, D., Fratzl, P., Roschger, P., Klaushofer, K., and Weinkamer, R. (2007). The bone mineralization density distribution as a fingerprint of the mineralization process. Bone *40*, 1308–1319.

Saito, M., and Marumo, K. (2010). Collagen cross-links as a determinant of bone quality: A possible explanation for bone fragility in aging, osteoporosis, and diabetes mellitus. Osteoporos. Int. *21*, 195–214.

Schaffler, M.B., Cheung, W.-Y., Majeska, R., and Kennedy, O. (2014). Osteocytes: master orchestrators of bone. Calcif. Tissue Int. *94*, 5–24.

Vom Scheidt, A., Hemmatian, H., Püschel, K., Krause, M., Amling, M., and Busse, B. (2019). Bisphosphonate treatment changes regional distribution of trabecular microstructure in human lumbar vertebrae. Bone *127*, 482–487.

Schindelin, J., Arganda-Carreras, I., Frise, E., Kaynig, V., Longair, M., Pietzsch, T., Preibisch, S., Rueden, C., Saalfeld, S., Schmid, B., et al. (2012). Fiji: an open-source platform for biological-image analysis. Nat. Methods *9*, 676–682.

Schmidt, F.N., Zimmermann, E.A., Campbell, G.M., Sroga, G.E., Püschel, K., Amling, M., Tang, S.Y., Vashishth, D., and Busse, B. (2017). Assessment of collagen quality associated with non-enzymatic cross-links in human bone using Fourier-transform infrared imaging. Bone *97*, 243–251.

Schmidt, F.N., Delsmann, M.M., Mletzko, K., Yorgan, T.A., Hahn, M., Siebert, U., Busse, B., Oheim, R., Amling, M., and Rolvien, T. (2018). Ultra-high matrix mineralization of sperm whale auditory ossicles facilitates high sound pressure and high-frequency underwater hearing. Proc. R. Soc. B *285*, 20181820.

Schmidt, F.N., Zimmermann, E.A., Walsh, F., Plumeyer, C., Schaible, E., Fiedler, I.A.K., Milovanovic, P., Rößle, M., Amling, M., Blanchet, C., et al. (2019). On the Origins of Fracture Toughness in Advanced Teleosts: How the Swordfish Sword's Bone Structure and Composition Allow for Slashing under Water to Kill or Stun Prey. Adv. Sci. *6*, 1900287.

Schrof, S., Varga, P., Galvis, L., Raum, K., and Masic, A. (2014). 3D Raman mapping of the collagen fibril orientation in human osteonal lamellae. J. Struct. Biol. *187*, 266–275.

Seeman, E. (2003). Periosteal bone formation — A neglected determinant of bone strength. N. Engl. J. Med. *349*, 320–323.

Seref-Ferlengez, Z., Kennedy, O.D., and Schaffler, M.B. (2015). Bone microdamage, remodeling and bone fragility: how much damage is too much damage? Bonekey Rep. *4*, 644.

Shahar, R., Banks-Sills, L., and Eliasy, R. (2003). Stress and strain distribution in the intact canine femur: finite element analysis. Med. Eng. Phys. *25*, 387–395.

Shapiro, F., and Wu, J.Y. (2019). Woven bone overview: Structural classification based on its integral role in developmental, repair and pathological bone formation throughout vertebrate groups. Eur. Cells Mater. *38*, 137–167.

Sharir, A., Stern, T., Rot, C., Shahar, R., and Zelzer, E. (2011). Muscle force regulates bone shaping for optimal load-bearing capacity during embryogenesis. Development *138*, 3247–3259.

Siris, E.S., Chen, Y.-T., Abbott, T.A., Barrett-Connor, E., Miller, P.D., Wehren, L.E., and Berger, M.L. (2004). Bone mineral density thresholds for pharmacological intervention to prevent fractures. Arch. Intern. Med. *164*, 1108–1112.

Skedros, J.G., Mason, M.W., Nelson, M.C., and Bloebaum, R.D. (1996). Evidence of structural and material adaptation to specific strain features in cortical bone. Anat. Rec. *246*, 47–63.

Skedros, J.G., Mendenhall, S.D., Kiser, C.J., and Winet, H. (2009). Interpreting cortical bone adaptation and load history by quantifying osteon morphotypes in circularly polarized light images. Bone *44*, 392–403.

Skedros, J.G., Kiser, C.J., and Mendenhall, S.D. (2011). A weighted osteon morphotype score outperforms regional osteon percent prevalence calculations for interpreting cortical bone adaptation. Am. J. Phys. Anthropol. *144*, 41–50.

van Staa, T.P., Dennison, E.M., Leufkens, H.G., and Cooper, C. (2001). Epidemiology of fractures in England and Wales. Bone *29*, 517–522.

Stock, S.R. (2015). The Mineral-Collagen Interface in Bone. Calcif. Tissue Int. *97*, 262–280.

Stockhausen, K.E., Qwamizadeh, M., M. Wölfel, E., Hemmatian, H., A. K. Fiedler, I., Flenner, S., Longo, E., Amling, M., Greving, I., O. Ritchie, R., et al. (2021). Collagen Fiber Orientation Is Coupled with Specific Nano-Compositional Patterns in Dark and Bright Osteons Modulating Their Biomechanical Properties. ACS Nano *15*, 455–467.

Su, X., Sun, K., Cui, F.Z., and Landis, W.J. (2003). Organization of apatite crystals in human woven bone. Bone *32*, 150–162.

Svedbom, A., Hernlund, E., Ivergård, M., Compston, J., Cooper, C., Stenmark, J., McCloskey, E. V, Jönsson, B., and Kanis, J.A. (2013). Osteoporosis in the European Union: a compendium of country-specific reports. Arch. Osteoporos. *8*, 137.

Tai, K., Dao, M., Suresh, S., Palazoglu, A., and Ortiz, C. (2007). Nanoscale heterogeneity promotes energy dissipation in bone. Nat. Mater. *6*, 454–462.

Taylor, M.E., Tanner, K.E., Freeman, M.A., and Yettram, A.L. (1996). Stress and strain distribution within the intact femur: compression or bending? Med. Eng. Phys. *18*, 122–131.

Turner, C.H., Rho, J., Takano, Y., Tsui, T.Y., and Pharr, G.M. (1999). The elastic properties of trabecular and cortical bone tissues are similar: results from two microscopic measurement techniques. J. Biomech. *32*, 437–441.

Varga, P., Pacureanu, A., Langer, M., Suhonen, H., Hesse, B., Grimal, Q., Cloetens, P., Raum, K., and Peyrin, F.F. (2013). Investigation of the three-dimensional orientation of mineralized collagen fibrils in human lamellar bone using synchrotron X-ray phase nano-tomography. Acta Biomater. *9*, 8118–8127.

Vashishth, D., Verborgt, O., Divine, G., Schaffler, M.B., and Fyhrie, D.P. (2000). Decline in osteocyte lacunar density in human cortical bone is associated with accumulation of microcracks with age. Bone *26*, 375–380.

Verbruggen, S.W., Kainz, B., Shelmerdine, S.C., Hajnal, J. V., Rutherford, M.A., Arthurs, O.J., Phillips, A.T.M., and Nowlan, N.C. (2018). Stresses and strains on the human fetal skeleton during development. J. R. Soc. Interface *15*.

Viguet-Carrin, S., Garnero, P., and Delmas, P.D. (2006). The role of collagen in bone strength. Osteoporos. Int. *17*, 319–336.

Wang, X., Bank, R.A., TeKoppele, J.M., and Mauli Agrawal, C. (2001). The role of collagen in determining bone mechanical properties. J. Orthop. Res. *19*, 1021–1026.

Wang, X., Shen, X., Li, X., and Agrawal, C.M. (2002). Age-related changes in the collagen network and toughness of bone. Bone *31*, 1–7.

Wang, Y., Azaïs, T., Robin, M., Vallée, A., Catania, C., Legriel, P., Pehau-Arnaudet, G., Babonneau, F., Giraud-Guille, M.M., and Nassif, N. (2012). The predominant role of collagen in the nucleation, growth, structure and orientation of bone apatite. Nat. Mater. *11*, 724–733.

Wang, Z.X., Lloyd, A.A., Burket, J.C., Gourion-Arsiquaud, S., and Donnelly, E. (2016). Altered distributions of bone tissue mineral and collagen properties in women with fragility fractures. Bone *84*, 237–244.

Weiner, S., Arad, T., Sabanay, I., and Traub, W. (1997). Rotated plywood structure of primary lamellar bone in the rat: Orientations of the collagen fibril arrays. Bone *20*, 509–514.

Willett, T.L., Dapaah, D.Y., Uppuganti, S., Granke, M., and Nyman, J.S. (2019). Bone collagen network integrity and transverse fracture toughness of human cortical bone. Bone *120*, 187–193.

Wittig, N.K., Palle, J., Østergaard, M., Frølich, S., Birkbak, M.E., Spiers, K.M., Garrevoet, J., and Birkedal, H. (2019). Bone Biomineral Properties Vary across Human Osteonal Bone. ACS Nano *13*, 12949–12956.

Wu, M., Fannin, J., Rice, K.M., Wang, B., and Blough, E.R. (2011). Effect of aging on cellular mechanotransduction. Ageing Res. Rev. *10*, 1–15.

Yeni, Y.N., and Norman, T.L. (2000). Calculation of porosity and osteonal cement line effects on the effective fracture toughness of cortical bone in longitudinal crack growth. J. Biomed. Mater. Res. *51*, 504–509.

Zheng, N., Fleisig, G.S., Escamilla, R.F., and Barrentine, S.W. (1998). An analytical model of the knee for estimation of internal forces during exercise. J. Biomech. *31*, 963–967.

Zimmermann, E.A., and Ritchie, R.O. (2015). Bone as a structural material. Adv. Healthc. Mater. *4*, 1287–1304.

Zimmermann, E.A., Schaible, E., Bale, H., Barth, H.D.H., Tang, S.Y.S., Reichert, P., Busse, B., Alliston, T., Ager, J.W., and Ritchie, R.O. (2011). Age-related changes in the plasticity and toughness of human cortical bone at multiple length scales. Proc. Natl. Acad. Sci. U. S. A. *108*, 14416–14421.

Zimmermann, E.A., Köhne, T., Bale, H.A., Panganiban, B., Gludovatz, B., Zustin, J., Hahn, M., Amling, M., Ritchie, R.O., and Busse, B. (2015a). Modifications to nano- and microstructural quality and the effects on mechanical integrity in Paget's disease of bone. J. Bone Miner. Res. *30*, 264–273.

Zimmermann, E.A., Busse, B., and Ritchie, R.O. (2015b). The fracture mechanics of human bone: Influence of disease and treatment. Bonekey Rep. *4*, 743.

Zimmermann, E.A., Riedel, C., Schmidt, F.N., Stockhausen, K.E., Chushkin, Y., Schaible, E., Gludovatz, B., Vettorazzi, E., Zontone, F., Püschel, K., et al. (2019). Mechanical Competence and Bone Quality Develop During Skeletal Growth. J. Bone Miner. Res. *34*, 1461–1472.

Zioupos, P., and Currey, J.D. (1998). Changes in the stiffness, strength, and toughness of human cortical bone with age. Bone *22*, 57–66.

Zysset, P.K., Guo, X.E., Hoffler, C.E., Moore, K.E., and Goldstein, S.A. (1999). Elastic modulus and hardness of cortical and trabecular bone lamellae measured by nanoindentation in the human femur. J. Biomech. *32*, 1005–1012.

9. Published Articles

9.1. Publication 1

J Bone Miner Res. 2019 Aug;34(8):1461-1472. doi: 10.1002/jbmr.3730. Epub 2019 Jun 17.

Mechanical Competence and Bone Quality Develop During Skeletal Growth

Elizabeth A Zimmermann [1], Christoph Riedel [1], Felix N Schmidt [1], Kilian E Stockhausen [1], Yuriy Chushkin [2], Eric Schaible [3], Bernd Gludovatz [4], Eik Vettorazzi [5], Federico Zontone [2], Klaus Püschel [6], Michael Amling [1], Robert O Ritchie [7,8], Björn Busse [1]

[1] Department of Osteology and Biomechanics, University Medical Center, Hamburg, Germany

[2] Beamline ID 10, European Synchrotron Radiation Facility, Grenoble, France

[3] Experimental Systems Group, Advanced Light Source, Berkeley, CA, USA

[4] School of Mechanical and Manufacturing Engineering, UNSW Sydney, NSW, Australia

[5] Department of Medical Biometry and Epidemiology, University Medical Center, Hamburg, Germany

[6] Department of Forensic Medicine, University Medical Center, Hamburg, Germany

[7] Department of Materials Science and Engineering, University of California, Berkeley, CA

[8] Materials Sciences Division, Lawrence Berkeley National Laboratory, Berkeley, CA, US


Volume 34
Number 8
August 2019
pp. 1385-1548
Journal of Bone and Mineral Research
JBMR®
Peripheral Growth Plate Chondrocytes Source of Bone Forming Cells
Independent Roles of Senescence and Estrogen Deficiency on Bone Loss
Use of FRAX® in Women on Aromatase Inhibitors
WILEY
Published monthly by
The American Society for Bone and Mineral Research
ASBMR

ORIGINAL ARTICLE

JBMR

Mechanical Competence and Bone Quality Develop During Skeletal Growth

Elizabeth A Zimmermann,[1] Christoph Riedel,[1] Felix N Schmidt,[1] Kilian E Stockhausen,[1] Yuriy Chushkin,[2] Eric Schaible,[3] Bernd Gludovatz,[4] Eik Vettorazzi,[5] Federico Zontone,[2] Klaus Püschel,[6] Michael Amling,[1] Robert O Ritchie,[7,8] and Björn Busse[1]*

[1]Department of Osteology and Biomechanics, University Medical Center, Hamburg, Germany
[2]Beamline ID 10, European Synchrotron Radiation Facility, Grenoble, France
[3]Experimental Systems Group, Advanced Light Source, Berkeley, CA, USA
[4]School of Mechanical and Manufacturing Engineering, UNSW Sydney, NSW, Australia
[5]Department of Medical Biometry and Epidemiology, University Medical Center, Hamburg, Germany
[6]Department of Forensic Medicine, University Medical Center, Hamburg, Germany
[7]Department of Materials Science and Engineering, University of California, Berkeley, CA, USA
[8]Materials Sciences Division, Lawrence Berkeley National Laboratory, Berkeley, CA, USA

ABSTRACT

Bone fracture risk is influenced by bone quality, which encompasses bone's composition as well as its multiscale organization and architecture. Aging and disease deteriorate bone quality, leading to reduced mechanical properties and higher fracture incidence. Largely unexplored is how bone quality and mechanical competence progress during longitudinal bone growth. Human femoral cortical bone was acquired from fetal ($n = 1$), infantile ($n = 3$), and 2- to 14-year-old cases ($n = 4$) at the mid-diaphysis. Bone quality was assessed in terms of bone structure, osteocyte characteristics, mineralization, and collagen orientation. The mechanical properties were investigated by measuring tensile deformation at multiple length scales via synchrotron X-ray diffraction. We find dramatic differences in mechanical resistance with age. Specifically, cortical bone in 2- to 14-year-old cases exhibits a 160% greater stiffness and 83% higher strength than fetal/infantile cases. The higher mechanical resistance of the 2- to 14-year-old cases is associated with advantageous bone quality, specifically higher bone volume fraction, better micronscale organization (woven versus lamellar), and higher mean mineralization compared with fetal/infantile cases. Our study reveals that bone quality is superior after remodeling/modeling processes convert the primary woven bone structure to lamellar bone. In this cohort of female children, the microstructural differences at the femoral diaphysis were apparent between the 1- to 2-year-old cases. Indeed, the lamellar bone in 2- to 14-year-old cases had a superior structural organization (collagen and osteocyte characteristics) and composition for resisting deformation and fracture than fetal/infantile bone. Mechanistically, the changes in bone quality during longitudinal bone growth lead to higher fracture resistance because collagen fibrils are better aligned to resist tensile forces, while elevated mean mineralization reinforces the collagen scaffold. Thus, our results reveal inherent weaknesses of the fetal/infantile skeleton signifying its inferior bone quality. These results have implications for pediatric fracture risk, as bone produced at ossification centers during children's longitudinal bone growth could display similarly weak points. © 2019 American Society for Bone and Mineral Research.

KEY WORDS: ANALYSIS/QUANTITATION OF BONE; BONE MODELING; BONE QUALITY; BONE REMODELING; HISTOMORPHOMETRY; OSTEOCYTES

Introduction

Bone's resistance to fracture is highly dependent on its bone quality, which encompasses the bone volume fraction, microstructural organization, damage, and nanoscale composition.[1] Indeed, aging and disease (such as osteoporosis, osteogenesis imperfecta, Paget's disease of bone, osteomalacia due to vitamin D deficiency, etc.) are linked to genetic, environmental, and disease-related factors that alter bone quality and in turn affect fracture resistance.[2–9] In terms of aging, high fracture incidence is found not only in elderly individuals but also in children and adolescents during longitudinal skeletal growth (<20 years).[10] Thirty percent of children experience at least one bone fracture, with roughly two-thirds of fractures occurring from low-energy traumas.[11–15] In contrast to elderly individuals where fracture risk increases due to imbalances in bone resorption and formation, increased fracture

Received in original form March 21, 2018; revised form February 25, 2019; accepted March 5, 2019. Accepted manuscript online June 17, 2019.
Address correspondence to: Björn Busse, PhD, Department of Osteology and Biomechanics, University Medical Center Hamburg-Eppendorf, Lottestr. 55a, 22529 Hamburg, Germany. E-mail: b.busse@uke.uni-hamburg.de
Additional Supporting information may be found in the online version of this article.
Journal of Bone and Mineral Research, Vol. 34, No. 8, August 2019, pp. 1461–1472
DOI: 10.1002/jbmr.3730

risk in children/adolescents has been postulated to be the result of a transitory weakness in the skeleton.[16,17] However, bone quality and mechanical competence at the tissue level during skeletal growth remain largely unexplored.

Like other materials, bones resist fracture through their multiscale structure that imparts resistance to deformation and crack growth. At the nanoscale, collagen and mineral assemble into fibrils, which promote strength and plastic deformation through mechanisms such as fibrillar stretching/sliding, sacrificial bonding, and nano-/micronscale cracking.[7,18–20] At the scale of hundreds of microns, secondary osteons resist crack propagation in mature tissue through crack deflection and crack bridging mechanisms.[21,22] Aging- and disease-related changes in bone quality, such as the mineralization or cross-linking profile at small length scales or the osteon density at larger length scales, have been shown to reduce the effectiveness of these mechanisms that resist deformation and fracture in bone.[6–9]

Although the main mechanisms of fracture resistance in mature bone tissue have been identified, it is unclear if the same mechanisms are active in longitudinally growing bone because of potential differences in bone quality. Most bones, particularly the long bones, vertebrae, and ilium, grow in length through endochondral ossification. Endochondral ossification progresses at ossification centers (eg, growth plates), where the extracellular matrix (ECM) surrounding the hypertrophic chondrocytes calcifies followed by chondrocyte apoptosis. Then, the remaining calcified ECM is used as a scaffold for the formation of bone, termed primary spongiosa or primary bone.[23–25] Later during the growth process and throughout life, the tissue structure is refined through bone remodeling, where cylindrical units of tissue 200 to 300 μm in diameter are resorbed by bone cells and filled in with new highly organized bone tissue called secondary osteons. However, the exact timing of bone remodeling in the primary spongiosa is not known.[25,26] Although endochondral ossification increases bone length, changes in bone diameter and cortex thickness occur during growth and throughout life through bone modeling processes by apposition or resorption at the periosteal and endocortical surfaces.[27,28]

Here, we investigate how bone quality and mechanical competence develop during skeletal growth. The chosen skeletal site is the femoral mid-diaphysis because the same region can be investigated at different stages of maturity in different age groups.[29] Based on bone's present microstructural features during growth, the cases were split into two groups: 1) fetal/infantile bone consisting of primary bone with no osteons; and 2) 2- to 14-year-old cases consisting of remodeled tissue (ie, secondary osteons). We investigate whether these two age groups associated with specific microstructural characteristics have critical differences in bone mechanical performance and quality. We hypothesize that the 2- to 14-year-old cases composed of osteonal bone will reveal a greater mean mineralization and a more longitudinally aligned collagen fibril network providing superior mechanical resistance in comparison to fetal/infantile cases composed of woven bone.

Materials and Methods

Materials

Cortical bone from the femoral mid-diaphysis was acquired from human cases. Individuals with bone pathologies that would affect bone quality or skeletal growth were not included in the study. This study has a cross-sectional design with bone samples originating from a caucasian female cohort with the following ages: 22 weeks of gestation, $n = 1$; 2 months, $n = 2$; 1 year, $n = 1$; 2 years, $n = 1$; 5 years, $n = 1$; 14 years, $n = 2$). The study was conducted in accordance with the local ethics regulations[30] and was approved by the State of Hamburg's General Medical Council Ethics Committee (WF-013/2011).

Histology

Femoral cross sections were fixed in 3.7% formaldehyde for 3 days, dehydrated, and embedded undecalcified in glycolmethacrylate (Technovit, Heraeus Kulzer GmbH, Wehrheim, Germany). Histological sections were removed with a rotation microtome (microTec, Techno-Med GmbH) and stained with von Kossa/van Gieson. Histomorphometry on stained sections was used to measure osteoid volume/bone volume (OV/BV), osteoid surface/bone surface (OS/BS), and osteoid thickness (O.Th) using OsteoMeasure (OsteoMetrics, Decatur, GA, USA).[31,32]

Circularly polarized light microscopy

Circularly polarized light (CPL) microscopy was used to assess the collagen fiber orientation.[33,34] Methylmethacrylate-embedded samples were ground to a thickness of 100 μm with an automatic grinding machine (Exakt, Norderstedt, Germany). Using an Olympus BX-61 microscope (Olympus, Hamburg, Germany) equipped with CPL filter sets, both brightfield and CPL images of the same region of interest (ROI) were captured in 8-bit grayscale. A masking procedure was applied to separate bone and non-bone areas (eg, porous spaces, lacunae), which were assigned a gray value of 0.[33] The grayscale of the bone pixels in each masked CPL image was measured and reported as the average brightness (based on gray levels 1 to 255).[35] When viewing bone under polarized light, collagen fibers that run parallel to the plane of the section appear bright, while fibers that run perpendicular to it appear dark. Oblique collagen fibers result in intermediate grayscale values.[33,36]

Mineralization

The bone mineral density distribution (BMDD) was determined with quantitative backscattered electron imaging (qBEI).[37] The scanning electron microscope (LEO 435 VP, Leo Electron Microscopy Ltd., Cambridge, UK) was operated in backscattered mode at 20 kV and 680 pA with a constant working distance of 20 mm. A block containing the entire medial side of the cross section was analyzed for each individual. Multiple images were taken at × 50 magnification with a pixel size of 2.3 μm^2 and stitched before the histogram analysis. The gray level was calibrated with aluminum and carbon standards, such that the gray level was linearly proportional to calcium content (light and dark pixels correspond with high and low calcium content, respectively). The bone mineralization distribution was characterized by the mean, peak, and standard deviation of the gray value distribution, which correspond to the mean calcium content (Ca Mean, Wt-%), the peak calcium content (Ca Peak, Wt-%), and degree of variance/heterogeneity (Ca Width, Wt-%), respectively. From qBEI, the percentage of bone mineralized below the 5th percentile (Ca Low, % B.Ar.) or above the 95th

percentile (Ca High, % B.Ar.) of a control BMDD, obtained from healthy individuals aged 31.4 ± 9.5 years, were calculated. Backscattered electron images were also used to calculate the cortical mineralized bone volume per tissue volume (BV/TV), the mean osteocyte lacunar area (Ot.Lc.Ar, μm²), and the number of osteocyte lacunae per bone area (N.Ot.Lc./B.Ar., #/mm²).

The mineral phase was also characterized with Fourier transform infrared (FTIR) imaging. Histological sections of cortical bone with a 5-μm thickness were scanned in transmission with a Spotlight 400 FTIR Imaging system (Perkin Elmer, Waltham, MA, USA). One section of the entire medial side of the cross section was analyzed per individual. Spectra were acquired over a spectral range of 570 to 4000 cm^{-1} at a 4-cm^{-1} spectral resolution with 32 scans/pixel. Images were scanned at a 25-μm step size. The spectra were automatically corrected for atmospheric effects and noise reduction. After background and PMMA subtraction, the FTIR parameters were calculated for each spectrum. Specifically, the mineral-to-matrix ratio was calculated through the area ratio of the amide I (1590 to 1725 cm^{-1}) and phosphate peaks (915 to 1180 cm^{-1}), the carbonate-to-phosphate ratio through the area ratio of the carbonate (850 to 900 cm^{-1}) and phosphate peaks, as well as the mineral maturity index through the area ratio of the 1030 cm^{-1} and 1110 cm^{-1} subbands.[38,39] For each parameter at the individual level, the distribution of values was fitted with a Gaussian curve. The mean value is reported for each FTIR parameter as well as the heterogeneity, which was measured by the FWHM of the Gaussian curve.

Mechanical properties

Deformation at the tissue, fibril, and mineral length scales was investigated with mechanical tensile tests during small and wide-angle X-ray scattering/diffraction (SAXS/WAXD) experiments (Supplemental Fig. S1) at beamline 7.3.3 at the Advanced Light Source synchrotron radiation facility (Lawrence Berkeley National Laboratory, Berkeley, CA, USA).[7,40,41] Here, multiple mechanical tests were performed for each case (fetal $n = 2$; 2 months $n = 2$; 2 months $n = 4$; 1 year $n = 3$; 2 years $n = 4$; 5 years $n = 2$; 14 years $n = 4$), except one 14-year-old case due to a lack of remaining material. Mechanical tests were performed on tissue from the posterior side of the diaphyseal femur.

Tensile tests are performed to measure overall bone strength. Simultaneously, fibril and mineral strains are measured through X-ray scattering because bone's ordered nano-level structure (ie, fibril's 67-nm periodicity and mineral's crystal structure) diffracts X-rays, allowing nanoscale deformation to be measured during tensile testing.[7,41] The experimental methods/analysis have been previously described.[7] Briefly, hydrated cortical tensile samples (15 mm × 1 mm × 250 μm) were loaded in tension (TST350 tensile stage, Linkam Scientific Instruments, Surrey, UK) with SAXS/WAXD data collected for 0.3 second every 10 seconds during the tests. Pilatus detectors were positioned ~4000 mm from the sample to collect SAXS data and 150 mm from the sample with an 18° angle to collect WAXD data using a 10-keV X-ray energy.

The analysis software IGOR Pro (Wavemetrics, Portland, OR, USA) and the custom macro NIKA were used to calibrate the image and convert 2D data to 1D.[42] Then, the first-order collagen peak and the mineral 002 peak in the 1D SAXS and WAXD data sets, respectively, were fit to detect changes in the average collagen and mineral d-spacing. The load was recorded during tensile testing and tissue stress was calculated by normalizing the load by the cross-sectional area. Additionally, tissue strain was measured by imaging the change in spacing of horizontal lines marked on the sample's surface, which were later analyzed using a custom-programmed image analysis software utilizing the software package Vision Assistant 8.5 (National Instruments, Austin, TX, USA). For each individual, ≥2 samples were tested with SAXS/WAXD. For each sample, the tissue stress, mineral strain, and fibril strain data were binned every 0.1% tissue strain and averaged on the individual level. The average and standard deviation are reported.

Synchrotron coherent diffraction X-ray imaging (CDI)

CDI was performed at beamline ID10 at the European Synchrotron Radiation Facility (Grenoble, France) on a 2-month-old and 14-year-old case. CDI results in a 3D image of the bone fragment. Methylmethacrylate was removed from histological sections with 2-methoxyethyl acetate followed by an alcohol series and demineralized water. Then, fragments of the bone sections were deposited onto Si_3N_4 membranes (Silson, Northampton, UK). The samples were rotated between tilts of −75° and 75° at 0.5° step sizes and the 2D diffraction pattern was taken at each step with 8-keV coherent X-rays. The 2D diffraction patterns were combined into a 3D diffraction pattern. A phase retrieval algorithm was applied to reconstruct the 3D electron density distribution from the 3D Fourier intensity data with a 14.7-nm voxel size.[43] The 2D image stack was filtered and thresholded to isolate large extrafibrillar mineralization. Then, the volume of each mineral particle was measured with FIJI image analysis software.

Statistics

All data are represented as mean ± standard deviation (SD). Data were aggregated on the individual level by averaging and separated into two groups based on microstructural observations: the 2- to 14-year-old samples contained osteons and the fetal to 1-year-old samples did not. Because of the small sample size, a nonparametric statistical analysis was used. Data were aggregated on the individual level and the Mann-Whitney *U* test was carried out with a significance level of $\alpha = 0.05$ using SPSS Statistics.

Results

Bone quality during skeletal growth

Densification of the cortex

In human cortical bone from the femoral mid-diaphysis, the bone volume fraction was analyzed with von Kossa/van Gieson-stained sections in a pediatric cohort. In the fetal/infantile cases (Fig. 1*A*, *B*), the bone's micron-level structure resembles a scaffold with long, porous channels and high amounts of unmineralized bone matrix (ie, osteoid). In contrast, the 2- to 14-year-old cases (Fig. 1*C*, *D*) exhibited a dense bone structure primarily consisting of mineralized tissue, without extensive areas containing osteoid. The bone volume fraction in the 2- to 14-year-old cases was 22% higher than the fetal/infantile cases ($P = 0.03$) (Fig. 1*E*). Additionally, bone formation decreased with age, with a 90% higher osteoid volume and 71% higher osteoid

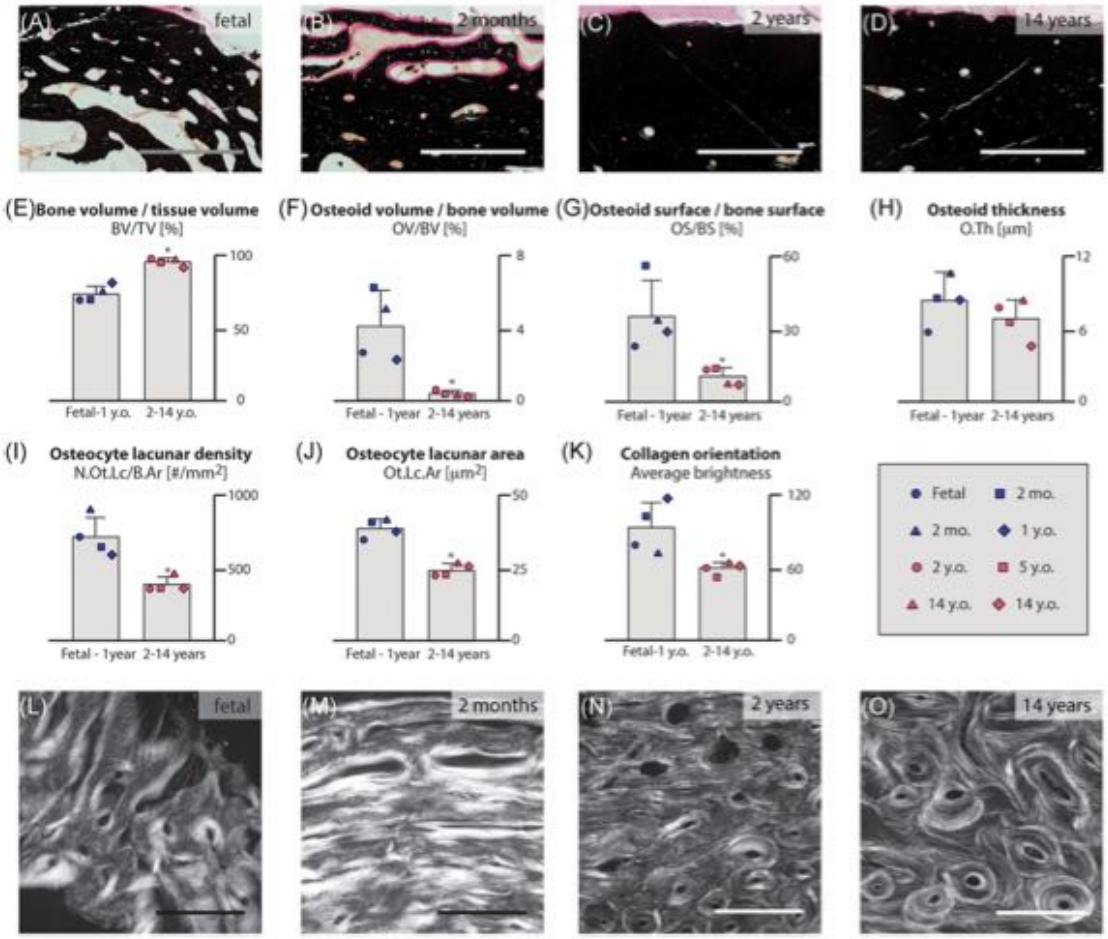

Fig. 1. Bone volume and collagen fiber organization during skeletal growth. Von Kossa/van Gieson-stained sections (mineralized bone: black; unmineralized osteoid: pink) show a porous scaffold-like cortex in (*A*) fetal and (*B*) infantile cases and a dense cortex in cases between (*C*) 2 and (*D*) 14 years. (*E*) Thus, fetal/infantile cases have a 22% lower BV/TV than the 2- to 14-year-old cases. Rapid bone formation in fetal/infantile cases is demonstrated by the greater (*F*) OV/TV and (*G*) OS/BS compared with 2- to 14-year-old cases. (*H*) However, osteoid thickness was not significantly different. (*I*) Osteocyte lacunar density is substantially higher in fetal to 1-year-old cases and the (*J*) osteocyte lacunae are enlarged in fetal to 1-year-old cases compared with 2- to 14-year-old cases. (*K–O*) Quantitative polarized light microscopy (bright: transverse fiber orientation; dark: longitudinal fiber orientation) measures collagen fiber orientation. (*K*) Here, the average brightness is significantly lower in the 2- to 14-year-old cases than the fetal/infantile cases implying that more fibers are longitudinally oriented in the older cases. Images show subsets of measured regions of interest. Histograms and bar graphs reflect characterizations of complete regions of interest. Data presented as mean ± SD. Mann-Whitney *U* test: $^*P < 0.05$. Scale bars = 500 µm. Data presented as a function of age in Supplemental Fig. S5

surface in the fetal/infantile bone versus the 2- to 14-year-old cases ($P = 0.03$) (Fig. 1*F*, *G*). However, the osteoid thicknesses were similar in both age groups, which suggests similar mineralization processes (Fig. 1*H*). A higher osteocyte lacunar density in the early phase of osteogenesis (ie, in woven bone) with shorter dendritic processes and no particular alignment within the bone matrix is evident (Fig. 1*I*), whereas the size of the osteocyte lacunae is larger in fetal to 1-year-old cases in comparison to 2- to 14-year-old cases (Fig. 1*J*). These histological data are also shown in Supplemental Fig. S5*A–F* as a function of age, where the same trends can be seen between the fetal/infantile cases and the 2- to 14-year-old cases.

Organization of collagen fibers

The porous bone scaffold in fetal/infantile cases and the dense bone structure in the 2- to 14-year-old cases were investigated in terms of collagen fiber organization with quantitative polarized light microscopy (Fig. 1*K–O*; Supplemental Figs. S2, S5*G*). Here, collagen fibers that are transversely aligned appear bright and fibers that are longitudinally aligned appear dark. In fetal and infantile cortical bone, the scaffold-like microstructure has an unorganized collagen fiber structure, with packets of dark and bright collagen fibers (Fig. 1*L*, *M*). This type of collagen fiber organization reflects woven bone. Whereas woven bone

dominates the fetal/infantile cases, the 2- to 14-year-old cases consisted of secondary remodeled osteonal bone (Fig. 1*N*, *O*). Here, the remodeled osteonal bone consists of secondary osteons with alternating bright and dark lines, called lamellae. These lamellae represent highly organized layers of collagen fibers. The alternating brightness signifies that the collagen fibers in neighboring lamellae alternate in orientation. Quantitative analysis of the brightness in the polarized light microscopy images (Fig. 1*K*; Supplemental Fig. S5*G*) shows that the fetal/infantile cases have a significantly higher brightness, indicating greater transversal collagen alignment than the 2- to 14-year-old cases. This implies that the collagen fibers are becoming preferentially longitudinally oriented in the 2- to 14-year-old cases.

Homogenization and elevation of mineral distribution

Trends in the amount and distribution of mineral with age during skeletal growth were investigated with quantitative backscattered electron imaging (qBEI) (Fig. 2), where the calcium content scales with the gray value (high mineralization: bright; low mineralization: dark). Here, in the fetal/infantile cases (Fig. 2*A*, *B*), the calcified cartilage precursor formed during endochondral ossification is visible within the scaffold (white arrows), due to its higher mineral content than the newly formed bone. Comparatively, in 2- to 14-year-old cases, secondary osteons indicative of bone remodeling at the femoral mid-diaphysis are visible (Fig. 2*C*, *D*) with qBEI by their circular appearance, darker color (from lower mineralization), and highly mineralized outer boundary (ie, cement line). QBEI analysis of the gray value histograms (Fig. 2*E*) indicate that the Ca Mean mineralization increases with age, such that Ca Mean is 10% greater in the 2- to 14-year-old cases than the fetal/infantile cases (Fig. 2*F*; Supplemental Fig. S6*A*); however, no significant difference was found for Ca Peak (Fig. 2*G*; Supplemental Fig. S6*B*). The high mineralization of the fetal case can be attributed to the high level of calcified cartilage. Further analysis of the Ca Width, which assesses the heterogeneity in the bone mineral density distribution (Fig. 2*H*; Supplemental Fig. S6*C*), indicated a decrease in the heterogeneity with age that was 34% lower in the 2- to 14-year-old cases. Furthermore, the primary bone has a greater proportion of low mineralized tissue under development than remodeled bone, but each have similar proportions of high mineralized tissue (Fig. 2*I*, *J*; Supplemental Fig. S6*D*, *E*).

These trends in mineralization are also visible in Fourier transform infrared (FTIR) spectroscopy images of the mineral-to-matrix ratio (MMR) (Fig. 3; Supplemental Fig. S3). Here, the MMR increases with age, such that it is 12% lower in the fetal/infantile cases (Fig. 3*E*; Supplemental Fig. S7*A*). The

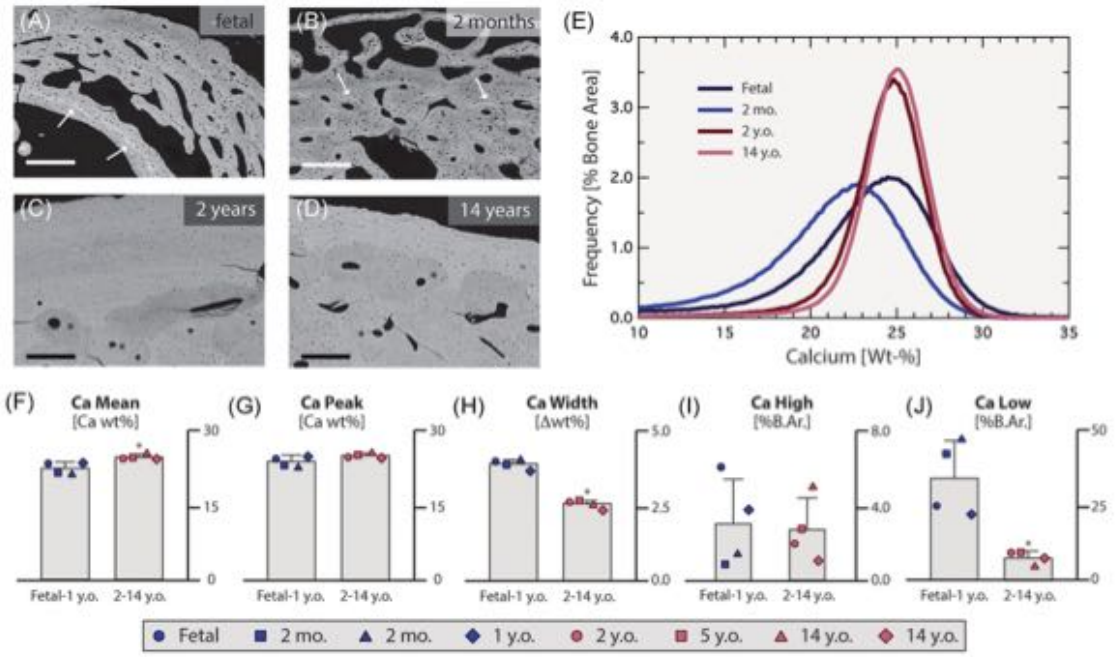

Fig. 2. Bone mineralization during skeletal growth. Quantitative backscattered electron imaging (qBEI) was used to measure the mineral density distribution (high mineralization: brighter; low mineralization: darker). In the (*A*) fetal and (*B*) infantile cases, calcified cartilage (white arrows) and areas with new bone formation (ie, low mineralization) were observed, while the (*C*) 2- to (*D*) 14-year-old cases exhibited secondary osteons (black asterisks). (*E*) Evaluation of the gray value histograms shows the trends in (*F*) Ca Mean, (*G*) Ca Peak, (*H*) Ca Width (signifying variance/heterogeneity), (*I*) Ca High and (*J*) Ca Low. Scale bar = 250 μm. Images show subsets of measured regions of interest. Histograms and bar graphs reflect characterizations of complete regions of interest. Data presented as mean ± SD. Mann-Whitney *U* test: $^*P < 0.05$. Data presented as a function of age in Supplemental Fig. S6

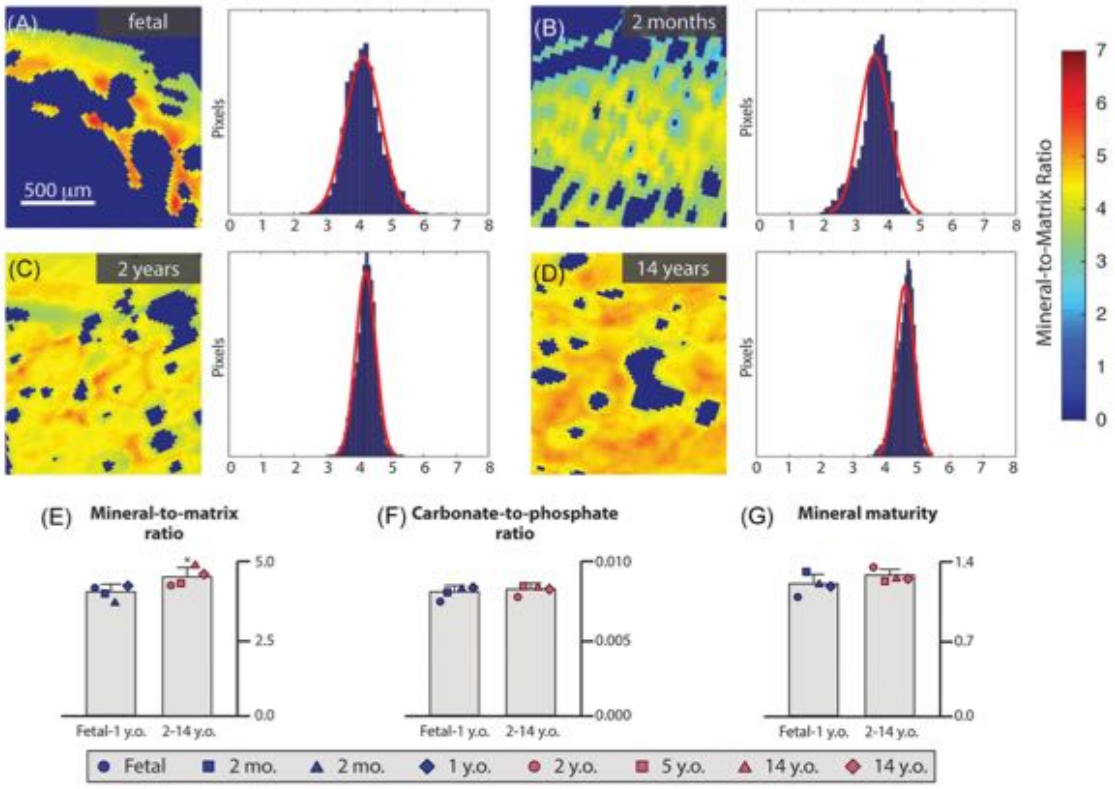

Fig. 3. Bone matrix quality during skeletal growth. Fourier transform infrared (FTIR) spectroscopy was used to image the quality of the bone matrix. (*A–D*) Images and histograms of the mineral-to-matrix ratio (MMR) confirm the differences in mineralization between the fetal/infantile cases and the 2- to 14-year-old cases. (*E*) The fetal/infantile cases have a 12% lower MMR. (*F*) The carbonate-to-phosphate ratio (CPR) and (*G*) mineral maturity were not significantly different. Data presented as mean ± SD. Images show subsets of measured regions of interest. Histograms and bar graphs reflect characterizations of complete regions of interest. Mann-Whitney *U* test: $^*P < 0.05$. Data presented as a function of age in Supplemental Fig. S7

heterogeneity of the MMR parameter also was significantly lower in the 2- to 14-year-old cases (Supplemental Fig. S7*D*). These trends in the MMR follow the complementary measurements in the Ca Mean, reported above. The carbonate-to-phosphate ratio (CPR) and the mineral maturity were also computed from the FTIR spectrum (Fig. 3*F*, *G*; Supplemental Figs. S3*C*, *D*; S4; S7) but neither showed a significant trend.

3D nanostructural images of the 2-month-old and 14-year-old samples were produced using synchrotron coherent diffraction imaging (CDI). Here, fibrils are visible with their characteristic 67-nm banding pattern (Fig. 4*A*, *B*). Additionally, large extrafibrillar mineral aggregates are observed on the fibrils' surface (Fig. 4*C*). The extrafibrillar mineral accounted for 3.1% of the volume in the 2-month-old sample and 5.3% in the 14-year-old sample. The distribution of extrafibrillar mineral volumes followed a log-normal distribution (Fig. 4*D*). Although all extrafibrillar mineral particles were generally plate-shaped with a 41 to 44-nm thickness, the 2-month-old cases contained smaller mineral aggregates (largest cross section: 0.19 × a 0.10 μm^2) than the 14-year-old cases (largest cross section: 0.45 × 0.36 μm^2).

Mechanical competence during skeletal growth

To investigate the multiscale mechanisms governing bone deformation, the mechanical resistance of the bone tissue from the pediatric cohort was measured at multiple length scales with tensile tests (measuring macroscale deformation) during synchrotron small-angle X-ray scattering (SAXS) and wide-angle X-ray diffraction (WAXD) experiments (measuring deformation at the fibril and mineral levels, respectively) (Fig. 5). As load is applied in the tensile test, the tissue first behaves elastically with a linear relationship between stress and strain (Fig. 5*A*, *B*), which is characterized by the elastic modulus and mechanistically originates from stretching of molecular-level bonds. Here, the modulus was 160% greater in the 2- to 14-year-old cases (Fig. 5*E*; Supplemental Fig. S8*A*) compared with the fetal/infantile cases.

After elastic stretching, the material begins to nonlinearly deform under mechanical load, which is characterized by permanent deformation (Fig. 5*A*, *B*). Here, the ultimate strength and failure strain describe the nonlinear behavior. The ultimate bone strength again is 83% greater in the 2-to 14-year-old cases than the fetal/infantile cases (Fig. 5*F*; Supplemental

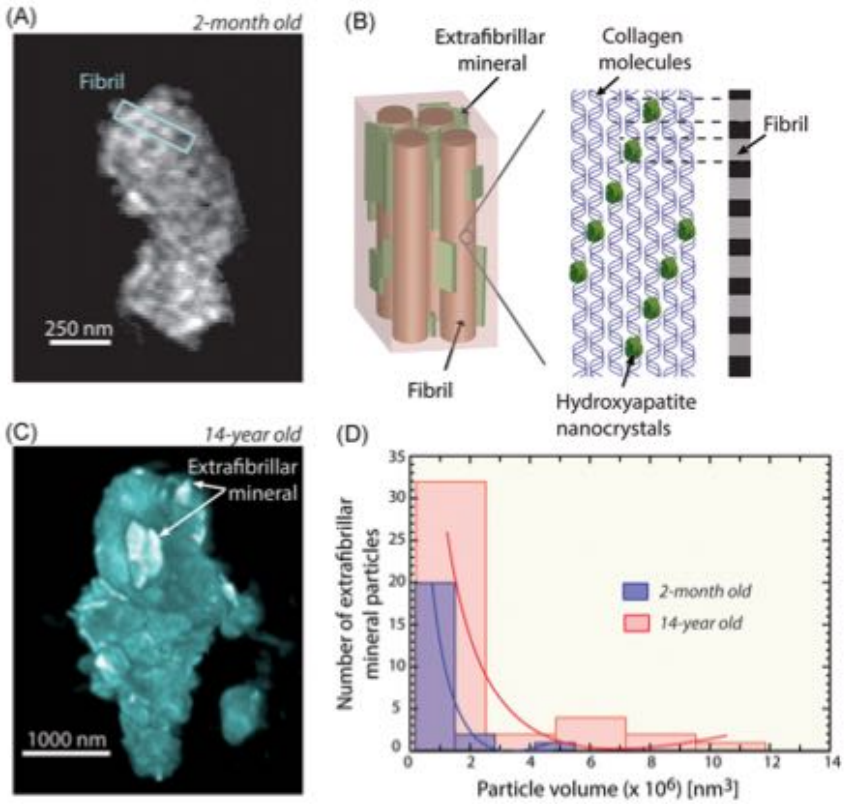

Fig. 4. Larger density and volume of extrafibrillar mineral with age. 3D nanostructural images of 2-month and 14-year-old bone were reconstructed at a 15-nm voxel size with synchrotron coherent X-ray diffraction imaging (CDI). (*A*) In 2D slices of the 2-month-old case, the fibril structure can be seen, where (*B*) the staggered spacing of collagen and mineral produces an alternating dark and bright pattern. (*C*) In the 3D reconstruction of the 14 year-old bone, large and bright extrafibrillar mineral particles are visible. (*D*) The extrafibrillar mineral particles are found in both the 2-month-old and 14-year-old cases; however, the size and density of extrafibrillar mineral was more abundant in the 14-year-old case. Here, the mineral particle volume follows a log-normal distribution, with the 14-year-old case having a 71% greater density of extrafibrillar mineral

Fig. S8*B*). The failure strain trends toward lower values at higher ages; however, the differences were not significant (Fig. 5*G*; Supplemental Fig. S8*C*).

The tissue's strength originates from deformation of its basic building blocks at the nanoscale. Here, mechanical loads applied to the tissue are transferred to the fibril, composed of collagen molecules and mineral nanoplatelets. Deformation in the fibril and mineral was measured during tensile tests with SAXS/WAXD. The fibril behavior was similar for each age group (Fig. 5*C*), where fibrils deform proportionally to applied tissue strain.

The differences in behavior at the nano-level are in the mineral deformation. WAXD measures tensile deformation in the mineral lattice of mineral platelets within and between collagen fibrils. As the samples are tested in tension, the mineral first stretches proportionally (ie, linear relationship) to tissue strain (Fig. 5*D*). The slope of the linear portion of the mineral versus tissue strain curve increases with age, with a significantly greater value in the 2- to 14-year-old cases (Fig. 5*H*; Supplemental Fig. S8*D*). Thus, the better micron-level organization (lamellar versus woven bone) in older cases may allow the mineral to deform more easily and contribute to the mechanical response. Then, in the fetal to 2-year-old samples, the linear relation between mineral and tissue strain becomes nonlinear. In the nonlinear region, the mineral strain plateaus around 0.44% in the fetal to 1-year-old cases and at 0.6% in the 2-year-old case (Fig. 5*D*). At the plateau, the mineral strain is constant as the tissue deforms, which may indicate sliding within/between fibrils or nonlinear deformation in the collagen matrix.

Discussion

During childhood and adolescence, the growth and development of long bones involve longitudinal growth through endochondral ossification, changes in diameter through periosteal/endocortical apposition/resorption, as well as bone remodeling. Our aim was to investigate bone quality and mechanical differences during the longitudinal growth of bones. Here, using the mid-femoral diaphysis at different ages during formation and maturation of the tissue, we investigated bone quality at a consistent skeletal site using

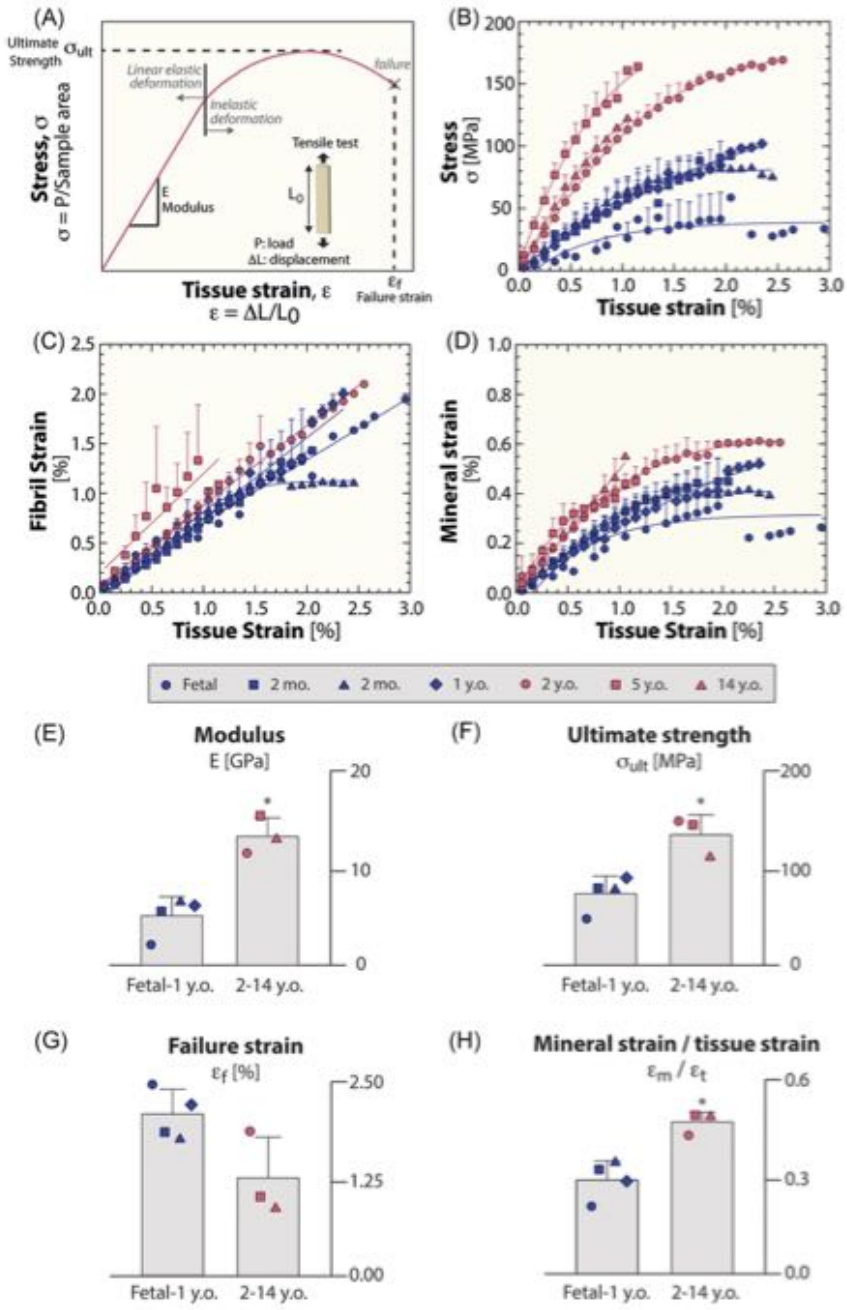

Fig. 5. Deformation mechanisms resisting fracture during skeletal growth. Synchrotron experiments investigated bone's nanoscale deformation. Here, tensile tests (test specimens ≥2/individual) were performed during synchrotron small-angle X-ray scattering (SAXS) and wide-angle X-ray diffraction (WAXD). (*A*, *B*) Tensile tests measuring stress (ie, applied load/sample area) and strain (ie, percent change in length) show differences in mechanical properties between the fetal/infantile cases and 2- to 14-year-old cases. Tissue stress, mineral strain, and fibril strain were binned every 0.1% tissue strain and were aggregated at the individual level. (*C*) Fibril deformation (SAXS) shows a linear increase in fibril strain during tensile tests for all cases. (*D*) Mineral deformation (WAXD) measurements indicate greater mineral strain in 2- to 14-year-old cases. The 2- to 14-year-old cases exhibited (*E*) 160% higher modulus and (*F*) 83% higher strength with trends toward lower (*G*) failure strain. (*H*) Additionally, the slope of the mineral strain versus tissue strain is 60% higher in the 2- to 14-year-old cases. Data presented as mean ± SD and were fit with linear or exponential curves. Mann-Whitney *U* test: $^*P < 0.05$. Data presented as a function of age in Supplemental Fig. S8

high-resolution materials science–based techniques and find that fetal/infantile bone tissue has an inferior bone quality and mechanical resistance than bone from 2- to 14-year-olds.

As the pediatric skeleton grows, the quality and form of the bone are shaped by ossification processes that grow the bone in length and in diameter as well as continue remodeling the existing structure. Fetal/infantile cases consisted of a porous, disorganized patchwork of collagen fiber orientations, characteristic of woven bone (Fig. 1*L*, *M*). Woven bone is known to be present during longitudinal growth, bone fracture healing, and bone modeling in adaptation to mechanical load.[25,44,45] The woven tissue consists of patches of collagen fibers with the same orientation, some oriented with the principal loading axis and others not (Fig. 1*L*, *M*). Conversely, highly organized lamellae found in secondary osteons were observed in the 2- to 14-year-old cases, which is a similar microstructural organization as adult bone. Indeed, studies in the development of long bones in mice show a similar porous scaffold-like cortex in fetal/infantile tissue with further densification near the time of walking.[46,47] Thus, investigation of the bone tissue at the femoral mid-diaphysis reflects that endochondral ossification results in deposition of woven bone and that around the age of one to 2 years (Supplemental Fig. S5*A*, *E*), bone remodeling processes replace the woven tissue with lamellar osteonal bone. This is also reflected by a similar collagen orientation in the age period of 2 to 14 years, possibly in response to changes in biomechanical loading.[34,36,48] Large differences in collagen orientation were observed in the fetal/infantile cases (Supplemental Fig. S5*G*). The fluctuation of the collagen orientation is linked to the disorganized nature of woven bone tissue and possibly due to the lower degree of mechanical stimuli experienced at this age.

The changes in bone quality during skeletal development additionally entail differences in the mineralization distribution. Specifically, the mean mineralization (Ca Mean) increased until about 2 years and then remained fairly constant with age (Fig. 2; Supplemental Fig. S6*A*). As a result, the 2- to 14-year-old cases had a 10% greater Ca Mean and a 34% lower heterogeneity than the fetal/infantile cases. Our data are in agreement with a recent study that found constant bone mineral density distribution in individuals between the ages of 1.5 to 23 years.[49] However, Currey et al.[50,51] found that ash content increased with age in children/adolescents. The bone mineral density distribution measured with qBEI may follow the same trends as the ash content.[52] Nevertheless, a discrepancy may be present due to the low number of cases tested in the studies of Currey and colleagues. Although qBEI measures do not inform about the mineral characteristics on a large three-dimensional volume of bone tissue (as in ash content), the main benefit is that spatial compositional data is provided and thus, the distribution of mineral can be quantitatively assessed. The differences in the mineralization distribution between the fetal/infantile and 2- to 14-year-old cases may be related to the collagen fiber organization. In our study, the 2- to 14-year-old cases consisted of secondary bone (ie, remodeled osteons); thus, it follows that the remodeling events may create a balanced mineral distribution as tissue is resorbed and renewed with age. Conversely, the fetal/infantile cases consisted of patches of woven bone. This disorganized collagen fiber structure incorporates less mineral than lamellar bone and/or may have a shorter mineralization period due to its rapid deposition. Correspondingly lower mineralization has been measured in woven bone found in disease states such as Paget's disease of bone and also in the bony callus formed during fracture healing.[8,44,53] CaLow exhibits similar trends with age as the collagen orientation (Supplemental Figs. S5*G*, S6*E*). CaLow has a broad range of values in fetal/infantile bone, whereas in the 2- to 14-year range, CaLow is fairly constant. This may represent the influence of mechanical loading (eg, walking) on the bone composition and structure.[54,55] After remodeling processes commence (2- to 14-year-old cases), which coincides with further biomechanical stimulation, the bone quality parameters (bone volume fraction, collagen orientation, mean mineralization, and mechanical properties) remain constant with age.

These differences in bone quality at the mid-diaphysis of the femur during pediatric growth translate into differences in mechanical properties. Here, strength and stiffness increased with age (Supplemental Fig. S8), such that the mechanical resistance of the fetal/infantile bone tissue was found to be significantly lower than the 2- to 14-year-old cases (Fig. 5*E*, *F*). Therefore, the fetal/infantile tissue is inherently weaker than the 2- to 14-year-old cases. In terms of a mechanistic explanation for the differences in mechanical resistance, we used synchrotron SAXS/WAXD measurements to investigate deformation in the collagen fibril and mineral, which are responsible for generating bone strength and stiffness. Our results show that the collagen fibrils deform similarly in all cases but that the contribution of the mineral to deformation increases with age (Fig. 5*D*, *H*; Supplemental Fig. S8); in the 2- to 14-year-old cases, the mineral has a greater contribution to deformation than in fetal/infantile cases (ie, greater mineral-strain to tissue-strain ratio). Changes in bone quality due to aging or disease are known to directly affect bone's mechanical resistance and ultimately fracture risk.[6–9] Here, we observed differences in bone volume fraction, collagen fiber orientation, and mineralization distribution between the fetal/infantile and 2- to 14-year-old cases. Mechanistically, the fetal/infantile bone tissue is inherently weaker because it consists of woven bone tissue (rather than osteonal lamellar bone; Fig. 1), which has overall a lower mean mineralization (Figs. 2*F*, 3*E*) and less longitudinally oriented collagen fibers (Fig. 1*K*).

Lower mean mineralization in the fetal/infantile cases translates into a lower modulus tissue (Fig. 5*E*). Previous studies on pathologic or callus tissue, which consists of woven bone, have shown a correspondingly lower modulus and hardness than healthy lamellar tissue.[8,44,53] Stiffness and strength result from the bone's inherent resistance to stretching and sliding of molecular level bonds. The "brittle, reinforcing" mineral phase has a higher stiffness and strength than the organic phase. Therefore, in bone, the stiffness and strength increase as the density of mineral gradually increases.[56]

Even though differences in collagen deformation were not observed with SAXS, the collagen fiber organization and orientation are critical to mechanical resistance; in particular, longitudinally oriented collagen is highly advantageous for resisting tensile loads.[57] Thus, even though similar deformation was observed in the collagen fibers at all ages (Fig. 5*C*), the 2- to 14-year-old cases have a higher percentage of collagen fibers oriented longitudinally (Fig. 1*K*) and thus the bone in these cases is better oriented to resist tensile deformation. Furthermore, the lamellar interfaces in the osteonal microscale structure of bone have been shown to resist crack growth by deflecting and bridging cracks.[21,22] However, areas of disorganized woven bone in Paget's disease of bone are unable to

deflect and bridge cracks.[8] Thus, the lack of lamellar surfaces in primary bone could limit the sacrificial bonding or microcracking to absorb energy during loading.[19,58] Thus, the micronscale bone structure of the fetal/infantile bone tissue has less mechanical resistance than the 2- to 14-year-old cases because of the unorganized collagen structure present in primary bone versus the highly oriented collagen fibers present in the remodeled osteons. Our mechanical data suggest a transition in the mechanical behavior with age (Supplemenal Fig. S8). The transition of the mechanical behavior seems to be mainly driven by mineral distribution (Supplemental Figs. S6*E*, S7*D*, S8) and the collagen orientation (Supplemental Fig. S5*G*). OV/BV and Ot.Lc.Ar (Supplemental Fig. S5*B*, *E*) do reflect the metabolic reorganization of the tissue with respect to aging and loading.

Our analysis used high-resolution materials science–based methods to quantify changes in the structure and mechanical properties of a rare pediatric cohort. However, the study design is a cross-sectional comparison of different individuals. Therefore, unknown interindividual differences (eg, genetic, variable growth/maturation, pre-/postpubertal growth stage, or environmental factors) may be affecting some of the observed differences. Second, the exact timing of endochondral ossification, modeling, and remodeling events as well as the specific timing of the transition to superior bone quality cannot be accurately assessed here due to the limited sample size and interindividual variability in young cohorts. Future work would try to represent all phases of growth at the mid-diaphysis as well as at the metaphyseal/epiphyseal ends near the growth plate with both sexes to understand age- and maturity-related variability.

In light of these limitations, our results show that the age of one to 2 years is a critical time for building strength and stiffness in the femoral mid-diaphysis. This change in bone structure and bone quality between one to 2 years of age coincides with walking in humans, which creates new mechanical demands on the femoral diaphysis of infants. Indeed, in addition to the effects of genetic and hormonal factors on skeletal development, mechanobiological signals and muscular forces play a critical role in determining bone size and shape.[47,59]

Fracture incidence is high in children/adolescents and in the elderly. Although fracture risk in the elderly occurs due to imbalances in bone remodeling, a different mechanism may be at play in children. In particular, the pubertal growth spurt in humans coincides with a decrease in areal bone mineral density (aBMD) and peak fracture incidence, with the most common fracture site being the distal forearm; thus, it has been suggested that the growth spurt may result in a transitory weakness in the skeleton.[11,13,16,17,60] Our results suggest that bone formed through endochondral ossification is mechanically weaker than remodeled bone because of its woven bone structure and lower mean mineralization. In particular, the high incidence of distal forearm fractures in children/adolescents could relate to the formation of low-quality bone (ie, woven microstructure, low bone volume fraction, low mean mineralization) adjacent to the growth plate, creating a mechanically weak zone. However, further work here is needed to confirm that primary bone at the distal forearm persists in children and/or adolescents, especially during peak growth periods, and results in increased fracture incidence.

In summary, during skeletal growth, ossification, modeling, and remodeling processes are actively elongating and shaping the bones that will eventually compose the mature skeleton. Here, at the femoral mid-diaphysis, we observed differences in bone quality; in fetal/infantile cases, the bone tissue consists of a scaffold-like structure of woven bone with high osteocyte lacunar density and size produced by endochondral ossification, whereas in the 2- to 14-year-old cases, remodeling of the bone structure results in a highly organized lamellar structure with a greater mean mineralization and bone volume fraction. We find that these dramatic changes in bone quality around one to 2 years of age leads to greater mechanical resistance, as collagen fibrils are better aligned to resist tensile forces and more mineral is present to reinforce the collagen scaffold. Thus, these results highlight the inherent low bone quality and mechanical weakness of the fetal/infantile skeleton. Furthermore, endochondral ossification may produce a similarly weak, low-quality bone structure at skeletal sites near growth plates (ie, proximal/distal ends of long bones).

Disclosures

All authors state that they have no conflicts of interest.

Acknowledgments

This project was supported by the Alexander von Humboldt Foundation and the German Research Foundation (DFG) under grant no. BU 2562/3-1/5-1. We acknowledge travel grants provided by the International Affairs, Strategy, and Partnership office of the University of Hamburg. We acknowledge use of the X-ray synchrotron beamline 7.3.3 at the Advanced Light Source at Lawrence Berkeley National Laboratory, which is funded by the Office of Science of the US Department of Energy under contract no. DE-AC02-05CH11231. We also acknowledge use of the beamline ID 10 at the European Synchrotron Radiation Facility. We thank Jerome Kieffer from the ESRF data analysis unit for acceleration of the phase retrieval program. Felix Schmidt acknowledges the Joachim Herz Foundation for a PhD scholarship in cooperation with the PIER Helmholtz Graduate School, University of Hamburg and DESY Hamburg.

Authors' roles: EAZ and BB designed the experiment. EAZ, CR, FNS, KES, YC, ES, BG, FZ, MA, ROR, and BB performed experiments, analyzed data, and interpreted the results. KP performed autopsies. YC, ES, EV, FZ, MA, and ROR contributed experimental tools, technical support, and conceptual advice. EAZ and BB wrote the manuscript. All authors revised the manuscript critically and approved the final version. BB and EAZ takes responsibility for the integrity of the data analysis.

References

1. Burr DB. Bone quality: understanding what matters. J Musculoskelet Neuronal Interact. 2004;4(2):184–6.
2. Zimmermann EA, Busse B, Ritchie RO. The fracture mechanics of human bone: influence of disease and treatment. Bonekey Rep. 2015;4:743.
3. Zebaze RMD, Ghasem-Zadeh A, Bohte A, et al. Intracortical remodelling and porosity in the distal radius and post-mortem femurs of women: a cross-sectional study. Lancet. 2010;375(9727):1729–36.

4. Karasik D, Rivadeneira F, Johnson ML. The genetics of bone mass and susceptibility to bone diseases. Nat Rev Rheumatol. 2016;12: 323–34.
5. Dempster DW, Compston JE, Meunier PJ. Bone histomorphometry and bone quality. Osteoporos Int. 2009;20(3):243–4.
6. Busse B, Bale HA, Zimmermann EA, et al. Vitamin D deficiency induces early signs of aging in human bone, increasing the risk of fracture. Sci Transl Med. 2013;5(193):193ra88.
7. Zimmermann EA, Schaible E, Bale H, et al. Age-related changes in the plasticity and toughness of human cortical bone at multiple length scales. Proc Natl Acad Sci USA. 2011;108(35):14416–21.
8. Zimmermann EA, Köhne T, Bale HA, et al. Modifications to nano- and microstructural quality and the effects on mechanical integrity in Paget's disease of bone. J Bone Miner Res. 2015;30(2):264–73.
9. Carriero A, Zimmermann EA, Paluszny A, et al. How tough is brittle bone? Investigating osteogenesis imperfecta in mouse bone. J Bone Miner Res. 2014;29(6):1392–401.
10. Donaldson LJ, Reckless IP, Scholes S, Mindell JS, Shelton NJ. The epidemiology of fractures in England. J Epidemiol Community Health. 2008;62(2):174–80.
11. Cooper C, Dennison EM, Leufkens HG, Bishop N, van Staa TP. Epidemiology of childhood fractures in Britain: a study using the general practice research database. J Bone Miner Res. 2004;19(12): 1976–81.
12. Landin L, Nilsson BE. Bone mineral content in children with fractures. Clin Orthop Rel Res. 1983;178:292–6.
13. Hedström EM, Svensson O, Bergström U, Michno P. Epidemiology of fractures in children and adolescents. Acta Orthop. 2010;81(1): 148–53.
14. Tiderius CJ, Landin L, Düppe H. Decreasing incidence of fractures in children: an epidemiological analysis of 1,673 fractures in Malmö, Sweden, 1993–1994. Acta Orthop Scand. 1999;70(6):622–6.
15. Goulding A, Cannan R, Williams SM, Gold EJ, Taylor RW, Lewis-Barned NJ. Bone mineral density in girls with forearm fractures. J Bone Miner Res. 1998;13(1):143–8.
16. Faulkner RA, Davison KS, Bailey DA, Mirwald RL, Baxter-Jones AD. Size-corrected BMD decreases during peak linear growth: implications for fracture incidence during adolescence. J Bone Miner Res. 2006;21(12):1864–70.
17. Bailey DA, Wedge JH, McCulloch RG, Martin AD, Bernhardson SC. Epidemiology of fractures of the distal end of the radius in children as associated with growth. J Bone Joint Surg Am. 1989;71(8): 1225–31.
18. Poundarik AA, Diab T, Sroga GE, et al. Dilatational band formation in bone. Proc Natl Acad Sci USA. 2012;109(47):19178–83.
19. Fantner GE, Hassenkam T, Kindt JH, et al. Sacrificial bonds and hidden length dissipate energy as mineralized fibrils separate during bone fracture. Nat Mater. 2005;4(8):612–6.
20. Gupta HS, Wagermaier W, Zickler GA, et al. Nanoscale deformation mechanisms in bone. Nano Lett. 2005;5(10):2108–11.
21. Koester KJ, Ager JW, Ritchie RO. The true toughness of human cortical bone measured with realistically short cracks. Nat Mater. 2008;7(8):672–7.
22. Nalla RK, Kinney JH, Ritchie RO. Mechanistic fracture criteria for the failure of human cortical bone. Nat Mater. 2003;2(3):164–8.
23. Scherft JP. Beginning endochondral ossification in embryonic mouse radii. J Ultrastruct Res. 1973;42(3):342–53.
24. Salle BL, Rauch F, Travers R, Bouvier R, Glorieux FH. Human fetal bone development: histomorphometric evaluation of the proximal femoral metaphysis. Bone. 2002;30(6):823–8.
25. Buckwalter JA, Glimcher MJ, Cooper RR, Recker R. Bone biology. J Bone Joint Surg Am. 1995;77(8):1276–89.
26. Rauch F. The dynamics of bone structure development during pubertal growth. J Musculoskelet Neuronal Interact. 2012;12(1):1–6.
27. Seeman E. Periosteal bone formation—a neglected determinant of bone strength. N Engl J Med. 2003;349(4):320–3.
28. Rauch F, Neu C, Manz F, Schoenau E. The development of metaphyseal cortex. Implications for distal radius fractures. during growth. J Bone Miner Res. 2001;16:1547–55.
29. Seeman E, Ghasem-Zadeh A. Challenges in the acquisition and analysis of bone microstructure during growth. J Bone Miner Res. 2016;31(12):2239–41.
30. Püschel K. Lehre und Forschung an Verstorbenen. Rechtsmedizin. 2016;26(2):115–9.
31. Dempster DW, Compston JE, Drezner MK, et al. Standardized nomenclature, symbols, and units for bone histomorphometry: a 2012 update of the report of the ASBMR Histomorphometry Nomenclature Committee. J Bone Miner Res. 2013;28(1):2–17.
32. Kulak CAM, Dempster DW. Bone histomorphometry: a concise review for endocrinologists and clinicians. Arq Bras Endocrinol Metab. 2010;54(2):87–98.
33. Goldman HM, Bromage TG, Thomas CDL, Clement JG. Preferred collagen fiber orientation in the human mid-shaft femur. Anat Rec A. 2003;272(1):434–45.
34. Boyde A, Riggs CM. The quantitative study of the orientation of collagen in compact bone slices. Bone. 1990;11(1):35–9.
35. Skedros JG, Mason MW, Nelson MC, Bloebaum RD. Evidence of structural and material adaptation to specific strain features in cortical bone. Anat Rec. 1996;246(1):47–63.
36. Bromage TG, Goldman HM, McFarlin SC, Warshaw J, Boyde A, Riggs CM. Circularly polarized light standards for investigations of collagen fiber orientation in bone. Anat Rec B. 2003;274(1):157–68.
37. Koehne T, Vettorazzi E, Küsters N, et al. Trends in trabecular architecture and bone mineral density distribution in 152 individuals aged 30–90 years. Bone. 2014;66:31–8.
38. Boskey A, Pleshko Camacho N. FT-IR imaging of native and tissue-engineered bone and cartilage. Biomaterials. 2007;28(15):2465–78.
39. Farlay D, Panczer G, Rey C, Delmas PD, Boivin G. Mineral maturity and crystallinity index are distinct characteristics of bone mineral. J Bone Miner Metab. 2010;28(4):433–45.
40. Hexemer A, Bras W, Glossinger J, et al. A SAXS/WAXS/GISAXS beamline with multilayer monochromator. J Phys Conf Ser. 2010;247(1):12007.
41. Zimmermann EA, Gludovatz B, Schaible E, et al. Mechanical adaptability of the Bouligand-type structure in natural dermal armour. Nat Commun. 2013;4:2634.
42. Ilavsky J. Nika: software for two-dimensional data reduction. J Appl Cryst. 2012;45(2):324–8.
43. Chushkin Y, Zontone F, Lima E, et al. Three-dimensional coherent diffractive imaging on non-periodic specimens at the ESRF beamline ID10. J Synchrotron Radiat. 2014;21(3):594–9.
44. Hoerth RM, Seidt BM, Shah M, et al. Mechanical and structural properties of bone in non-critical and critical healing in rat. Acta Biomater. 2014;10:4009–19.
45. Holguin N, Brodt MD, Sanchez ME, Silva MJ. Aging diminishes lamellar and woven bone formation induced by tibial compression in adult C57Bl/6. Bone. 2014;65:83–91.
46. Bortel EL, Duda GN, Mundlos S, Willie BM, Fratzl P, Zaslansky P. Long bone maturation is driven by pore closing: a quantitative tomography investigation of structural formation in young C57BL/6 mice. Acta Biomater. 2015;22:92–102.
47. Sharir A, Stern T, Rot C, Shahar R, Zelzer E. Muscle force regulates bone shaping for optimal load-bearing capacity during embryogenesis. Development. 2011;138(15):3247–59.
48. Portigliatti Barbos M, Bianco P, Ascenzi A, Boyde A. Collagen orientation in compact bone: II. Distribution of lamellae in the whole of the human femoral shaft with reference to its mechanical properties. Metab Bone Dis Res Res. 1984;5(6):309–15.
49. Fratzl-Zelman N, Roschger P, Misof BM, et al. Normative data on mineralization density distribution in iliac bone biopsies of children, adolescents and young adults. Bone. 2009;44(6):1043–8.
50. Currey JD, Brear K, Zioupos P. The effects of ageing and changes in mineral content in degrading the toughness of human femora. J Biomech. 1996;29(2):257–60.
51. Currey JD, Butler G. The mechanical properties of bone tissue in children. J Bone Joint Surg. 1975;57(6):810–4.
52. Skedros JG, Bloebaum RD, Bachus KN, Boyce TM, Constantz B. Influence of mineral content and composition on graylevels in

backscattered electron images of bone. J Biomed Mater Res. 1993;27(1):57–64.

53. Manjubala I, Liu Y, Epari DR, et al. Spatial and temporal variations of mechanical properties and mineral content of the external callus during bone healing. Bone. 2009;45:185–92.
54. Boskey AL, Coleman R. Aging and bone. J Dent Res. 2010;89(12): 1333–48.
55. Lynch ME, Main RP, Xu Q, et al. Tibial compression is anabolic in the adult mouse skeleton despite reduced responsiveness with aging. Bone. 2011;49(3):439–46.
56. Landis WJ, Librizzi JJ, Dunn MG, Silver FH. A study of the relationship between mineral content and mechanical properties of turkey gastrocnemius tendon. J Bone Miner Res. 1995;10(6):859–67.
57. Wagermaier W, Gupta HS, Gourrier A, Burghammer M, Roschger P, Fratzl P. Spiral twisting of fiber orientation inside bone lamellae. Biointerphases. 2006;1(1):1.
58. Zimmermann EA, Ritchie RO. Bone as a structural material. Adv Healthcare Mater. 2015;4(9):1287–304.
59. Nowlan NC, Bourdon C, Dumas G, Tajbakhsh S, Prendergast PJ, Murphy P. Developing bones are differentially affected by compromised skeletal muscle formation. Bone. 2010;46(5): 1275–85.
60. Landin LA. Fracture patterns in children. Analysis of 8,682 fractures with special reference to incidence, etiology and secular changes in a Swedish urban population 1950-1979. Acta Orthop Scand Suppl. 1983;202:1–109.

9.2. Publication 2

ACS Nano. 2021 Jan 26;15(1):455-467. doi: 10.1021/acsnano.0c04786. Epub 2021 Jan 6.

Collagen Fiber Orientation is Coupled with Specific Nano-Compositional Patterns in Dark and Bright Osteons Modulating Their Biomechanical Properties

Kilian E. Stockhausen [1], Mahan Qwamizadeh [1], Eva M. Wölfel [1,3,4], Haniyeh Hemmatian [1], Imke A. K. Fiedler [1,3], Silja Flenner [2], Elena Longo [2], Michael Amling [1], Imke Greving [2], Robert O. Ritchie [5], Felix N. Schmidt [1,3,§], Björn Busse [1,4,5,§]

[1] Department of Osteology and Biomechanics, University Medical Center, Lottestr. 55a, 22529, Hamburg, Germany

[2] Institute of Materials Research, Helmholtz-Zentrum Geesthacht, Max-Planck-Straße 1, 21502, Geesthacht, Germany

[3] Forum Medical Technology Health Hamburg (FMTHH), Butenfeld 34, 22529, Hamburg, Germany

[4] Interdisciplinary Competence Center for Interface Research (ICCIR), Martinistr. 52, 20251, Hamburg, Germany

[5] Materials Sciences Division, Lawrence Berkeley National Laboratory, 1 Cyclotron Road, Berkeley CA 94720, USA

[§] Contributed equally

ACS NANO

www.acsnano.org

ARTICLE

Collagen Fiber Orientation Is Coupled with Specific Nano-Compositional Patterns in *Dark* and *Bright* Osteons Modulating Their Biomechanical Properties

Kilian E. Stockhausen, Mahan Qwamizadeh, Eva M. Wölfel, Haniyeh Hemmatian, Imke A. K. Fiedler, Silja Flenner, Elena Longo, Michael Amling, Imke Greving, Robert O. Ritchie, Felix N. Schmidt,[#] and Björn Busse[*,#]

Cite This: *ACS Nano* 2021, 15, 455–467

Read Online

ACCESS | Metrics & More | Article Recommendations | Supporting Information

ABSTRACT: **Bone continuously adapts to its mechanical environment by structural reorganization to maintain mechanical strength. As the adaptive capabilities of bone are portrayed in its nano- and microstructure, the existence of *dark* and *bright* osteons with contrasting preferential collagen fiber orientation (longitudinal and oblique-angled, respectively) points at a required tissue heterogeneity that contributes to the excellent fracture resistance mechanisms in bone. *Dark* and *bright* osteons provide an exceptional opportunity to deepen our understanding of how nanoscale tissue properties influence and guide fracture mechanisms at larger length scales. To this end, a comprehensive structural, compositional, and mechanical assessment is performed using circularly polarized light microscopy, synchrotron nanocomputed tomography, focused ion beam/scanning electron microscopy, quantitative backscattered electron imaging, Fourier transform infrared spectroscopy, and nanoindentation testing. To predict how the mechanical behavior of osteons is affected by shifts in collagen fiber orientation, finite element models are generated. Fundamental disparities between both osteon types are observed: *dark* osteons are characterized by a higher degree of mineralization along with a higher ratio of inorganic to organic matrix components that lead to higher stiffness and the ability to resist plastic deformation under compression. On the contrary, *bright* osteons contain a higher fraction of collagen and provide enhanced ductility and energy dissipation due to lower stiffness and hardness.**

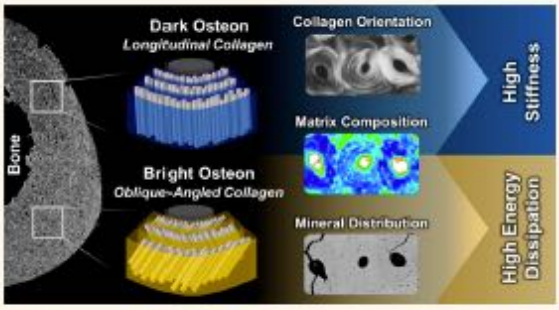

KEYWORDS: *bone, osteon, collagen fiber orientation, mineral aggregates, biomechanics*

During bone remodeling, cortical bone is continuously reorganized in response to mechanical stimuli to ensure adequate bone quality on all hierarchical levels.[1,2] In this process, osteoclasts remove bone tissue and void volumes are subsequently filled in by osteoblasts with new bone matrix to form osteons.[3] Osteons are the basic structural unit of cortical bone and consist of concentric lamellar structures surrounding a central Haversian canal. While osteons are predominantly oriented parallel to the long axis of the bone, the orientation of collagen fibers within individual lamellae can differ considerably leading to a number of proposed models over the years.[4−8] While no universal model for the collagen arrangement in bone exists, an impact of preferentially aligned collagen fibers and bone mineral particles on the biomechanical function is postulated. The collagen fibers are reinforced by bone mineral particles to form a spatially related composite material where the mineral long axis is coaligned with the collagen fibers that provides bone its unique mechanical properties.[9,10] More recently, the understanding of mineral and collagen assembly has advanced with

Received: June 8, 2020
Accepted: December 11, 2020
Published: January 6, 2021

https://dx.doi.org/10.1021/acsnano.0c04786
ACS Nano 2021, 15, 455−467

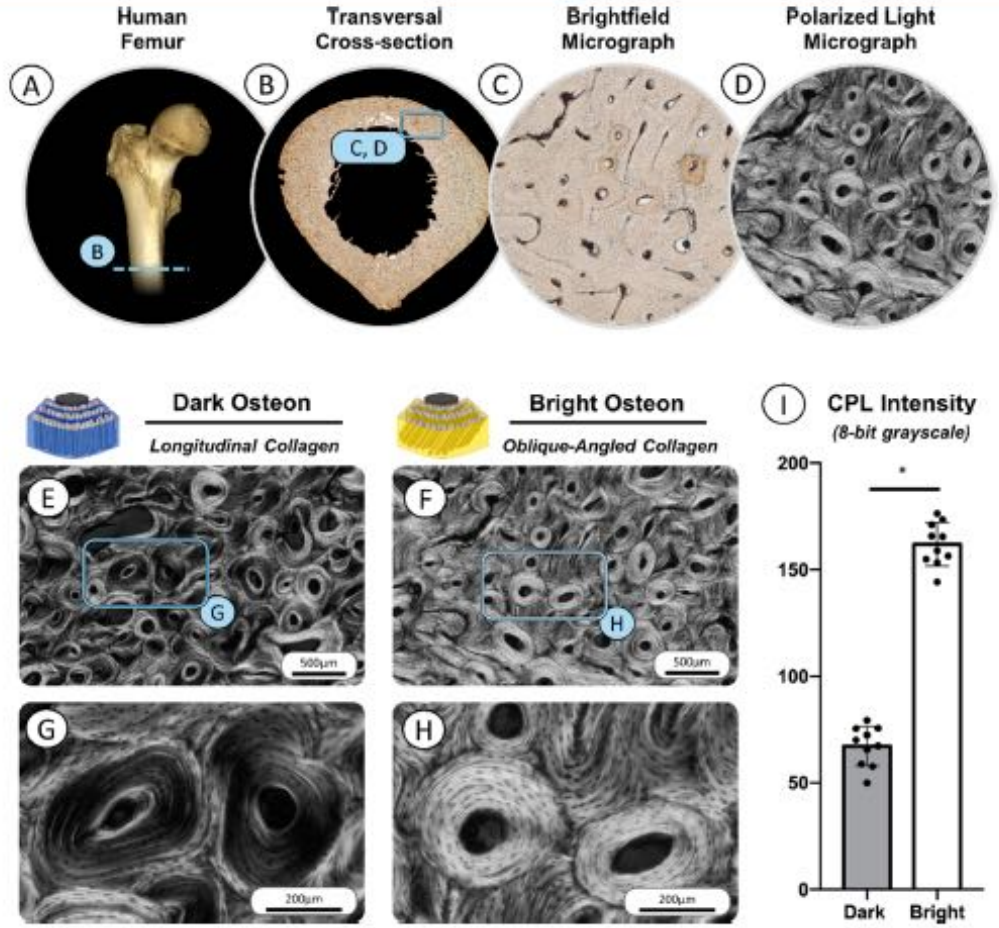

Figure 1. (A, B) Femoral bone was obtained during autopsy, and cross sections were cut from the mid-diaphysis. (C) At the microstructural level, femoral cortical bone is composed of secondary remodeled osteons surrounded by interstitial bone. (D) Preferential collagen fiber orientation (CFO) remains hidden under brightfield microscopy but can be visualized using circularly polarized light microscopy (CPL): osteons composed of oblique orientated collagen fibers appear bright, while osteons composed of collagen fibers parallel with the osteon axis appear dark.[48] (E–H) CPL was used to identify 20 osteons of contrasting preferential CFO for subsequent assessment. (I) Brightness of the masked CPL images reflects the predominant collagen fiber orientation.

studies showing that bone mineral is fractal-like and hierarchically assembled at the nanoscale[11] and that localized differences between the orientation of mineral nanocrystals and collagen fibrils exist within single lamellae that might add an additional layer of mechanical adaptation toward compressive loading.[12]

During skeletal growth and throughout life, the mechanical behavior of bone is closely correlated to its structure and composition, even though the mechanical properties in juvenile bone are explained by different intrinsic properties compared to adult bone.[13,14] In health, bone is able to withstand complex physiological loading patterns by capable fracture resistance mechanisms, both intrinsic and extrinsic.[15–17] Many factors guide the fracture resistance of bone including the structural integrity on the nano- and microscale, the bone mineral density distribution, the mineral quality, and the accumulation of microcracks.[18–21] This extends to the organic part of the matrix where alterations in collagen quality have been shown to have an adverse effect on the mechanical competence.[22–24] The importance of collagen for fracture resistance is emphasized by clinically challenging disorders like osteogenesis imperfecta or Paget's disease, both of which are characterized by impaired collagen formation and organization leading to increased fracture susceptibility.[25–27] Additionally, the orientation of collagen fibers is considered as an contributor to bone's ability to resist fracture.[28,29] When viewed under polarized light, the predominant collagen fiber orientation (CFO) can be quantified; osteons composed of oblique orientated collagen fibers appear bright, while osteons composed of collagen fibers parallel to the osteon axis appear dark.[30,31] Structurally, *bright* osteons are characterized by predominant CFOs of ±45° with respect to the osteon axis, whereas *dark* osteons are distinguished by longitudinal collagen fibers.[31]

So far, most studies seized on the idea that *dark* osteons are better able to resist tensile forces and bending while *bright* osteons, assembled of oblique-angled collagen fibrils, can better withstand compressive forces and torsion.[32,33] It was proposed that the collagen fiber organization is an excellent predictor of cortical bone strength and that the distribution

https://dx.doi.org/10.1021/acsnano.0c04786
ACS Nano 2021, 15, 455–467

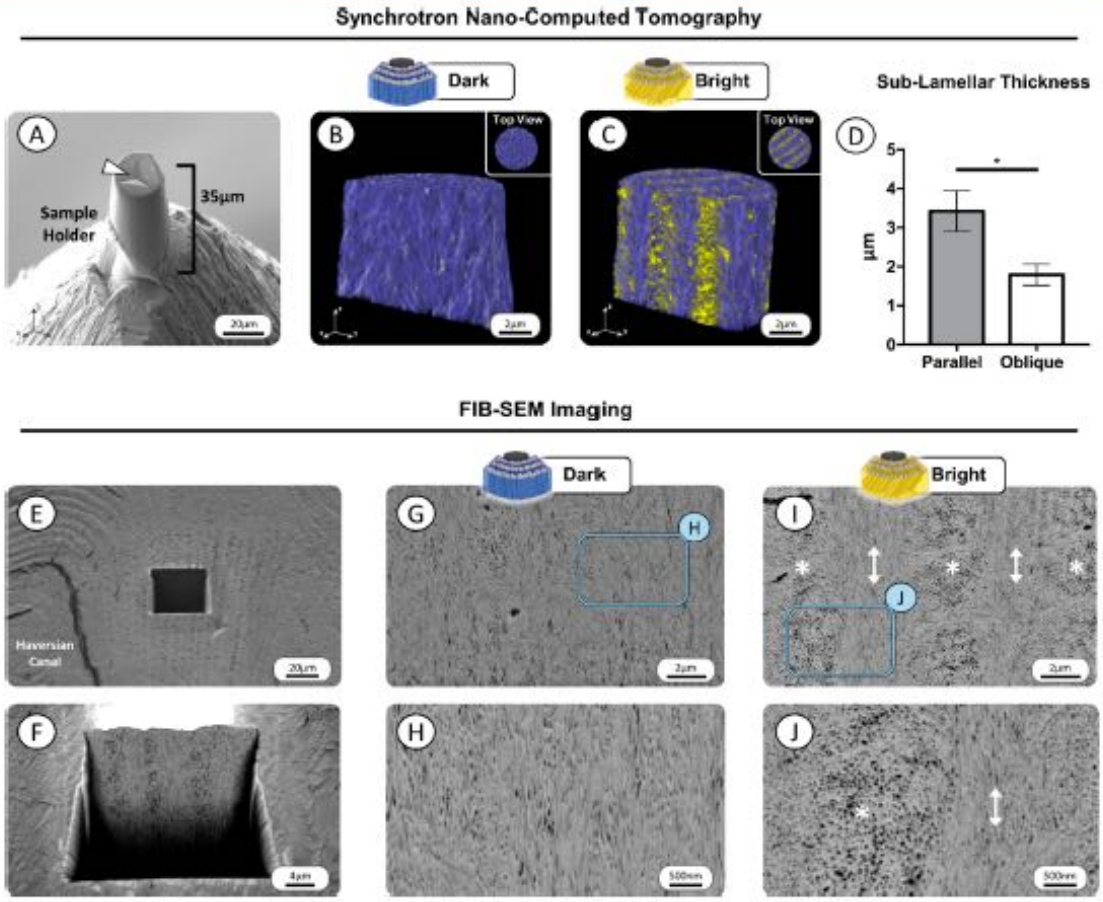

Figure 2. (A) Using FIB-SEM, cylindrical bone volumes below the nanoindentations (white arrow) were extracted. (B) Using synchrotron nanocomputed tomography with Zernike phase contrast the nanoscale collagen orientation is visualized. Structurally rather homogeneous, collagen fibers run predominantly parallel to the long axis in *dark* osteons. (C) In *bright* osteons, a lamellar pattern of volumes being composed of parallel fibers (blue) and oblique-angled fibers (yellow) with respect to the osteon axis becomes evident. (D) Parallel-fibered lamellae were found to be significantly thicker compared to lamellae composed of oblique-angled fibers. (E, F) FIB-SEM imaging was used to visualize the internal structure within *dark* and *bright* osteons. (E, H) Transversely oriented trenches were milled into the osteon to expose an imaging plane with radial-longitudinal orientation with respect to the Haversian canal. (G, H) Consistent with the tomography findings, *dark* osteons are characterized by collagen fibers running predominantly parallel to the long axis. (I, J) *Bright* osteons display the characteristic lamellar pattern with fibrils being oriented parallel (double-headed arrows) and oblique-angled to the analyzed plane (asterisk). The sublamellar thicknesses conform with the values reported in (D).

pattern of both osteon types, neglecting the degree of mineralization, corresponds to that of the loading forces acting on the bone.[34−36] In quadrupedal mammalians, where angulation of the joints leads to significant bending stresses,[37,38] the distribution of *dark* and *bright* osteons coincides with the distribution of tensile and compressive stresses.[39−41] The dependency of population densities of distinct osteon types with specific loading modes suggests that collagen fibers align according to specific strain modes and serve different mechanical functions.[42−44] However, in bipedal human femoral bone, the diaphysis is primarily loaded in compression with little impact of bending and tensile forces.[45−47] In view of this rather uniform loading scenario, spatial changes in the preferential CFO of osteons might serve further mechanical functions beyond the resistance to tensile and compressive stresses indicating a more profound mechanical function of *dark* and *bright* osteons. This is further supported by the fact that, even though the overall CFO pattern appeared nonrandomly distributed, no single pattern of CFO was found to exist in the human diaphyseal femur, suggesting that the microstructure is sensitive to individual adaptation.[30] In this study, we aim to reinterpret the role of *dark* and *bright* osteons in bone that is predominantly under compression to elucidate the necessity of both types to coexist within the femoral diaphysis.

While the structural properties of *dark* and *bright* osteons have been studied in the past, the composition and its impact on mechanical properties are still unknown. As bone derives its strength and toughness from its hierarchical assembly, *dark* and *bright* osteons provide an exceptional opportunity to deepen our understanding of how nanoscale tissue properties influence and guide fracture mechanisms at larger length scales. To this end, we applied synchrotron nanocomputed tomography, quantitative backscattered electron imaging

https://dx.doi.org/10.1021/acsnano.0c04786
ACS Nano 2021, 15, 455−467

(qBEI), focused ion beam milling combined with scanning electron microscopy (FIB-SEM), Fourier transform infrared spectroscopy (FTIR), and nanoindentation testing to assess the structure, composition and biomechanical properties of 20 *dark* and *bright* osteons. In order to predict how the preferential CFO affects the biomechanical behavior of bone on the overlying hierarchical levels, finite element models are generated. We hypothesize that osteons with contrasting types of preferential CFO (oblique-angled *versus* longitudinal) present with distinct differences in compositional and local biomechanical properties. Despite the compression-dominant loads present in the femur, this would indicate that individual osteons are highly sensitive to their mechanical surrounding and serve different mechanical functions providing bone locally with more stiffness or ductility where needed.

RESULTS AND DISCUSSION

As the adaptive capabilities of bone to the mechanical environment are portrayed in its microstructure and composition, the existence of *dark* and *bright* osteons with contrasting predominant CFO types points at a required heterogeneity of the tissue matrix beneficial for the unique properties of bone. To unravel the necessity of both types of osteons to exist within the femoral diaphysis we comprehensively assess the structure, composition, and mechanical properties of *dark* osteons composed of collagen fibers running parallel to the long axis and *bright* osteons predominantly built from oblique-angled fibers. In the human femoral mid-diaphysis, circularly polarized light microscopy (CPL) was employed to identify and quantify the preferential CFO of individual osteons that remains hidden under brightfield microscopy (Figure 1A–D). Increasing brightness corresponds to a shift in predominant CFO toward more oblique-angled collagen fibers (Figure 1E–H). Quantitative analysis in individual osteons excluding the Haversian canal area consistently shows significantly higher brightness in *bright* compared to *dark* osteons (67.22 ± 9.31 *versus* 162.00 ± 10.17, $p < 0.001$) (Figure 1I). The marked differences in brightness values obtained by CPL highlight fundamental structural variations in terms of the predominant CFO between different osteons within the same individual. Comparing undecalcified and decalcified ground sections in terms of CPL brightness, it was found that both samples displayed similar brightness values independent of the mineralization state (Figure S1). This clearly shows that the changes in CPL brightness are attributable to orientation shifts of optically anisotropic collagen and are not affected by the mineralization profile of individual osteons.

The changes in CFO, as detected by CPL, are verified using synchrotron nanocomputed tomography with Zernike phase contrast and FIB-SEM imaging (Figure 2). Utilizing phase contrast, phase variations of the beam propagating through the bone specimen can be visualized allowing for the assessment of the spatial organization of collagen fibers.[49,50] In the three-dimensional visualization obtained, it was found that in *dark* osteons collagen fibers indeed run parallel with the long axis of the bone (Figure 2B). No transition between neighboring lamellae is visible supporting the reported view that *dark* osteons are structurally rather homogeneous.[31] On the other hand, *bright* osteons display a considerable degree of heterogeneity within its CFO. Here, a distinct lamellar pattern with changing CFO is present similar to the proposed plywood structural models of osteons. (Figure 2C and Supporting Information videos 1 and 2). An arching of collagen fibers is observed with fiber angles ranging from +90 to −90° with respect to the long axis of the osteons where the longitudinally oriented fraction of collagen fibers corresponds to the darkened lamellae of the otherwise *bright* osteon under CPL. The thickness of the lamellae composed of longitudinally oriented collagen fibers was found to be significantly higher compared to lamellae built from oblique-angled fibers (3.42 ± 0.55 μm *versus* 1.79 ± 0.27 μm, $p < 0.001$) (Figure 2D) which is consistent with previous studies.[51] The structural organization is further validated by FIB-SEM imaging where transversely oriented trenches were milled into the osteon to expose the internal matrix organization (Figure 2E,F). Here, a higher degree of CFO homogeneity was observed in *dark* osteons with collagen fibers running predominantly parallel to the long axis. In agreement with the nanocomputed tomography findings and consistent with previously published data,[52] *bright* osteons are composed of lamellae with oblique-angled collagen fibers that are bordered by lamellae built from parallel-oriented fibers (Figure 2G–J). Interestingly, the lamellar layout of *bright* osteons is also represented in quantitative backscattered electron images (qBEI) of transversely sectioned osteons, where individual lamellae with a thickness of ~6 μm are clearly visible whereas the lamellar pattern is hardly evident in the *dark* osteons (Figure 3A,B).

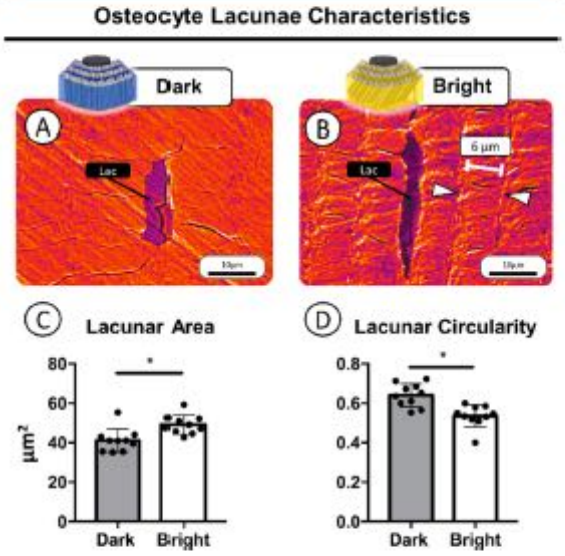

Figure 3. (A, B) Structurally, no lamellar pattern is visible in *dark* osteons whereas *bright* osteons display a lamellar pattern with ~6 μm total thickness (white arrows) around osteocyte lacunae (lac). (C, D) The osteocyte lacunar area is smaller in size in *dark* osteons and is characterized by a higher circularity index indicating a rounder shape.

Here it is important to mention that the lamellar thickness as assessed in qBEI images refers to the total thickness of a repeating unit of lamellae.[53] As visualized by nanocomputed tomography and FIB-SEM imaging, a lamellar unit contains one sublamellae of predominantly parallel-oriented and one sublamellae of oblique-angled collagen fibers. Significant variations in osteocyte lacunar area and shape between both osteon types were also measured from the acquired qBEI

https://dx.doi.org/10.1021/acsnano.0c04786
ACS Nano 2021, 15, 455–467

images. Osteocyte lacunar areas are smaller in size in *dark* osteons compared to *bright* osteons (41.17 ± 5.92 μm^2 *versus* 49.21 ± 4.83 μm^2, $p < 0.001$) and are characterized by a higher circularity index (0.631 ± 0.059 *versus* 0.536 ± 0.056, $p < 0.001$) representative of a rounder shape (Figure 3C,D). As osteoblasts are aligned with the collagen fibers they lay down during the formation phase,[54] this supports the view that the long axis of the osteocyte lacunae is aligned with the preferential CFO.[55] No difference in osteocyte lacunar density was measured between *dark* and *bright* osteons (0.00083 ± 0.00024 *versus* 0.00091 ± 0.00033 #/μm^2, $p = 0.588$). Despite the differences in osteocyte lacunar area and collagen fiber orientation, the canaliculi were found to be oriented perpendicular to the osteonal lamellae and extending radially from the central Haversian canal in both osteon types (Figure S2 and Supporting Information videos 1 and 2).

The content of mineral between the two structurally opposing types of osteons was quantified using qBEI where lower brightness values signify a lower and higher brightness values a higher mineral content (Figure 4A,B). Both qBEI histograms of *dark* and *bright* osteons present an inverse log-normal frequency distribution, but the *dark* osteons are characterized by a higher peak and a smaller tail at the low-calcium end (Figure 4C). Quantitative analysis of the qBEI histograms revealed significant differences in the mineral distribution. A higher mean calcium content (Ca_{mean}) was quantified in osteons with a predominant longitudinal collagen fiber orientation. The Ca_{mean} is 5.68% higher in *dark* osteons compared to the *bright* ones (26.25 ± 0.32 *versus* 24.84 ± 0.34 Ca wt %, $p < 0.001$) (Figure 4D). The peak calcium content (Ca_{peak}) displays the same pattern with a 5.42% higher peak mineralization in *dark* osteons (26.67 ± 0.36 *versus* 25.30 ± 0.32 Ca wt %, $p < 0.001$) (Figure 4E). In support of the higher mean and peak calcium content, *dark* osteons have a higher percentage of bone area exhibiting a high mineral content (Ca_{high} $p < 0.001$) and a lower percentage of bone area with a low mineral content (Ca_{low}, $p < 0.001$) (Figure 4F,G) compared to *bright* osteons. Overall, the qBEI data shows a higher bone mineral content in osteons with preferentially longitudinal oriented collagen fibers indicating a connection between the CFO and degree of mineralization. Since osteons undergo quick primary mineralization during remodeling followed by secondary mineralization that proceeds over longer periods of time, cortical bone presents with a heterogeneous mineralization profile.[56,57] Consequently, a higher mean calcium content usually points toward a higher tissue age and maturation.[58−60] From our findings regarding the mineralization, this would infer that *dark* osteons are on average older and more mature compared to *bright* osteons. However, this seems unlikely as this would require a continuous change in collagen fiber orientation from oblique-angled to longitudinal over time.

To assess how the higher degree of mineralization is associated with changes in the organic phase, FTIR was performed to assess the ratio of mineral-to-matrix (MMR). Here, the differences measured by qBEI are supported by the FTIR results: *dark* osteons are characterized by a higher MMR compared to *bright* osteons (3.21 ± 0.17 *versus* 2.80 ± 0.18, $p < 0.001$) which corresponds to an increase of 14.77% (Figure 5A−D). Moreover, the MMR positively correlates with the mean calcium content showing that *dark* osteons indeed contain more mineral ($r = 0.7292$, $p < 0.001$) (Figure 5E). Consistent with previous studies,[61,62] a ring of elevated MMR

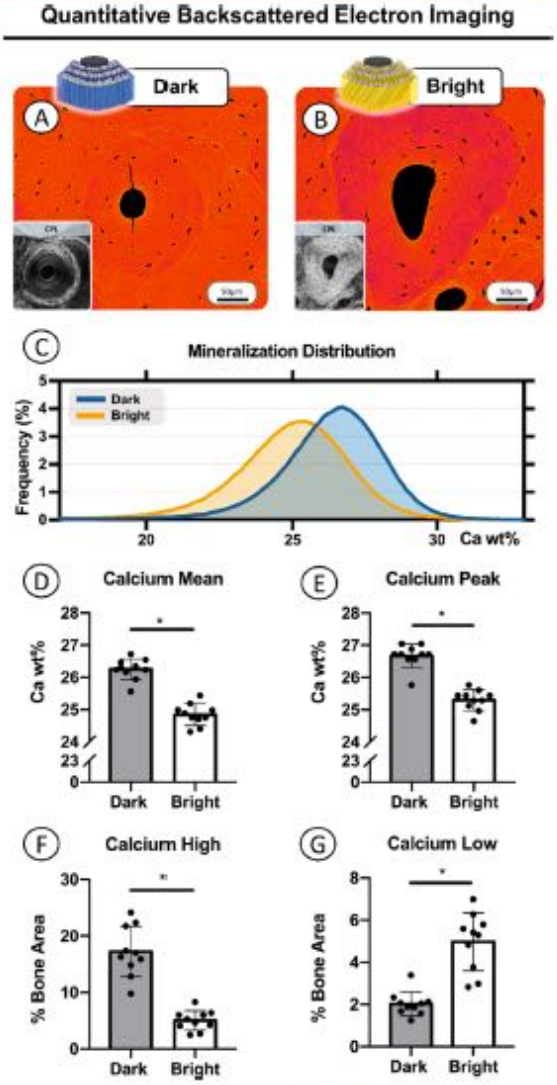

Figure 4. (A, B) Using qBEI, the mineral density is quantified. (C) Histogram analysis reveals a higher mineralization in *dark* osteons. (D, E) Both mean and peak calcium contents are increased. (F, G) Accordingly, a smaller percentage of bone area is regarded as lowly mineralized, and a higher percentage as highly mineralized.

was measured toward the center of the Haversian canal, both in *dark* and *bright* osteons. It was found that the thickness of the ring with elevated MMR correlates positively with the osteon wall thickness ($r = 0.681$, $p < 0.001$). Calculating the ratio of the high-MMR ring thickness and the osteon wall thickness revealed no statistical differences between *dark* and *bright* osteons (0.223 ± 0.037 *versus* 0.2144 ± 0.030 μm, $p = 0.603$) (Figure S3). The higher MMR was accompanied by a higher carbonate-to-phosphate ratio (CPR) in *dark* osteons (0.01463 ± 0.00044 *versus* 0.01370 ± 0.00028, 6.79% higher, $p < 0.001$) which also correlated positively with the mean calcium content ($r = 0.4914$, $p < 0.001$) (Figure 5F,G). The higher amount of carbonate substitution for phosphate in the mineral crystals is often linked to more mature and crystalline

https://dx.doi.org/10.1021/acsnano.0c04786
ACS Nano 2021, 15, 455−467

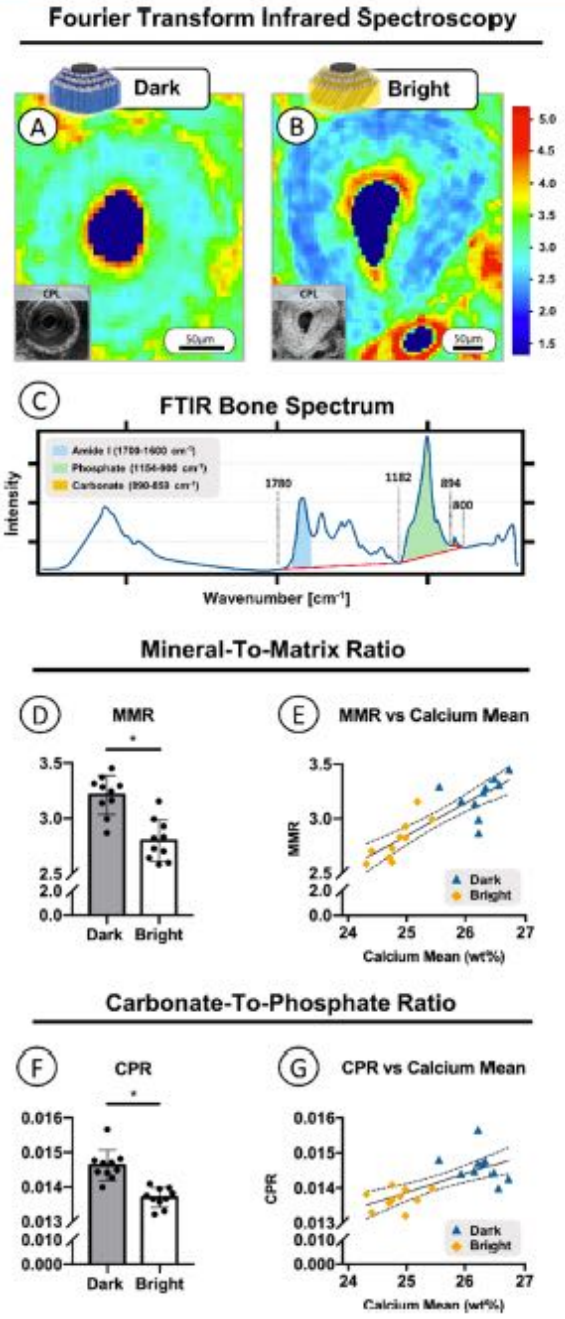

Figure 5. (A, B) Representative maps of the mineral-to-matrix ratio (MMR) of *dark* and *bright* osteons where each pixel represents individual spectra. (C, D) Differences measured by qBEI are supported by the FTIR results: *dark* osteons are characterized by a higher MMR compared to *bright* osteons, which correlates positively with the mean calcium content. (E, F) Amount of carbonate substitution for phosphate (CPR) in the mineral crystals is increased and correlates positively with the mean calcium content.

mineral crystals. In general, MMR and CPR increase with advancing age,[63,64] and regardless of developmental age, the highest CPRs are present in the oldest bone.[65,66] However, CPR may also be an indicator of mineralization speed and secondary hypermineralization[67] which points toward a favored accelerated mineralization in *dark* osteons for biomechanical purposes.

Taken together, our findings suggest that the bone matrix is sensitive to structural and compositional adaptions on the osteonal level which define its localized biomechanical competence. As the inorganic mineral phase of the bone matrix has a higher stiffness compared to the organic collagen phase, the degree and quality of mineralization is also an indicator for the mechanical competence of bone.[68−71] We speculate that the revealed differences in mineral content between *dark* and *bright* osteons are related to their specific ultrastructure and play a functional role in providing biomechanical competence rather than being a result of tissue aging.

To link the structural and compositional disparities of *dark* and *bright* osteons to the local biomechanical properties, nanoindentation testing was performed (Figure 6A,B). In agreement with the observed trends in the mineralization pattern assessed by qBEI and FTIR, both the hardness and stiffness measured *via* nanoindentation are significantly higher in *dark* osteons indicating a greater resistance to deformation. The elastic modulus was 31.05% higher in the *dark* osteons (25.28 ± 1.12 GPa *versus* 19.29 ± 1.54 GPa, $p < 0.001$) (Figure 6C). Correspondingly, the hardness was 33.33% higher in *dark* osteons compared to *bright* osteons (0.96 ± 0.08 GPa *versus* 0.72 ± 0.09 GPa, $p < 0.001$) (Figure 6D). The mean calcium content correlated positively with the elastic modulus and hardness ($r(E) = 0.885$, $r(H) = 0.788$, $p < 0.001$) (Figure 6E,F) and the preferential CFO negatively ($r(E) = 0.888$, $r(H) = 0.766$, $p < 0.001$) (Figure 6G,H).

As an interim summary, it can be noted that both types of osteons are clearly distinguished in terms of their structure, composition, and biomechanical properties. *Dark* osteons with longitudinal CFO are characterized by a higher degree of mineralization along with a higher ratio of inorganic to organic matrix components that lead to higher stiffness (higher elastic modulus) and the ability to resist plastic deformation (higher hardness). On the contrary, *bright* osteons with oblique-angled CFO contain a higher fraction of collagen and could provide enhanced ductility and energy dissipation due to lower stiffness and hardness.

Since nanoindentation testing displays biomechanical properties on the lamellar level of osteons, the mechanical behavior of *dark* and *bright* osteons itself is not fully represented. To predict how changes in CFO on the nanoscale affect the tissue-level biomechanical properties, finite element models were generated. The fundamental building blocks of the matrix, namely the mineralized collagen fibrils, were modeled as representative volume elements (RVEs) taking into account their orthotropic mechanical properties. The overlying hierarchical levels (mineralized collagen fibers, osteonal lamellae, and full osteons) were then modeled for different orientations of the collagen fibrils leading to two key findings. First, the implications of the observed structural and compositional disparities between *dark* and *bright* osteons on the mechanical properties as assessed by nanoindentation have been validated by the outcomes of the FEM models. Shifting the fiber orientation from 45° to 0° resulted in the effective

https://dx.doi.org/10.1021/acsnano.0c04786
ACS Nano 2021, 15, 455−467

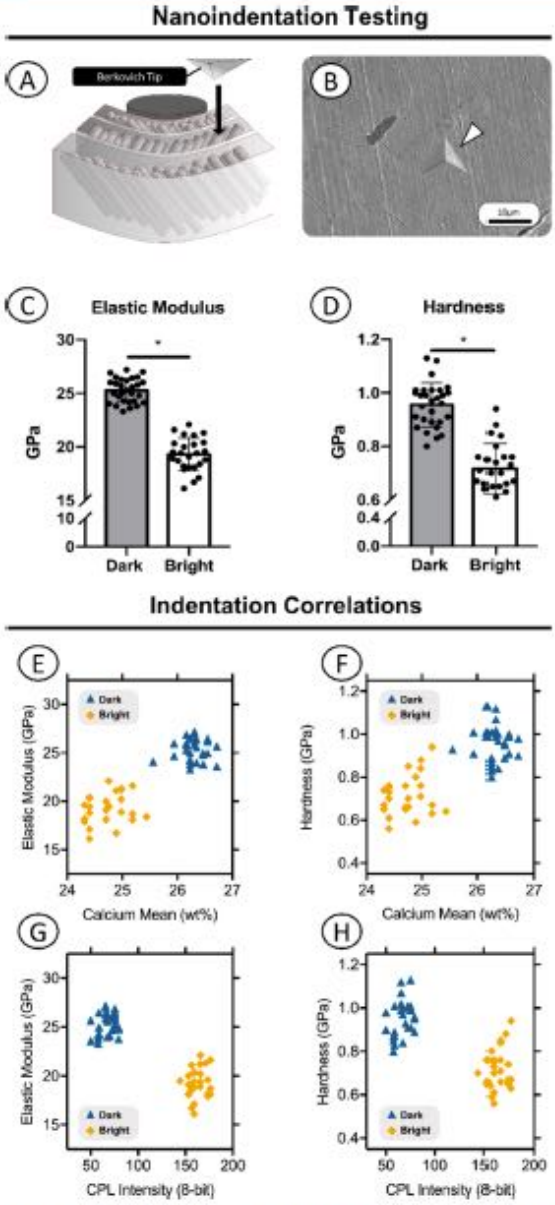

Figure 6. (A) Local biomechanical properties were assessed by nanoindentation testing and (B) successful indents were verified using electron microscopy (white arrow). (C, D) The elastic modulus and hardness are significantly higher in *dark* osteons. (E, F) Both parameters correlated positively with the mean calcium content and (G, H) negatively with the predominant collagen orientation.

modulus in the direction of indentation (E_i) being increased 26.70% for the lamellar level (Table 1). The FEM model predicts an elastic modulus of 26.15 GPa for *dark* and 20.64 GPa for *bright* osteons, which is in good agreement with the experimentally measured values of 25.28 ± 1.12 and 19.29 ± 1.54 GPa, respectively (considering the nanoindentation results being representative of the lamellar level). The detailed engineering elastic constants of the coated fiber and lamellae RVE are summarized in Table 1.

Second, the obtained elastic constants were used to predict the effective elastic modulus E_{eff} of whole osteons (Table 2). On the osteonal level, the influence of the higher mineralized and, hence, stiffer interstitial bone on the mechanical properties becomes evident: the higher the assumed elastic modulus of the interstitial bone the higher the effective modulus of the osteon RVE. Still, a clear difference between different types of collagen orientation is observed: for *dark* osteons (0°), E_{eff} is 14.38% higher compared to *bright* osteons (45°) (averaged over equal assumed elastic modulus of interstitial bone). When comparing *dark* osteons to osteons with alternating CFO between neighboring lamellae, E_{eff} is 7.20% higher in *dark* osteons. However, alternating lamellae results in 6.70% higher E_{eff} when compared to *bright* osteons. This clearly shows the adaptive capabilities and biomechanical implications of *dark* and *bright* osteons to either serve as a stiff building block of bone or to conduce as an energy dissipating module, both to prevent fractures on larger length scales.

Although we are aware of the established view that CFO pattern should reflect the loading history of the femur, with *dark* osteons occupying volumes that are subjected to tensile stress and *bright* osteons being present in areas under compression, based on the compositional results obtained in this study we propose an alternative view on the existence of *dark* and *bright* osteons and their mechanical functions. We postulate that *dark* osteons are predominantly found in regions where a higher degree of stiffness is required since more deformation is created in low stiffness materials when they are subjected to uniaxial stress, either compression or tension. From a mechanistic point of view, it is beneficial for the human femur to have less lateral movement along the anterior and posterior axis, thus a higher fraction of osteons with longitudinally oriented collagen fibers with a higher mineral content that provides additional stiffness.[72] On the other hand, regions that experience some bending stresses (while still being predominantly loaded in compression) would benefit from oblique-angled collagen fibers with a lower mineral content and an improved ability to dissipate energy. In general, nano- and microscale heterogeneity of the bone matrix composition and mechanical properties is considered beneficial for the mechanical competence at larger length scales.[73−75] In healthy bone, continuous remodeling processes maintain a constant tissue heterogeneity for better damage resistance. Healthy bone can hamper the initiation and propagation of microcracks while enabling remodeling processes to repair the affected bone volume. The mineralization profile of individual osteons,[61] the higher mineralization and accumulation of cross-links in interstitial bone[76] and the stiffness mismatch at cement lines[77] all contribute to tissue heterogeneity that guides the toughening mechanisms of bone. Based on our findings, we believe that structural heterogeneity at the osteonal level extends to the organic phase of the matrix: bone tissue can react to changed loading modes to modulate its nanostructural arrangement in functional interaction with its compositional properties to build more *dark* osteons in case of increased need of stiffness (compressive/tensile loading) or *bright* osteons to dissipate energy.

It can also be speculated that the osteon heterogeneity might be another mechanism that preserves the mechanical competence of bone. Rather than being considered "old" tissue, the nanostructural heterogeneity could serve as a

https://dx.doi.org/10.1021/acsnano.0c04786
ACS Nano 2021, 15, 455−467

Table 1. FEM Calculated Elastic Moduli for the Coated Collagen Fiber and Osteonal Lamellar Level Assuming 0 and 45° of Collagen Fiber Orientation[a]

RVE, orientation	E_1	E_2	E_3	G_{12}	G_{13}	G_{23}	ν_{21}	ν_{21}	ν_{13}	ν_{31}	ν_{23}	ν_{32}
coated fiber, 0°	26.40	11.42	6.77	7.58	3.29	1.90	0.255	0.110	0.306	0.079	0.258	0.153
coated fiber, 45°	20.81	11.74	9.51	5.36	4.51	4.31	0.201	0.114	0.391	0.179	0.208	0.168
lamella, 0°	26.15	11.38	6.73	7.53	3.27	1.89	0.253	0.111	0.306	0.079	0.258	0.153
lamella, 45°	20.64	11.70	9.45	5.34	4.48	4.29	0.200	0.114	0.391	0.179	0.208	0.168

[a]All modulus units are in GPa.

Table 2. Effective Elastic Modulus of the Osteon RVE in the Direction of Indentation for Different Lamellar CFO Scenarios and Elastic Moduli of Interstitial Bone

CFO (deg)	E(interstitial) (GPa)	E(effective) (GPa)
0	30.07	25.75
0	27.08	24.66
0	23.74	23.44
45	30.07	22.66
45	27.08	21.57
45	23.74	20.35
0, 45, −45	30.07	24.10
0, 45, −45	27.08	23.01
0, 45, −45	23.74	21.79

remodeling regulator that guides the remodeling activity. Previous studies have shown that osteons targeted by osteoclasts have lower elastic moduli and hardness and are characterized by a lower mineral quantity than nonresorbable areas.[78] Applying these findings to our study implicates that osteons composed of longitudinally oriented collagen fibers with a higher mineral content are considered more desirable in certain loading scenarios and less prone to osteoclast-mediated bone resorption. As a consequence, our data could be indicative of the fact that osteoclastic resorption does not proceed in a random manner and serves more functions apart from the removal of microdamage. Additionally, the CFO and compositional heterogeneity between *dark* and *bright* osteons could promote the detection of microdamage; as deformation can spread out over greater distances due to the nanoscale heterogeneity of the bone matrix, the mechano-sensitive osteocytes, residing inside the bone matrix and sampling their mechanical environment might detect damage and initiate remodeling processes more quickly.[79−82]

While our study used high-resolution techniques to assess changes in the structure, composition, and mechanical properties in individual osteons of contrasting orientation, the osteons were selected from the femoral cross-section of one individual. Therefore, interindividual variations by genetic predisposition, environmental factors, and lifestyle choices may have not been addressed. However, the focus of this study was to approach the compositional changes accompanied by different collagen orientations. By confining to one individual, we were able to focus and address these changes and eliminate potential interindividual factors of influence. Also, CPL reflects the predominant CFO without direct visualization of the collagen fibers and, hence, provides only an average measure of the CFO. However, in combination with phase-contrast nanocomputed tomography and FIB-SEM imaging, the variability in ultrastructural matrix organization was confirmed in three dimensions and at high-resolution. It was shown that CPL is an imaging modality that is able to indirectly visualize variations in CFO at the nanoscale. Moreover, in order to implement our spatially correlated analytical approach to evaluate multiple bone quality parameters in the same plane of selected osteons, the use of undecalcified bone specimen was necessary. Hence, the mineral phase is also included in the nanotomograms and contributes to the structural appearance. However, it has been shown that the orientations of mineral particles and collagen fibers are dependent on each other with the crystallographic c-axes being aligned with the fiber axes, so that the collagen fiber orientation can be inferred.[10,50,83] Therefore, despite not resolving individual collagen fibrils, phase contrast tomography provides sufficient resolution and high sensitivity to mass density fluctuations that allows for the assessment of the ultrastructural matrix organization. Finally, the amount of collagen- and mineral-bound water could not be directly assessed which is known to affect the mechanical properties.[84,85] It has been shown that the water content is inversely correlated with the mineral content as collagen-bound water is gradually replaced by hydroxyapatite.[86] As we quantified a lower mean and peak mineral content in *bright* osteons, it can be inferred that these osteons contain a higher amount of bound water. Previous studies have demonstrated that bound water is a substantial contributing factor to the mechanical behavior of bone as it provides collagen ductility and postyield toughness.[87,88] This further supports our findings that *bright* osteons provide the bone matrix enhanced ductility and energy dissipating abilities. Further studies both *in silico* and *ex vivo* are needed to elucidate the role of *dark* and *bright* osteons on fracture mechanics on larger length scales and the whole bone level.

CONCLUSION

It is commonly accepted that *dark* osteons are found in regions of tensile stress and *bright* osteons in regions under compression. Here, we have shown that these osteon types show distinct structural and compositional differences reflecting important mechanical characteristics that locally adapt the bone matrix to its mechanical environment. In particular, *dark* osteons with longitudinally oriented collagen fibers and a higher degree of mineralization constitute to more stiffness and the ability to resist elastic and plastic deformation in tension and compression whereas *bright* osteons with oblique-angled fibers provide ductility and the ability to dissipate energy more efficiently where needed. Furthermore, we show that beyond the change in preferential collagen fiber orientation there are fundamental disparities between different types of osteons that result in altered mechanical competence potentially serving as an additional fracture resistance mechanism.

METHODS

Sample Collection. Healthy femoral bone was obtained during autopsy at the Department of Forensic Medicine at the University Medical Center Hamburg-Eppendorf (Hamburg, Germany) from a

https://dx.doi.org/10.1021/acsnano.0c04786
ACS Nano 2021, 15, 455−467

44-year old organ donor in line with previously published protocols (PV 3486).[39] Femoral cross sections from the mid-diaphysis were cut using a diamond saw (EXAKT Advanced Technologies GmbH, Norderstedt, Germany) and fixed in 3.7% formaldehyde for 3 days. Thereafter, the sample was dehydrated in an increasing alcohol series and embedded undecalcified in glycolmethacrylate (Technovit 7200, Heraeus Kulzer GmbH, Wehrheim, Germany). Using an automatic grinding machine (EXACT Advances Technologies GmbH, Norderstedt, Germany) the sample was ground to a thickness of 100 μm.

Circularly Polarized Light Microscopy. Using circularly polarized light microscopy (CPL), the predominant CFO can be visualized. When viewed under polarized light, osteons composed of oblique orientated collagen fibers appear bright, while osteons composed of collagen fibers parallel with the osteon axis appear dark. An Olympus BX-61 microscope (Olympus Europa, Hamburg, Germany) equipped with circularly polarizing filter sets was used to discern *dark* and *bright* osteons of different preferential collagen orientation. Prior to any other measurements, a total of 20 (10 *dark* and 10 *bright*) fully remodeled osteons with an uninterrupted periphery were selected unbiasedly from the anterolateral quadrant of the cross-section for subsequent structural, compositional and mechanical analysis. By adhering to one bone region a selection bias of osteons that might be subjected to variational mechanical characteristics on a regional bone level is avoided. To exclude primary osteons from the analysis, osteons were selected only if they were surrounded by at least two partially resorbed osteons. An uninterrupted periphery in form of a hypermineralized cement line was further verified using quantitative backscattered electron imaging. In the analyzed area, 14.59% and 17.52% of all osteons that matched the selection criteria appeared fully *dark* and *bright*, respectively. Haversian canals and surrounding interstitial bone were masked and assigned a gray value of 0. The grayscale of the bone pixels in each masked osteon was measured and reported as the average brightness (based on gray levels 1−255). To confirm that the osteons included in the study were oriented perpendicular to the analyzed cross-sectional plane, microcomputed tomography was performed where the orientation of the Haversian canal was assessed in the orthogonal projections (Figure S4). Finally, to verify that the brightness variations detected by CPL are attributable to changes in preferential CFO and to deconvolute the influence of localized differences in bone mineral density, a control experiment comparing undecalcified and decalcified ground sections in terms of CPL brightness was performed. The anterior quadrant of a femoral cross-section was divided into two parts, and one-half was decalcified in 20% EDTA for 8 days. Successful decalcification of the sample was checked radiographically using a cabinet X-ray system (Faxitron, Inc., USA). Further sample preparation toward ground sections was identical and as described above.

Quantitative Backscattered Electron Imaging. Quantitative backscattered electron imaging (qBEI) was applied to evaluate the osteonal bone mineral density distribution (BMDD) and morphology of osteocyte lacunae. The coplanar polished surface of the bone specimen was carbon-coated, and the sample was mounted in a scanning electron microscope (GeminiSEM, Zeiss AG, Oberkochen, Germany). The microscope was operated in backscattered electron mode at 20 keV and at a constant working distance of 20 mm. Images were acquired with 300× magnification. The intensity of backscattered electrons correlates with the mean atomic number of the investigated material.[39,48] Brightness and contrast of the recorded 8-bit images were calibrated using carbon and aluminum standards: the gray values assigned to carbon and aluminum were 4.8 and 222, respectively. As the gray value of unmineralized osteoid (<0.2 wt % calcium) was measured to be 4.8 and that of pure hydroxyapatite (39.68 wt % calcium) was 255, the measurement accuracy was 0.16 wt % calcium.[39] The obtained gray values for each pixel were averaged to provide a mean value for the full osteon. Osteonal areas were isolated and surrounding tissue was excluded from evaluation. The following compositional qBEI parameters were derived from the backscattered electron images using a custom-made MATLAB routine: Mean calcium content of the BMDD (Ca_{mean}), most frequent calcium content (Ca_{peak}), percentage of bone area which is mineralized below the fifth percentile or above the 95th percentile (Ca_{low} and Ca_{high}). Additionally, the area, circularity index and density of osteocyte lacunae were assessed.

Focused Ion Beam-Scanning Electron Microscopy. Focused ion beam-scanning electron microscopy (FIB-SEM) imaging was used to visualize the internal structure within *dark* and *bright* osteons (Crossbeam 340, Zeiss AG, Oberkochen, Germany).[48] Using the secondary electron mode, ion milling was performed to expose imaging planes with radial-longitudinal orientation with respect to the Haversian canal. A coarse trench was milled at 30 kV and 30 nA, followed by polishing of the exposed image plane at 30 kV and 2 nA. Finally, images were acquired at 2 kV (InlensDuo, Zeiss) and postprocessed using a band-pass filter to remove curtaining artifacts.[90]

Fourier Transform Infrared Spectroscopy. Fourier transform infrared spectroscopy (FTIR) in attenuated total reflection-mode was performed to assess the composition of the individual osteons.[76] FTIR spectra were collected with a FTIR Spotlight 400 (PerkinElmer, Waltham, Massachusetts, USA) over an area of 750 × 750 μm to create a map, where each pixel represents individual spectra. For each osteon, spectra were acquired at a 6.25 μm spatial resolution over a spectral range of 4000−570 cm^{-1} at a resolution of 4 cm^{-1} and with 16 scans per pixel averaged. The areas under the curve of the amide I peak (1700−1600 cm^{-1}), the phosphate peak (1154−900 cm^{-1}) and the carbohydrate peak (890−850 cm^{-1}) were integrated to measure the mineral-to-matrix ratio (MMR) and carbonate-to-phosphate ratio (CPR).[76] To account for baseline shifts a local baseline has been used for each integrated peak. Two basepoints at local minima have been selected for the carbonate peak (894−800 cm^{-1}), for the phosphate peak (1182−800 cm^{-1}) and for the amide I peak (1780−1182 cm^{-1}). Only the enclosed area between the respective local baseline and the spectrum was used for integration and calculation of the ratios. Osteonal areas were isolated and surrounding tissue was excluded from evaluation.

Nanoindentation Testing. Nanoindentation testing (G200, Keysight Technologies, Santa Rosa, CA) was used for biomechanical assessment of the individual osteons.[48] For each osteon, four indents, one per osteonal quadrant, were performed at half the distance between the osteon center and periphery. Using a depth-sensing continuous stiffness method, indentations with 2 μm depth were performed with a Berkovich tip preceded and followed by calibration on fused silica. The hardness H and the elastic modulus E were calculated according to Oliver and Pharr with the NanoSuite software provided by the manufacturer.[91]

Synchrotron Nanocomputed Tomography. Synchrotron nanocomputed tomography with Zernike phase contrast was performed at the P05 beamline[92,93] operated by the Helmholtz Zentrum Geesthacht (HZG) at the PETRA III storage ring of the German Electron Synchrotron (DESY) to visualize the ultrastructural organization of 16 osteons (n = 8 per group) beneath the nanoindentations in 3D.[49,50] The samples were prepared using FIB-SEM. The nanoindentations were localized and cylindrical volumes with a diameter of 25 μm were extracted and placed on a cone-shaped sample holder using a micromanipulator. A full field transmission X-ray microscope equipped with a Fresnel Zone Plate of 130 μm diameter, a beam shaping optics and Zernike phase rings, was used for acquiring the tomograms at an energy of 11 keV. These optics were designed and manufactured at the Paul Scherrer Institute. An X-ray sCMOS camera (Hamamatsu C12849−101U, 6.5 μm pixel size, 2048 × 2048 pixel, 16 bit image depth) with a 10 μm Gadox scintillator was used as a detector. The effective pixel size of the system was 18.65 nm and a binning factor of 2 was applied. The resolution was determined in 3D using Fourier Shell correlations (FSCs). By applying the 1/2-bit criterion, the average FSC-based spatial resolution was calculated to be 77.7 nm. To ensure that the ultrastructural organization is not affected by plastic deformation below the nanoindent, the analyzed volume of interest was chosen to start 5 μm below the sample surface.

Finite Element Modeling. To predict how the mechanical properties of bone at different hierarchical levels are affected by changes in the predominant CFO, multiscale modeling using the

https://dx.doi.org/10.1021/acsnano.0c04786
ACS Nano 2021, 15, 455−467

Finite Element Method (FEM) was applied.[94−96] Periodic boundary conditions (PBCs) were applied to simulate the orthotropic mechanical properties in different hierarchical levels by modeling finite representative volume elements (RVEs).[97] Here, the hierarchical levels of (i) mineral-coated collagen fibers, (ii) osteonal lamellae, and (iii) remodeled secondary osteons were modeled based on two different orientations of mineralized collagen fibrils (0° and 45°) to represent *dark* and *bright* osteons. The volume fractions of the coated fiber level (87.4% mineralized collagen fibril, 12.6% extrafibrillar hydroxyapatite) and the orthotropic elastic constants of mineralized collagen fibrils were adapted from Hamed *et al.*[98,99] The hydroxyapatite foam was assumed to be isotropic with the bulk and shear modulus being K_{HA} = 57.8 GPa and μ_{HA} = 31.4 GPa, respectively.[100] Osteonal lamellae were composed of the homogenized coated fiber RVE (97.5% volume fraction) interspersed with ellipsoidal lacunar cavities (2.25%)[101] with a mean size of 18.9 μm × 9.2 μm × 4.8 μm.[102] The characteristics for the osteon RVE were extracted from the qBEI images (osteon diameter = 300 μm, Haversian canal diameter = 90 μm, lamellar thickness = 6 μm, number of lamellae = 11). Each lamella was assigned a collagen fiber orientation of 0° or 45°. Three scenarios of CFO were considered: (1) all lamellae contain collagen fibers with 0° orientation (*dark* osteon), (2) all lamellae contain fibers oriented 45° (*bright* osteon), and (3) lamellae alternate in terms of CFO between 0° and 45°. Three elastic moduli were assumed for the stiffer surrounding interstitial bone (+15% of elastic modulus of osteonal bone with 0°, 25°, and 45° orientation corresponding to 30.07, 27.08, and 23.74 GPa, respectively).[103] Nine orthotropic material properties according to the elastic material stress−strain relation were calculated at each hierarchical level.

ABAQUS/CAE 6.14-4 was used to create the RVEs. The General/Static solver was employed for the computation and the mesh independency has been checked for the solution to be converged. 11900 and 47421 eight-node linear brick elements with reduced integration (C3D8R) were used to mesh the coated fiber and osteon RVE, respectively. The osteonal lamellae were meshed with 11983 10-node quadratic tetrahedron elements (C3D10). A python script was developed to calculate the average stress and strain components within the model to numerically compute the mechanical properties of the homogenized RVE.

Statistical Analysis. Normality of the data was assessed by Shapiro−Wilk tests. To determine statistical differences between *dark* and *bright* osteons independent *t* tests were performed. Pearson product-moment correlations were used to check for correlations between structural, compositional, and mechanical properties. Statistical tests were performed using SPSS with a level of significance of $\alpha = 0.05$.

ASSOCIATED CONTENT

Supporting Information

The Supporting Information is available free of charge at https://pubs.acs.org/doi/10.1021/acsnano.0c04786.

3D assessment of osteon orientation by coregistration of microcomputed tomography scan and CPL micrograph, CPL micrographs comparing undecalcified and decalcified ground sections, spatial assessment of canalicular network by nanocomputed tomography, and spatial distribution of high-MMR zone (PDF)

Video of nanocomputed tomography stack obtained from *a dark* osteon (MP4)

Video of nanocomputed tomography stack obtained from a *bright* osteon (MP4)

AUTHOR INFORMATION

Corresponding Author

Björn Busse − *Department of Osteology and Biomechanics, University Medical Center, 22529 Hamburg, Germany; Interdisciplinary Competence Center for Interface Research (ICCIR), 20251 Hamburg, Germany; Materials Sciences Division, Lawrence Berkeley National Laboratory, Berkeley, California 94720, United States;* orcid.org/0000-0002-3099-8073; Email: b.busse@uke.uni-hamburg.de

Authors

Kilian E. Stockhausen − *Department of Osteology and Biomechanics, University Medical Center, 22529 Hamburg, Germany;* orcid.org/0000-0001-8923-8936

Mahan Qwamizadeh − *Department of Osteology and Biomechanics, University Medical Center, 22529 Hamburg, Germany*

Eva M. Wölfel − *Department of Osteology and Biomechanics, University Medical Center, 22529 Hamburg, Germany; Forum Medical Technology Health Hamburg (FMTHH), 22529 Hamburg, Germany; Interdisciplinary Competence Center for Interface Research (ICCIR), 20251 Hamburg, Germany*

Haniyeh Hemmatian − *Department of Osteology and Biomechanics, University Medical Center, 22529 Hamburg, Germany*

Imke A. K. Fiedler − *Department of Osteology and Biomechanics, University Medical Center, 22529 Hamburg, Germany; Forum Medical Technology Health Hamburg (FMTHH), 22529 Hamburg, Germany*

Silja Flenner − *Institute of Materials Research, Helmholtz-Zentrum Geesthacht, 21502 Geesthacht, Germany*

Elena Longo − *Institute of Materials Research, Helmholtz-Zentrum Geesthacht, 21502 Geesthacht, Germany*

Michael Amling − *Department of Osteology and Biomechanics, University Medical Center, 22529 Hamburg, Germany*

Imke Greving − *Institute of Materials Research, Helmholtz-Zentrum Geesthacht, 21502 Geesthacht, Germany*

Robert O. Ritchie − *Materials Sciences Division, Lawrence Berkeley National Laboratory, Berkeley, California 94720, United States;* orcid.org/0000-0002-0501-6998

Felix N. Schmidt − *Department of Osteology and Biomechanics, University Medical Center, 22529 Hamburg, Germany; Forum Medical Technology Health Hamburg (FMTHH), 22529 Hamburg, Germany*

Complete contact information is available at: https://pubs.acs.org/10.1021/acsnano.0c04786

Author Contributions

#F.N.S. and B.B. contributed equally.

Notes

The authors declare no competing financial interest.

ACKNOWLEDGMENTS

We acknowledge the Helmholtz-Zentrum Geesthacht outstation at DESY (Hamburg, Germany), a member of the Helmholtz Association HGF, for the provision of experimental facilities. Parts of this research were carried out at the Imaging Beamline P05 at PETRA III, and we thank D. Laipple for assistance in the sample preparation. We acknowledge the input and support on the study by K. Püschel, A. vom Scheidt and C. Plumeyer. M.Q. and H.H. are fellows of the Alexander von Humboldt foundation. B.B. is supported by the German Research Foundation (DFG) under Grant No. BU 2562/3-1. I.G. and E.L. acknowledge funding by the German Research

Foundation (DFG) under Grant No. 192346071 – SFB 986, Z2. Further funding was received from the Interdisciplinary Center for Interface Research (ICCIR) on behalf of the Hamburg University of Technology (TUHH) and the University Medical Center Hamburg-Eppendorf (UKE).

REFERENCES

(1) Milovanovic, P.; Busse, B. Inter-site Variability of the Human Osteocyte Lacunar Network: Implications for Bone Quality. *Curr Osteoporos Rep.* **2019**, *17* (3), 105–115.
(2) Milovanovic, P.; Busse, B. Phenomenon of osteocyte lacunar mineralization: indicator of former osteocyte death and a novel marker of impaired bone quality? *Endocr. Connect.* **2020**, *9* (4), R70–R80.
(3) Lassen, N. E.; Andersen, T. L.; Ploen, G. G.; Søe, K.; Hauge, E. M.; Harving, S.; Eschen, G. E. T.; Delaisse, J.-M. Coupling of Bone Resorption and Formation in Real Time: New Knowledge Gained from Human Haversian BMUs. *J. Bone Miner. Res.* **2017**, *32*, 1395–1405.
(4) Gebhardt, W. Über Funktionell Wichtige Anordnungsweisen Der Feineren Und Gröberen Bauelemente Des Wirbeltierknochens. *Dev. Genes Evol.* **1905**, *20*, 187–322.
(5) Ascenzi, A.; Bonucci, E. The Compressive Properties of Single Osteons. *Anat. Rec.* **1968**, *161*, 377–391.
(6) Ascenzi, A.; Bonucci, E. The Tensile Properties of Single Osteons. *Anat. Rec.* **1967**, *158*, 375–386.
(7) Giraud-Guille, M. M. Twisted Plywood Architecture of Collagen Fibrils in Human Compact Bone Osteons. *Calcif. Tissue Int.* **1988**, *42*, 167–180.
(8) Reznikov, N.; Shahar, R.; Weiner, S. Bone Hierarchical Structure in Three Dimensions. *Acta Biomater.* **2014**, *10*, 3815–3826.
(9) Fratzl, P.; Gupta, H. S.; Paschalis, E. P.; Roschger, P. Structure and Mechanical Quality of the Collagen-Mineral Nano-Composite in Bone. *J. Mater. Chem.* **2004**, *14*, 2115–2123.
(10) McNally, E.; Nan, F.; Botton, G. A.; Schwarcz, H. P. Scanning Transmission Electron Microscopic Tomography of Cortical Bone Using Z-Contrast Imaging. *Micron* **2013**, *49*, 46–53.
(11) Reznikov, N.; Bilton, M.; Lari, L.; Stevens, M. M.; Kröger, R. Fractal-Like Hierarchical Organization of Bone Begins at the Nanoscale. *Science* **2018**, *360*, eaao2189.
(12) Grünewald, T. A.; Liebi, M.; Wittig, N. K.; Johannes, A.; Sikjaer, T.; Rejnmark, L.; Gao, Z.; Rosenthal, M.; Guizar-Sicairos, M.; Birkedal, H.; Burghammer, M. Mapping the 3D Orientation of Nanocrystals and Nanostructures in Human Bone: Indications of Novel Structural Features. *Sci. Adv.* **2020**, *6*, eaba4171.
(13) Lefèvre, E.; Farlay, D.; Bala, Y.; Subtil, F.; Wolfram, U.; Rizzo, S.; Baron, C.; Zysset, P.; Pithioux, M.; Follet, H. Compositional and Mechanical Properties of Growing Cortical Bone Tissue: A Study of the Human Fibula. *Sci. Rep.* **2019**, *9*, 17639.
(14) Zimmermann, E. A.; Riedel, C.; Schmidt, F. N.; Stockhausen, K. E.; Chushkin, Y.; Schaible, E.; Gludovatz, B.; Vettorazzi, E.; Zontone, F.; Püschel, K.; Amling, M.; Ritchie, R. O.; Busse, B. Mechanical Competence and Bone Quality Develop during Skeletal Growth. *J. Bone Miner. Res.* **2019**, *34*, 1461–1472.
(15) Zimmermann, E. A.; Ritchie, R. O. Bone as a Structural Material. *Adv. Healthcare Mater.* **2015**, *4*, 1287–1304.
(16) Zimmermann, E. A.; Schaible, E.; Bale, H.; Barth, H. D.; Tang, S. Y.; Reichert, P.; Busse, B.; Alliston, T.; Ager, J. W.; Ritchie, R. O. Age-Related Changes in the Plasticity and Toughness of Human Cortical Bone at Multiple Length Scales. *Proc. Natl. Acad. Sci. U. S. A.* **2011**, *108*, 14416–14421.
(17) Zimmermann, E. A.; Busse, B.; Ritchie, R. O. The Fracture Mechanics of Human Bone: Influence of Disease and Treatment. *BoneKEy Rep.* **2015**, *4*, 743.
(18) Vom Scheidt, A.; Hemmatian, H.; Püschel, K.; Krause, M.; Amling, M.; Busse, B. Bisphosphonate Treatment Changes Regional Distribution of Trabecular Microstructure in Human Lumbar Vertebrae. *Bone* **2019**, *127*, 482–487.
(19) Milovanovic, P.; Zimmermann, E. A.; Riedel, C.; vom Scheidt, A.; Herzog, L.; Krause, M.; Djonic, D.; Djuric, M.; Puschel, K.; Amling, M.; Ritchie, R. O.; Busse, B. Multi-Level Characterization of Human Femoral Cortices and Their Underlying Osteocyte Network Reveal Trends in Quality of Young, Aged, Osteoporotic and Antiresorptive-Treated Bone. *Biomaterials* **2015**, *45*, 46–55.
(20) McCalden, R. W.; McGeough, J. A.; Barker, M. B.; Court-Brown, C. M. Age-Related Changes in the Tensile Properties of Cortical Bone. The Relative Importance of Changes in Porosity, Mineralization, and Microstructure. *J. Bone Joint Surg. Am.* **1993**, *75*, 1193–1205.
(21) O'Brien, F. J.; Taylor, D.; Lee, T. C. Microcrack Accumulation at Different Intervals during Fatigue Testing of Compact Bone. *J. Biomech.* **2003**, *36*, 973–980.
(22) Willett, T. L.; Dapaah, D. Y.; Uppuganti, S.; Granke, M.; Nyman, J. S. Bone Collagen Network Integrity and Transverse Fracture Toughness of Human Cortical Bone. *Bone* **2019**, *120*, 187–193.
(23) Fiedler, I. A. K.; Schmidt, F. N.; Wölfel, E. M.; Plumeyer, C.; Milovanovic, P.; Gioia, R.; Tonelli, F.; Bale, H. A.; Jähn, K.; Besio, R.; Forlino, A.; Busse, B. Severely Impaired Bone Material Quality in Chihuahua Zebrafish Resembles Classical Dominant Human Osteogenesis Imperfecta. *J. Bone Miner. Res.* **2018**, *33*, 1489–1499.
(24) Wang, X.; Shen, X.; Li, X.; Agrawal, C. M. Age-Related Changes in the Collagen Network and Toughness of Bone. *Bone* **2002**, *31*, 1–7.
(25) Carriero, A.; Zimmermann, E. A.; Paluszny, A.; Tang, S. Y.; Bale, H.; Busse, B.; Alliston, T.; Kazakia, G.; Ritchie, R. O.; Shefelbine, S. J. How Tough Is Brittle Bone? Investigating Osteogenesis Imperfecta in Mouse Bone. *J. Bone Miner. Res.* **2014**, *29*, 1392–1401.
(26) Rauch, F.; Glorieux, F. H. Osteogenesis Imperfecta. *Lancet* **2004**, *363*, 1377–1385.
(27) Zimmermann, E. A.; Köhne, T.; Bale, H. A.; Panganiban, B.; Gludovatz, B.; Zustin, J.; Hahn, M.; Amling, M.; Ritchie, R. O.; Busse, B. Modifications to Nano- and Microstructural Quality and the Effects on Mechanical Integrity in Paget's Disease of Bone. *J. Bone Miner. Res.* **2015**, *30*, 264–273.
(28) Viguet-Carrin, S.; Garnero, P.; Delmas, P. D. The Role of Collagen in Bone Strength. *Osteoporosis Int.* **2006**, *17*, 319–336.
(29) Ritchie, R. O. The Conflicts between Strength and Toughness. *Nat. Mater.* **2011**, *10*, 817–822.
(30) Bromage, T. G.; Goldman, H. M.; McFarlin, S. C.; Warshaw, J.; Boyde, A.; Riggs, C. M. Circularly Polarized Light Standards for Investigations of Collagen Fiber Orientation in Bone. *Anat. Rec.* **2003**, *274*, 157–168.
(31) Ascenzi, M. G.; Ascenzi, A.; Benvenuti, A.; Burghammer, M.; Panzavolta, S.; Bigi, A. Structural Differences between "Dark" and "Bright" Isolated Human Osteonic Lamellae. *J. Struct. Biol.* **2003**, *141*, 22–33.
(32) McMahon, J. M.; Boyde, A.; Bromage, T. G. Pattern of Collagen Fiber Orientation in the Ovine Calcaneal Shaft and Its Relation to Locomotor-Induced Strain. *Anat. Rec.* **1995**, *242*, 147–158.
(33) Riggs, C. M.; Vaughan, L. C.; Evans, G. P.; Lanyon, L. E.; Boyde, A. Mechanical Implications of Collagen Fibre Orientation in Cortical Bone of the Equine Radius. *Anat. Embryol.* **1993**, *187*, 239–248.
(34) Ascenzi, A. The Micromechanics *versus* the Macromechanics of Cortical Bone - A Comprehensive Presentation. *J. Biomech. Eng.* **1988**, *110*, 357–363.
(35) Martin, R. B.; Ishida, J. The Relative Effects of Collagen Fiber Orientation, Porosity, Density, and Mineralization on Bone Strength. *J. Biomech.* **1989**, *22*, 419–426.
(36) Martin, R. B.; Boardman, D. L. The Effects of Collagen Fiber Orientation, Porosity, Density, and Mineralization on Bovine Cortical Bone Bending Properties. *J. Biomech.* **1993**, *26*, 1047–1054.

https://dx.doi.org/10.1021/acsnano.0c04786
ACS Nano 2021, 15, 455–467

(37) Shahar, R.; Banks-Sills, L.; Eliasy, R. Stress and Strain Distribution in the Intact Canine Femur: Finite Element Analysis. *Med. Eng. Phys.* **2003**, *25*, 387−395.
(38) Bergmann, G.; Siraky, J.; Rohlmann, A.; Koelbel, R. A Comparison of Hip Joint Forces in Sheep, Dog and Man. *J. Biomech.* **1984**, *17*, 907−921.
(39) Boyde, A.; Riggs, C. M. The Quantitative Study of the Orientation of Collagen in Compact Bone Slices. *Bone* **1990**, *11*, 35−39.
(40) Skedros, J. G.; Mason, M. W.; Nelson, M. C.; Bloebaum, R. D. Evidence of Structural and Material Adaptation to Specific Strain Features in Cortical Bone. *Anat. Rec.* **1996**, *246*, 47−63.
(41) Mason, M. W.; Skedros, J. G.; Bloebaum, R. D. Evidence of Strain-Mode-Related Cortical Adaptation in the Diaphysis of the Horse Radius. *Bone* **1995**, *17*, 229−237.
(42) Riggs, C. M.; Lanyon, L. E.; Boyde, A. Functional Associations between Collagen Fibre Orientation and Locomotor Strain Direction in Cortical Bone of the Equine Radius. *Anat. Embryol.* **1993**, *187*, 231−238.
(43) Skedros, J. G.; Mendenhall, S. D.; Kiser, C. J.; Winet, H. Interpreting Cortical Bone Adaptation and Load History by Quantifying Osteon Morphotypes in Circularly Polarized Light Images. *Bone* **2009**, *44*, 392−403.
(44) Skedros, J. G.; Kiser, C. J.; Mendenhall, S. D. A Weighted Osteon Morphotype Score Outperforms Regional Osteon Percent Prevalence Calculations for Interpreting Cortical Bone Adaptation. *Am. J. Phys. Anthropol.* **2011**, *144*, 41−50.
(45) Duda, G. N.; Schneider, E.; Chao, E. Y. S. Internal Forces and Moments in the Femur during Walking. *J. Biomech.* **1997**, *30*, 933−941.
(46) Taylor, M. E.; Tanner, K. E.; Freeman, M. A.; Yettram, A. L. Stress and Strain Distribution within the Intact Femur: Compression or Bending? *Med. Eng. Phys.* **1996**, *18*, 122−131.
(47) Zheng, N.; Fleisig, G. S.; Escamilla, R. F.; Barrentine, S. W. An Analytical Model of the Knee for Estimation of Internal Forces during Exercise. *J. Biomech.* **1998**, *31*, 963−967.
(48) Zimmermann, E. A.; Fiedler, I. A. K.; Busse, B. Breaking new ground in mineralized tissue: Assessing tissue quality in clinical and laboratory studies. *J. Mech. Behav. Biomed. Mater.* **2021**, *113*, 104138.
(49) Langer, M.; Pacureanu, A.; Suhonen, H.; Grimal, Q.; Cloetens, P.; Peyrin, F. X-Ray Phase Nanotomography Resolves the 3D Human Bone Ultrastructure. *PLoS One* **2012**, *7*, 1−7.
(50) Varga, P.; Pacureanu, A.; Langer, M.; Suhonen, H.; Hesse, B.; Grimal, Q.; Cloetens, P.; Raum, K.; Peyrin, F. Investigation of the Three-Dimensional Orientation of Mineralized Collagen Fibrils in Human Lamellar Bone Using Synchrotron X-Ray Phase Nano-Tomography. *Acta Biomater.* **2013**, *9*, 8118−8127.
(51) Reznikov, N.; Shahar, R.; Weiner, S. Three-Dimensional Structure of Human Lamellar Bone: The Presence of Two Different Materials and New Insights into the Hierarchical Organization. *Bone* **2014**, *59*, 93−104.
(52) Grandfield, K.; Vuong, V.; Schwarcz, H. P. Ultrastructure of Bone: Hierarchical Features from Nanometer to Micrometer Scale Revealed in Focused Ion Beam Sections in the TEM. *Calcif. Tissue Int.* **2018**, *103*, 606−616.
(53) Pazzaglia, U. E.; Congiu, T.; Marchese, M.; Spagnuolo, F.; Quacci, D. Morphometry and Patterns of Lamellar Bone in Human Haversian Systems. *Anat. Rec.* **2012**, *295*, 1421−1429.
(54) Jones, S. J.; Boyde, A.; Pawley, J. B. Osteoblasts and Collagen Orientation. *Cell Tissue Res.* **1975**, *159*, 73−80.
(55) Kerschnitzki, M.; Wagermaier, W.; Roschger, P.; Seto, J.; Shahar, R.; Duda, G. N.; Mundlos, S.; Fratzl, P. The Organization of the Osteocyte Network Mirrors the Extracellular Matrix Orientation in Bone. *J. Struct. Biol.* **2011**, *173*, 303−311.
(56) Currey, J. D. The Adaption of Mechanical Properties to Different Functions. *Bones: Structure and Mechanics*, 2nd ed.; Princeton University Press, 2002; Vol. 2, pp 144−145.
(57) Bala, Y.; Farlay, D.; Delmas, P. D.; Meunier, P. J.; Boivin, G. Time Sequence of Secondary Mineralization and Microhardness in Cortical and Cancellous Bone from Ewes. *Bone* **2010**, *46*, 1204−1212.
(58) Grynpas, M. Age and Disease-Related Changes in the Mineral of Bone. *Calcif. Tissue Int.* **1993**, *53*, 57−64.
(59) Busse, B.; Bale, H. A.; Zimmermann, E. A.; Panganiban, B.; Barth, H. D.; Carriero, A.; Vettorazzi, E.; Zustin, J.; Hahn, M.; Ager, J. W.; Püschel, K.; Amling, M.; Ritchie, R. O. Vitamin D Deficiency Induces Early Signs of Aging in Human Bone, Increasing the Risk of Fracture. *Sci. Transl. Med.* **2013**, *5*, 188−193.
(60) Schmidt, F. N.; Zimmermann, E. A.; Walsh, F.; Plumeyer, C.; Schaible, E.; Fiedler, I. A. K.; Milovanovic, P.; Rößle, M.; Amling, M.; Blanchet, C.; Gludovatz, B.; Ritchie, R. O.; Busse, B. On the Origins of Fracture Toughness in Advanced Teleosts: How the Swordfish Sword's Bone Structure and Composition Allow for Slashing under Water to Kill or Stun Prey. *Adv. Sci.* **2019**, *6*, 1970072.
(61) Wittig, N. K.; Palle, J.; Østergaard, M.; Frølich, S.; Birkbak, M. E.; Spiers, K. M.; Garrevoet, J.; Birkedal, H. Bone Biomineral Properties Vary across Human Osteonal Bone. *ACS Nano* **2019**, *13*, 12949−12956.
(62) Roschger, A.; Roschger, P.; Wagermaier, W.; Chen, J.; van Tol, A. F.; Repp, F.; Blouin, S.; Berzlanovich, A.; Gruber, G. M.; Klaushofer, K.; Fratzl, P.; Weinkamer, R. The Contribution of the Pericanalicular Matrix to Mineral Content in Human Osteonal Bone. *Bone* **2019**, *123*, 76−85.
(63) Boskey, A. L.; Imbert, L. Bone Quality Changes Associated with Aging and Disease: A Review. *Ann. N. Y. Acad. Sci.* **2017**, *1410*, 93−106.
(64) McCreadie, B. R.; Morris, M. D.; Chen, T.; Rao, D. S.; Finney, W. F.; Widjaja, E.; Goldstein, S. A. Bone Tissue Compositional Differences in Women with and without Osteoporotic Fracture. *Bone* **2006**, *39*, 1190−1195.
(65) Boskey, A. L.; Donnelly, E.; Boskey, E.; Spevak, L.; Ma, Y.; Zhang, W.; Lappe, J.; Recker, R. R. Examining the Relationships between Bone Tissue Composition, Compositional Heterogeneity, and Fragility Fracture: A Matched Case-Controlled FTIRI Study. *J. Bone Miner. Res.* **2016**, *31*, 1070−1081.
(66) Paschalis, E. P.; Betts, F.; DiCarlo, E.; Mendelsohn, R.; Boskey, A. L. FTIR Microspectroscopic Analysis of Normal Human Cortical and Trabecular Bone. *Calcif. Tissue Int.* **1997**, *61*, 480−486.
(67) Schmidt, F. N.; Delsmann, M. M.; Mletzko, K.; Yorgan, T. A.; Hahn, M.; Siebert, U.; Busse, B.; Oheim, R.; Amling, M.; Rolvien, T. Ultra-High Matrix Mineralization of Sperm Whale Auditory Ossicles Facilitates High Sound Pressure and High-Frequency Underwater Hearing. *Proc. R. Soc. London, Ser. B* **2018**, *285*, 20181820.
(68) Landis, W. J.; Librizzi, J. J.; Dunn, M. G.; Silver, F. H. A Study of the Relationship between Mineral Content and Mechanical Properties of Turkey Gastrocnemius Tendon. *J. Bone Miner. Res.* **1995**, *10*, 859−867.
(69) Follet, H.; Boivin, G.; Rumelhart, C.; Meunier, P. The Degree of Mineralization Is a Determinant of Bone Strength: A Study on Human Calcanei. *Bone* **2004**, *34*, 783−789.
(70) Donnelly, E.; Boskey, A. L.; Baker, S. P.; van der Meulen, M. C. H. Effects of Tissue Age on Bone Tissue Material Composition and Nanomechanical Properties in the Rat Cortex. *J. Biomed. Mater. Res., Part A* **2009**, *9999A*, 1048−1056.
(71) Rho, J. Y.; Zioupos, P.; Currey, J. D.; Pharr, G. M. Microstructural Elasticity and Regional Heterogeneity in Human Femoral Bone of Various Ages Examined by Nano-Indentation. *J. Biomech.* **2002**, *35*, 189−198.
(72) Nair, A. K.; Gautieri, A.; Buehler, M. J. Role of Intrafibrillar Collagen Mineralization in Defining the Compressive Properties of Nascent Bone. *Biomacromolecules* **2014**, *15*, 2494−2500.
(73) Seref-Ferlengez, Z.; Kennedy, O. D.; Schaffler, M. B. Bone Microdamage, Remodeling and Bone Fragility: How Much Damage Is Too Much Damage? *BoneKEy Rep.* **2015**, *4*, 644.
(74) Donnelly, E.; Meredith, D. S.; Nguyen, J. T.; Gladnick, B. P.; Rebolledo, B. J.; Shaffer, A. D.; Lorich, D. G.; Lane, J. M.; Boskey, A. L. Reduced Cortical Bone Compositional Heterogeneity with

https://dx.doi.org/10.1021/acsnano.0c04786
ACS Nano 2021, 15, 455−467

Bisphosphonate Treatment in Postmenopausal Women with Intertrochanteric and Subtrochanteric Fractures. *J. Bone Miner. Res.* **2012**, *27*, 672–678.
(75) Boivin, G. Y.; Chavassieux, P. M.; Santora, A. C.; Yates, J.; Meunier, P. J. Alendronate Increases Bone Strength by Increasing the Mean Degree of Mineralization of Bone Tissue in Osteoporotic Women. *Bone* **2000**, *27*, 687–694.
(76) Schmidt, F. N.; Zimmermann, E. A.; Campbell, G. M.; Sroga, G. E.; Püschel, K.; Amling, M.; Tang, S. Y.; Vashishth, D.; Busse, B. Assessment of Collagen Quality Associated with Non-Enzymatic Cross-Links in Human Bone Using Fourier-Transform Infrared Imaging. *Bone* **2017**, *97*, 243–251.
(77) Milovanovic, P.; vom Scheidt, A.; Mletzko, K.; Sarau, G.; Püschel, K.; Djuric, M.; Amling, M.; Christiansen, S.; Busse, B. Bone Tissue Aging Affects Mineralization of Cement Lines. *Bone* **2018**, *110*, 187–193.
(78) Pernelle, K.; Imbert, L.; Bosser, C.; Auregan, J. C.; Cruel, M.; Ogier, A.; Jurdic, P.; Hoc, T. Microscale Mechanical and Mineral Heterogeneity of Human Cortical Bone Governs Osteoclast Activity. *Bone* **2017**, *94*, 42–49.
(79) Tai, K.; Dao, M.; Suresh, S.; Palazoglu, A.; Ortiz, C. Nanoscale Heterogeneity Promotes Energy Dissipation in Bone. *Nat. Mater.* **2007**, *6*, 454–462.
(80) Klein-Nulend, J.; Bacabac, R. G.; Bakker, A. D. Mechanical Loading and How It Affects Bone Cells: The Role of the Osteocyte Cytoskeleton in Maintaining Our Skeleton. *Eur. Cell. Mater.* **2012**, *24*, 278–291.
(81) Klein-Nulend, J.; Bakker, A. D.; Bacabac, R. G.; Vatsa, A.; Weinbaum, S. Mechanosensation and Transduction in Osteocytes. *Bone* **2013**, *54*, 182–190.
(82) Milovanovic, P.; Zimmermann, E. A.; Hahn, M.; Djonic, D.; Püschel, K.; Djuric, M.; Amling, M.; Busse, B. Osteocytic Canalicular Networks: Morphological Implications for Altered Mechanosensitivity. *ACS Nano* **2013**, *7*, 7542–7551.
(83) Stock, S. R. The Mineral-Collagen Interface in Bone. *Calcif. Tissue Int.* **2015**, *97*, 262–280.
(84) Nyman, J. S.; Ni, Q.; Nicolella, D. P.; Wang, X. Measurements of Mobile and Bound Water by Nuclear Magnetic Resonance Correlate with Mechanical Properties of Bone. *Bone* **2008**, *42*, 193–199.
(85) Nyman, J. S.; Gorochow, L. E.; Adam Horch, R.; Uppuganti, S.; Zein-Sabatto, A.; Manhard, M. K.; Does, M. D. Partial Removal of Pore and Loosely Bound Water by Low-Energy Drying Decreases Cortical Bone Toughness in Young and Old Donors. *J. Mech. Behav. Biomed. Mater.* **2013**, *22*, 136–145.
(86) Wehrli, F. W.; Fernández-Seara, M. A. Nuclear Magnetic Resonance Studies of Bone Water. *Ann. Biomed. Eng.* **2005**, *33*, 79–86.
(87) Granke, M.; Does, M. D.; Nyman, J. S. The Role of Water Compartments in the Material Properties of Cortical Bone. *Calcif. Tissue Int.* **2015**, *97*, 292–307.
(88) Nyman, J. S.; Roy, A.; Shen, X.; Acuna, R. L.; Tyler, J. H.; Wang, X. The Influence of Water Removal on the Strength and Toughness of Cortical Bone. *J. Biomech.* **2006**, *39*, 931–938.
(89) Roschger, P.; Fratzl, P.; Eschberger, J.; Klaushofer, K. Validation of Quantitative Backscattered Electron Imaging for the Measurement of Mineral Density Distribution in Human Bone Biopsies. *Bone* **1998**, *23*, 319–326.
(90) Schindelin, J.; Arganda-Carreras, I.; Frise, E.; Kaynig, V.; Longair, M.; Pietzsch, T.; Preibisch, S.; Rueden, C.; Saalfeld, S.; Schmid, B.; Tinevez, J.-Y.; White, D. J.; Hartenstein, V.; Eliceiri, K.; Tomancak, P.; Cardona, A. Fiji: An Open-Source Platform for Biological-Image Analysis. *Nat. Methods* **2012**, *9*, 676–682.
(91) Oliver, W. C.; Pharr, G. M. An Improved Technique for Determining Hardness and Elastic Modulus Using Load and Displacement Sensing Indentation Experiments. *J. Mater. Res.* **1992**, *7*, 1564–1583.
(92) Ogurreck, M.; Wilde, F.; Herzen, J.; Beckmann, F.; Nazmov, V.; Mohr, J.; Haibel, A.; Müller, M.; Schreyer, A. The Nanotomography Endstation at the PETRA III Imaging Beamline. *J. Phys.: Conf. Ser.* **2013**, *425*, 182002.
(93) Flenner, S.; Storm, M.; Kubec, A.; Longo, E.; Döring, F.; Pelt, D. M.; David, C.; Müller, M.; Greving, I. Pushing the Temporal Resolution in Absorption and Zernike Phase Contrast Nanotomography: Enabling Fast *In Situ* Experiments. *J. Synchrotron Radiat.* **2020**, *27*, 1339–1346.
(94) Qwamizadeh, M.; Liu, P.; Zhang, Z.; Zhou, K.; Wei Zhang, Y. Hierarchical Structure Enhances and Tunes the Damping Behavior of Load-Bearing Biological Materials. *J. Appl. Mech.* **2016**, *83*, 51009.
(95) Qwamizadeh, M.; Lin, M.; Zhang, Z.; Zhou, K.; Zhang, Y. W. Bounds for the Dynamic Modulus of Unidirectional Composites with Bioinspired Staggered Distributions of Platelets. *Compos. Struct.* **2017**, *167*, 152–165.
(96) Qwamizadeh, M.; Zhou, K.; Zhang, Y. W. Damping Behavior Investigation and Optimization of the Structural Layout of Load-Bearing Biological Materials. *Int. J. Mech. Sci.* **2017**, *120*, 263–275.
(97) Omairey, S. L.; Dunning, P. D.; Sriramula, S. Development of an ABAQUS Plugin Tool for Periodic RVE Homogenisation. *Eng. Comput.* **2019**, *35*, 567–577.
(98) Hamed, E.; Jasiuk, I.; Yoo, A.; Lee, Y. H.; Liszka, T. Multi-Scale Modelling of Elastic Moduli of Trabecular Bone. *J. R. Soc., Interface* **2012**, *9*, 1654–1673.
(99) Hamed, E.; Lee, Y.; Jasiuk, I. Multiscale Modeling of Elastic Properties of Cortical Bone. *Acta Mech.* **2010**, *213*, 131–154.
(100) Hellmich, C.; Ulm, F.-J. Micromechanical Model for Ultrastructural Stiffness of Mineralized Tissues. *J. Eng. Mech.* **2002**, *128*, 898–908.
(101) Buenzli, P. R.; Sims, N. A. Quantifying the Osteocyte Network in the Human Skeleton. *Bone* **2015**, *75*, 144–150.
(102) Dong, P.; Haupert, S.; Hesse, B.; Langer, M.; Gouttenoire, P.-J. J.; Bousson, V. V.; Peyrin, F. F. 3D Osteocyte Lacunar Morphometric Properties and Distributions in Human Femoral Cortical Bone Using Synchrotron Radiation Micro-CT Images. *Bone* **2014**, *60*, 172–185.
(103) Rho, J. Y.; Tsui, T. Y.; Pharr, G. M. Elastic Properties of Human Cortical and Trabecular Lamellar Bone Measured by Nanoindentation. *Biomaterials* **1997**, *18*, 1325–1330.

https://dx.doi.org/10.1021/acsnano.0c04786
ACS Nano 2021, 15, 455–467

10. Abstract

Bone derives its mechanical competence from its hierarchical structure which is established during skeletal growth and maintained by remodeling processes throughout life. In this process, the micro- and nanostructure of the bone matrix is extensively altered and adapted to new mechanical demands. However, a higher fracture incidence is not only observed in aging and disease but also in children and adolescents. While the main drivers of fracture resistance are established in mature bone, it remains unclear how bone quality is altered during longitudinal bone growth. In healthy adults, the presence of secondary osteons and interstitial bone highlights an extensive remodeling history. When viewed under polarized light, osteons can appear dark or bright based on their preferential collagen fiber orientation (longitudinal and transverse, respectively). As the adaptability of bone is reflected in its micro- and nanostructural arrangement, the formation of *dark* and *bright* osteons points at a tissue heterogeneity that is advantageous for its mechanical strength. In the context of this thesis, the organization and orientation of collagen fibers was investigated in mid-diaphyseal human femoral bone and related to important compositional and mechanical properties of bone quality. Specifically, bone was obtained from fetal to 14-years old cases and a 44-year-old individual, and comprehensively assessed to scrutinize the structure-composition relationship in cortical bone.

A distinct coupling of preferential collagen fiber orientation and mineralization patterns was verified. In particular, the fetal/infantile cases are characterized by a disorganized woven bone matrix in which collagen fibers are preferentially transversely aligned. With ongoing age and near the time of walking, woven bone is replaced by highly organized lamellar bone and the collagen orientation is shifted towards more longitudinally aligned fibers. Compositionally, a higher bone mineral density is quantified in the 2- to 14-years old cases that is also more homogeneously distributed. The structural and compositional disparities result in significant differences in mechanical competence where the older cases demonstrate both higher stiffness and strength emphasizing the inferior bone quality of the fetal/infantile skeleton. Fundamental structural and compositional discrepancies are also quantified in *dark* and *bright* osteons. Longitudinally fibered *dark* osteons are characterized by a higher mineral content and a higher ratio of inorganic to organic matrix components that lead to higher stiffness. In contrast, *bright* osteons display a lamellar architecture with changing collagen fiber orientation between neighboring lamellae, contain relatively more collagen, are more ductile and provide better energy dissipation capabilities.

Taken together, both during skeletal growth and in healthy mature bone, the preferential collagen fiber orientation is associated with specific mineralization profiles that, in conjunction, guide the mechanical properties. The presented findings underline that the bone matrix is sensitive to structural and compositional adaptions at the nanoscale and provide new insight into how nanoscale tissue properties can influence fracture mechanisms at larger length scales.

11. Zusammenfassung

Knochen erlangt seine mechanische Belastbarkeit durch seinen hierarchischen Aufbau, der sich während des skelettalen Wachstums entwickelt und durch kontinuierliche Knochenumbauprozesse erhalten wird. In Zuge dessen wird die Matrix sowohl mikro- als auch nanostrukturell angepasst, um neuen mechanischen Anforderungen besser entgegenwirken zu können. Dennoch ist ein erhöhtes Frakturrisiko nicht nur im Alter und bei Knochenkrankheiten dokumentiert, sondern auch bei Kindern und Jugendlichen. Während die zugrunde liegenden Mechanismen der Frakturresistenz in vollentwickeltem Knochen weitestgehend erforscht sind, ist unklar, wie sich die Knochenmaterialqualität während des skelettalen Wachstums verändert. In gesunden Erwachsenen unterstreichen sekundäre Osteone und Schaltlamellen umfassende stattgefundene Knochenumbauprozesse. Polarisationsoptisch betrachtet können Osteone sowohl dunkel als auch hell erscheinen: in Abhängigkeit der vorrangigen Kollagenfaserorientierung (longitudinal oder transversal). Die Existenz *dunkler* und *heller* Osteone weist auf eine Heterogenität der Matrix hin, die die Belastbarkeit optimiert. Im Rahmen der vorliegenden Arbeit wurde die Organisation und Orientierung der Kollagenfasern in der humanen femoralen Knochenmatrix untersucht und in Zusammenhang mit weiteren kompositionellen und mechanischen Parametern gestellt. Hierbei wurden Proben von fetalen bis 14 Jahre alten Fällen sowie eines 44-Jahre alten Individuums untersucht.

Es konnte ein klarer Zusammenhang zwischen der Kollagenfaserorientierung und spezifischen Mineralisationsmustern aufgezeigt werden. Im fetalen/infantilen Alter besteht die Knochenmatrix aus Geflechtknochen, in dem die Kollagenfasern primär transversal orientiert sind. Mit fortschreitendem Alter und Beginn des freien Gehens wird der Geflechtknochen durch organisierten Lamellenknochen ersetzt, und die Kollagenfasern sind vorrangig longitudinal orientiert. Der strukturelle Umbau wird von kompositionellen Änderungen begleitet. Hier weisen die 2 bis 14 Jahre alten Fälle eine erhöhte und homogenere Mineralisierung auf, die mehr Steifigkeit verleiht. Strukturelle und kompositionelle Unterschiede konnten ebenfalls zwischen *hellen* und *dunklen* Osteonen nachgewiesen werden. *Dunkle* Osteone mit longitudinalem Kollagen sind höher mineralisiert und haben ein höheres Verhältnis von anorganischen zu organischen Matrixbestandteilen, was zu erhöhter Steifigkeit führt. Im Gegensatz dazu sind *helle* Osteone lamellar aufgebaut, wobei sich die Kollagenfaserorientierung zwischen benachbarten Lamellen verändert. Sie enthalten einen höheren Anteil an Kollagen und können durch ihre größere Duktilität mehr Energy ableiten.

Die Ergebnisse dieser Arbeit zeigen, dass die Kollagenfaserorientierung im humanen Knochen mit bestimmten Mineralisationsmustern gekoppelt ist, die die mechanische Kompetenz maßgeblich beeinflussen. Die beiden Studien unterstreichen die Fähigkeit der Knochenmatrix sich sowohl strukturell als auch kompositionell gegenüber mechanischen Belastungen anzupassen und offenbaren wie das Frakturverhalten durch Anpassungen auf der Nanoebene beeinflusst werden kann.

12. Declaration of Contribution to Publications

Publication 1:

Mechanical Competence and Bone Quality Develop During Skeletal Growth

I hereby declare my own contributions to the article “Mechanical Competence and Bone Quality Develop During Skeletal Growth”: I planned and performed experiments to evaluate the microstructural appearance and preferential collagen fiber orientation by circularly polarized light microscopy in the femoral diaphysis of the developing skeleton. Subsequently, I analyzed the obtained data, performed statistical analysis, and interpreted the results taking into account additional compositional and mechanical data acquired in other experiments. I contributed to the writing of the manuscript, revised and approved the final version of the manuscript.

Publication 2:

Collagen Fiber Orientation is Coupled with Specific Nano-Compositional Patterns in Dark and Bright Osteons Modulating Their Biomechanical Properties

I hereby declare my own contributions to the article “Collagen Fiber Orientation is Coupled with Specific Nano-Compositional Patterns in Dark and Bright Osteons Modulating Their Biomechanical Properties”: I designed the study and planned all experiments of the presented work. I secured beamtime at the German Electron Synchrotron (DESY) and prepared and organized the experimental procedure. I prepared the samples and performed the experiments. I collected structural (polarized light microscopy, synchrotron nano-computed tomography), compositional (quantitative backscattered electron imaging, Fourier transform infrared spectroscopy) and mechanical information (nanoindentation), evaluated and interpreted the obtained data. I performed the statistical analysis, wrote the manuscript, designed the figures and revised the manuscript during the revision process.

13. Acknowledgements

An dieser Stelle möchte ich mich bei all den Personen bedanken, ohne deren Unterstützung diese Doktorarbeit nicht möglich gewesen wäre.

Besonderer Dank gilt zunächst meinem Doktorvater Prof. Dr. Björn Busse, der mir durch seine wertvollen Ratschläge und anhaltende Hilfe ein wichtiger Begleiter in dieser Phase meiner akademischen Laufbahn war.

Großer Dank geht ebenfalls an Prof. Dr. Michael Amling, durch dessen Motivation und Einsatz der multidisziplinäre wissenschaftliche Diskurs am Institut für Osteologie und Biomechanik etabliert wurde.

Meinen großartigen Mitdoktoranden Annika vom Scheidt, Felix Schmidt, Eva Wölfel, Imke Fiedler und Simon von Kroge, die ich nach den gemeinsamen Jahren auch zu meinen Freunden zähle, danke ich herzlichst: Für zahlreiche und konstruktive fachliche Diskussionen und Ratschläge sowie für die vielen nicht-wissenschaftlichen und motivierenden Gespräche, die meinen Weg zur fertigen Doktorarbeit bereichert haben.

Für eine freundschaftliche Arbeitsatmosphäre und wissenschaftlichen Austausch danke ich zudem den Kolleginnen und Kollegen, die mich in meiner Zeit am Institut für Osteologie und Biomechanik begleitet haben: Katharina Jähn-Rickert, Sandra Perkovic, Christine Plumeyer, Christoph Riedel, Haniyeh Hemmatian, Mahan Qwamizadeh, Mona Neven, Michael Hahn, Elke Leicht, Olga Winter, Frau Dietzmann und Elizabeth Zimmermann.

Meinen Eltern Ingeborg und Wolfgang sowie meinem Bruder Luca und meiner Oma danke ich von Herzen für ihre liebevolle und uneingeschränkte Unterstützung und Geduld. Danke für euren großen Beistand in allen Etappen dieses herausfordernden Weges: Für die mitgegebene Begeisterung für die Naturwissenschaften, euren Rückhalt und eure Hilfe. Außerdem danke ich meiner Freundin Celina für ihre Geduld und ihren Halt. Deine Liebe und dein Zuspruch waren von großer Bedeutung für das Gelingen dieser Arbeit.

14. Curriculum Vitae

Lebenslauf wurde aus datenschutzrechtlichen Gründen entfernt.

15. Eidesstattliche Versicherung

Ich versichere ausdrücklich, dass ich die Arbeit selbständig und ohne fremde Hilfe verfasst, andere als die von mir angegebenen Quellen und Hilfsmittel nicht benutzt und die aus den benutzten Werken wörtlich oder inhaltlich entnommenen Stellen einzeln nach Ausgabe (Auflage und Jahr des Erscheinens), Band und Seite des benutzten Werkes kenntlich gemacht habe.
Ferner versichere ich, dass ich die Dissertation bisher nicht einem Fachvertreter an einer anderen Hochschule zur Überprüfung vorgelegt oder mich anderweitig um Zulassung zur Promotion beworben habe.
Ich erkläre mich einverstanden, dass meine Dissertation vom Dekanat der Medizinischen Fakultät mit einer gängigen Software zur Erkennung von Plagiaten überprüft werden kann.

Unterschrift: .....